Radiation induced activation of potassium-channels: The role of ROS and calcium

Die Rolle von ROS und Calcium bei der Kalium-Kanal Aktivierung nach ionisierender Strahlung

TECHNISCHE
UNIVERSITÄT
DARMSTADT

Vom Fachbereich Biologie der Technischen Universität Darmstadt
zur Erlangung des akademischen Grades
eines Doctor rerum naturalium
genehmigte Dissertation von
Diplom-Biologin Christine Silvia Gibhardt
aus Kassel

1. Referent: Prof. Dr. Gerhard Thiel
2. Referent: Prof. Dr. Marco Durante
Eingereicht am: 23.06.2014
Mündliche Prüfung am: 08.09.2014
Darmstadt 2014
D17

Table of contents

1. **Abstract** **1**

1.1. Abstract 1

1.2. Zusammenfassung 3

2. **Introduction** **5**

2.1. General introduction 5

2.2. Ion-channels 5

2.2.1. Ion-channels and their role in cell cycle regulation 5

2.2.2. Calcium-activated potassium-channels: the hIK channel 7

2.3. Calcium 9

2.4. Ionizing radiation 10

2.4.1. Heavy-ion irradiation 10

2.4.2. X-ray irradiation 11

2.4.3. Laser irradiation 11

2.5. Reactive oxygen species 12

2.6. Redox-buffering in cells 14

2.7. Motivation 15

3. **Matherial and methodes** **16**

3.1. Chemicals 16

3.2. Plasmids 16

3.2.1. Plasmid amplification 16

3.3. Cell culture 17

3.3.1. Cell culture for microscopy 17

3.3.2. Cell culture for electrophysiological recordings 17

3.4. Patch clamp recordings 18

3.5. Fluorescence microscopy 19

3.6. Cell irradiation 19

3.7. Matlab simulation 20

3.8. Statistical analysis 20

4. CHAPTER 1 - Activation of potassium-channels by ROS and calcium 21

4.1. Activation of the hIK channel in A549 cells by ROS and calcium 21

4.2. Activation of heterologous expressed hIK channels in HEK293 cells by ROS, calcium and X-ray irradiation 27

4.3. ROS stimulated increase of the cytosolic calcium concentration 32

5. CHAPTER 2 - Generation of ROS by UV-laser micro-irradiation 36

5.1. Establishing fluorescence based sensor proteins for *in vivo* monitoring of ROS and ROS buffering in cells after UV-laser micro-irradiation 36

5.2. UV-laser micro-irradiation generates a rapid burst of H_2O_2 in the irradiated compartment 38

5.3. Cytoplasm and nucleus have different redox-buffering capacities 41

6. CHAPTER 3 - Real-time detection of ROS after X-ray and heavy-ion irradiation 47

6.1. Generation of reactive oxygen species after X-ray irradiation 47

6.2. Generation of reactive oxygen species after heavy-ion irradiation 52

7. Discussion 54

7.1. Radiation, ROS and Ca^{2+} induced hIK channel activation and membrane hyperpolarization 54

7.2. Real-time detection of ROS after ionizing radiation 57

7.3. Cellular and physiological consequences of ionizing radiation induced hIK channel activation 62

7.4. Conclusion 63

8. References 64

9. Apendix 83

9.1. Abbreviations 83

9.2. List of figures 85

9.3. Own Work - List of contributions 86

9.4. Declaration - Ehrenwörtliche Erklärung 87

9.5. Acknowledgements 88

9.6. Curriculum vitae 90

1. Abstract

1.1. Abstract

Ionizing radiation (IR), in particular photons, is a quasi-universal tool in medical diagnostics and in tumor therapy. The negative side effects of this high-energy photon irradiation, which often cause secondary cancers or cell invasiveness, are well documented. The classical paradigm still is that all these effects can be traced back to irradiation induced DNA damage. Damage to other cellular compartments has been neglected for a long time. Recent research, however, has demonstrated that a calcium-activated K^+-channel (hIK-channel) is activated by different types of ionizing radiation, e.g. γ-irradiation (Kuo et al., 1993), X-ray, α-particles and heavy-ion irradiation (Roth, 2013). The elevated K^+ conductance results in a membrane hyperpolarization; the latter is a known signal for cell cycle progression.

In the present thesis I elucidate the signal cascade, which is activated by IR and which finally activates hIK channels. In order to examine whether excursion in the concentration of cellular hydrogen peroxide (H_2O_2), or of the free concentration of Ca^{2+} ($[Ca^{2+}]_{cyt}$) are involved in signaling after IR, I employed several genetically encoded fluorescence sensors. The generation of reactive oxygen species (ROS), especially H_2O_2, was measured before and immediately after cells were challenged with either 405 nm UV laser micro-irradiation, X-rays or heavy-ion irradiation with a sensor for H_2O_2 (HyPer) and a sensor for the glutathione redox-buffer (Grx1-roGFP2). The latter is a sink for all ROS, which are eliminated in a cell by the oxidation of glutathione. These measurements provide for the first time robust quantitative data on the generation of ROS directly after irradiation in single living cells with a high temporal and spatial resolution. The data show that ROS molecules are generated immediately after the irradiation stress. They are rapidly buffered by an efficient redox-buffer system, which involves glutathione. When the buffer is exhausted the concentration of ROS is increasing throughout the cell; the latter could be monitored directly by an increase in the concentration of H_2O_2, a known second messenger in the cell.

This general pattern is observed with some variations after exposing cells to X-ray stress (1-10 Gy) and 405 nm UV-irradiation (0.5-4.5 mJ/µm²). The latter micro-irradiation experiments of the cells with laser light provide the additional information that the ROS response is maximal in the compartment, which is directly irradiated and that an irradiation of the nucleus generates about 2 to 3 times more H_2O_2 than the equivalent irradiation of the cytosol. Also an irradiation of cells with heavy-ions causes an increase in H_2O_2 concentration, but the response is more variable and not all cells reveal an increase in H_2O_2. Further experiments suggest that the rise in H_2O_2, which is generated in cells as a responds to irradiation stress, is sufficient to trigger a signal cascade, involving an increase in $[Ca^{2+}]_{cyt}$. The latter hypothesis is supported by the finding that an incubation of A549 cells and HEK293 cells in a buffer with H_2O_2 is triggering an elevation in $[Ca^{2+}]_{cyt}$. This was measured with a FRET based Ca^{2+} sensor (YC3.60). The fact that challenging the same cells with the identical amount of H_2O_2 is sufficient to stimulate the Ca^{2+}-activated hIK channel suggests that channel activation is mediated via a H_2O_2 induced increase in $[Ca^{2+}]_{cyt}$. This upstream part of the signaling cascade is independent of the cell type and found in HEK293 cells and A549 cells. The increase in membrane conductance, which is downstream of these events, is only elevated in cells like A549 cells, which express the hIK channel. When hIK channels are transiently expressed in HEK293 cells, also these cells, which are in their native form insensitive to IR, respond to the radiation stress with an increase in membrane conductance. Collectively the data show that cells, which functionally express hIK channels, are sensitive to ionizing irradiation. The activation of these Ca^{2+} sensitive channels, which can have severe impacts on the differentiation of cells, is based on an elevation in $[Ca^{2+}]_{cyt}$ in these cells; the latter gain is the result of a rapid elevation of ROS molecules in the nucleus but also in the cytosol of cells, which under went an exposure to ionizing irradiation.

1.2. Zusammenfassung

Ionisierende Strahlung wird vor allem in der klinischen Diagnose und in der Tumor-Therapie eingesetzt. Die Tatsache, dass diese Art der Bestrahlung negative Nebeneffekte hat und zu sekundären Tumoren führen kann, ist seit langem bekannt. Bisher wurde die Wirkung von ionisierender Strahlung wie z.B. Röntgen- oder Schwerionen-Strahlung hauptsächlich in Bezug auf Schädigung der DNA und dessen Auswirkungen interpretiert und untersucht. Gut dokumentiert ist, dass DNA-Schäden wie Doppelstrangbrüche, Einzelstrangbrüche oder Basenschäden direkt oder durch eine fehlerhafte Reparatur zu Veränderungen im Erbgut führen können.

Erst seit einigen Jahren sind auch andere zelluläre Bestandteile außerhalb des Zellkerns in den Fokus der Untersuchungen gerückt. Vor kurzem konnte gezeigt werden, dass unterschiedliche Arten von ionisierender Strahlung, wie γ- (Kuo et al., 1993), Röntgen-, α- und Schwerionen-Strahlung (Roth, 2013), zu einer Aktivierung von Calcium-abhängigen Kalium-Kanälen, sogenannter hIK Kanäle, führt. Die erhöhte Kalium-Leitfähigkeit, führt zur Hyperpolarisation der Zellmembran und kann damit Einflüsse auf Zellproliferation und Migration haben.

In der vorliegenden Arbeit wurde die Signalkaskade, welche die Aktivierung von hIK Kanälen nach Bestrahlung zur Folge hat, genauer untersucht. Die Entstehung von reaktiven Sauerstoffspezies (ROS) wurde mit Hilfe von proteinbasierten Fluoreszenz-Sensoren mit einer hohen zeitlichen und räumlich Auflösung nach Bestrahlung von Zellen mit verschiedenen Strahlenarten, wie 405 nm UV Mikro-Bestrahlung, Röntgen- und Schwerionen-Strahlung, detektiert. Dabei konnte zum ersten Mal in lebenden Zellen sowohl die direkte Entstehung von Wasserstoffperoxid (H_2O_2) mit dem Sensor HyPer, als auch indirekt die Pufferung der ROS durch das zelluläre Redox-Puffer-System mit dem Sensor Grx1-roGFP2 gezeigt werden. Letzterer gibt ein Maß für die Menge an oxidiertem Glutathion. Die Daten zeigen, dass ROS unmittelbar nach Bestrahlung gebildet werden und schnell durch ein sehr effizientes Redox-Puffer System abgefangen werden. Wenn die Puffer Kapazität ausgeschöpft ist, steigt die ROS Konzentration in der gesamten Zelle an. Letzteres wurde direkt durch eine erhöhte Konzentration des als Signalmolekül bekannten H_2O_2 gemessen.

Die Entstehung von ROS wurde mit einigen Variationen sowohl nach Röntgenstrahlung (1-10 Gy), als auch nach UV Strahlung mit 405 nm (0,5-4,5 mJ/μm^2) gemessen. Die Laser Mikro-Bestrahlung konnte zusätzlich zeigen, dass die Konzentration an entstandenen ROS im bestrahlten zellulären Kompartiment am höchsten war, wobei im Zellkern 2 bis 3 mal mehr H_2O_2 entstand als im Cytosol. Auch nach Bestrahlung mit Schwerionen wurde eine erhöhte H_2O_2 Konzentration festgestellt. Jedoch reagierten nicht alle Zellen auf die Bestrahlung.

Des Weiteren konnte gezeigt werden, dass das entstandene H_2O_2 eine Calcium-Signalkaskade in den verwendeten Zellen auslöst. Die Erhöhung der cytosolischen Calcium Konzentration wurde dabei mit einem FRET basierten Ca^{2+} Sensor (YC3.60) gemessen. Durch die gleiche Menge H_2O_2 konnten außerdem hIK Kanäle direkt aktiviert werden. Diese erhöhte Membranleitfähigkeit konnte nur in den Zellen, die hIK Kanäle exprimieren, beobachtet werden. HEK293 Zellen, die in ihrer nativen Form nicht auf Strahlung reagieren, konnten durch die Überexpression von hIK Kanälen strahlenempfindlich gemacht werden.

Zusammenfassend zeigen die Daten, dass Zellen die funktionale hIK-Kanäle besitzen auf ionisierende Strahlung reagieren. Die durch die Strahlung entstandenen ROS lösen eine Erhöhung der cytosolischen Calcium Konzentration aus, wodurch wiederum die hIK Kanäle aktiviert werden. Die Aktivierung dieser Calcium-abhängigen Kaliumkanäle hat gravierende Effekte auf die Zelldifferenzierung.

2. Introduction

2.1. General introduction

Ionizing radiation (IR) generates various effects in cells among which DNA damage is considered the most severe one. DNA double strand breaks, single strand breaks or base damage can be created directly by irradiation of the DNA with low-LET (linear-energy-transfer) irradiation or indirectly by reactive oxygen species. The former accounts for about 1/3 the latter for 2/3 of the DNA damage (Azzam *et al.*, 2012).

Damage to other compartments of the cell has been for a long time neglected in radiation biology. But considering the cytosol of a mammalian cell with many organelles and a crowded packaging with proteins and vesicles it seems obvious that the DNA is not the only target of ionizing radiation. Notably the most prominent molecule in cells is water, which makes out about 80 % of a cell. Also membranes are very abundant in cells and the first barrier for ionizing radiation. In the context of the large size of membranes as targets for ionizing irradiation also membrane proteins became in recent years a subject of interest in radiation biology. In this context it was for example found that potassium-channels are activated in A549 cells upon irradiation with different types of ionizing radiation, e.g. γ-irradiation (Kuo *et al.*, 1993) X-ray, α-particles and heavy-ion irradiation (Roth, 2013). In the latter study it was found that one particular potassium (K^+) channel, the human intermediate-conductance calcium-activated K^+ (hIK) channel, is in particular sensitive to ionizing irradiation. This channel is activated in a dose dependent manner within 3 to 10 minutes after exposure to sparse or dense ionizing radiation. Activation by IR occurs to be indirect. The finding that a cytosolic Ca^{2+}-buffer decreases the sensitivity of this channel to IR suggest a calcium mediated signaling cascade, which connects a primary radiation response with channel activation (Roth, 2013).

2.2. Ion-channels

Ion-channels are transmembrane protein tunnels, which enable the selective flow of ions across membranes; they are present is all cell membranes including the plasma membrane and the membrane of organelles. The activity of ion-channels is characterized by a stochastic switching between an open and a closed conformation, a process which is called gating (Hille, 2001). Gating and hence the activity of ion-channels can be regulated via different chemical and physical stimuli. The most prominent regulators are chemical ligands or voltage.

Ion-channels play important roles in many physiological progresses. They are key players in the nervous system, in muscle movement or in the regulation of the heartbeat. Due to their prominent involvement in many cellular functions, it is obvious that aberrant functions of ion-channels are the cause of many diseases (reviewed in Celesia, 2001; Kim, 2014).

2.2.1. Ion-channels and their role in cell cycle regulation

In the last decades it was found that ion-channels are involved in processes beyond neuron firing and muscle movement. One of the emerging roles of channels is their role in the regulation of cell cycle regulation. There is experimental evidence which shows that they can control the onset of apoptosis and modulate proliferation and migration of cells (Wang, 2004). With this importance of channels in cell differentiation it is not surprising to find that they are also involved in many aspects of cancer development (Becchetti, 2011; Kunzelmann, 2005; Yang and Brackenbury, 2013; Felipe *et al.*, 2006). The most prominent ion-channel expressed in tumor cells is the hERG channel (KCNH2, Kv11.1) (Asher *et al.*, 2011, 2010; Bogin, 2004; Camacho, 2006; Felipe *et al.*, 2006; Huber, 2013; Kunzelmann, 2005; Lansu & Gentile, 2013; Leanza *et al.*, 2014; Ouadid-Ahidouch & Ahidouch, 2013; Ousingsawat, 2007; Pardo *et al.*, 2005; Pardo, 2004; Patt *et al.*, 2004; Prevarskaya *et al.*, 2010). The hERG channel is expressed in a variety of tumor cells and it has been shown that hERG channel activity is involved in many down-stream signal cascades, e.g. integrin adhesion and therefore migration and infiltration of tumor cells.

Regarding the contrasting role of ion-channels, which favors on one side apoptosis and on the other side cell proliferation, it is currently believed that these membrane proteins have the role of molecular switches. The fade of cells is determined by a fine balance between proliferation or apoptosis and ion-channel activity favors depending on the type of channel or on the physiological context one or the other pathway. One hypothesis that explains the regulation of proliferation and apoptosis is illustrated in Fig. 1.

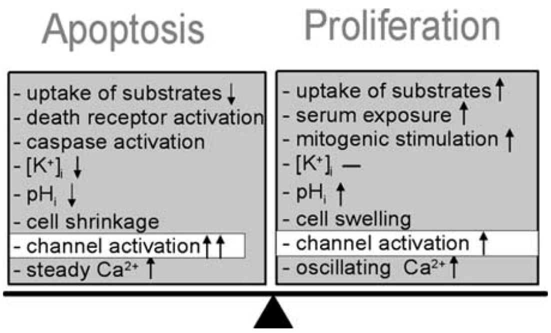

Fig. 1 **Ion-channels are molecular switches.**

Schematic illustration of environmental and intracellular factors determining the cell fate whether in the direction of apoptosis or proliferation. Ion-channel activity as well as the intracellular potassium concentration and calcium signaling maintain important factors in the determination of the cell fate. (Kunzelmann, 2005)

The role of ion-channels in the regulation of cell differentiation is frequently discussed in the context of the channels to modulate the membrane potential (Sundelacruz *et al.*, 2009; Yang and Brackenbury, 2013; Blackiston *et al.*, 2010; Prevarskaya *et al.*, 2007). There is evidence that the membrane potential of cells is depolarized in the early G1 phase. Cell cycle progression is then accompanied with a membrane hyperpolarization, which is essential for the transition from late G1 to S phase. This hyperpolarization is achieved by the activation of potassium-channels which drive the potential close to the negative Nernst potential for K^+ (Wonderlin & Strobl, 1996). Different types of potassium-channels were so far found, which all have the ability to hyperpolarize the cell membrane upon activation. Hence, it appears as if there is not one specific potassium-channel required for this purpose in all cell types. In T-lymphocytes for example, the voltage-gated Kv1.3 channel is clearly associated with progression from G1 to S phase (Deutsch *et al.*, 1991), whereas the Eag1 channel (KCNH1, Kv10.1) plays this role in various cell types (Borowiec *et al.*, 2011; Brüggemann *et al.*, 1997; García-Becerra *et al.*, 2010; Kamosinska *et al.*, 1997; Pardo *et al.*, 2005; Pardo & Stühmer, 2008; Pardo & Sühmer, 2008; Pardo, 2004). The latter channel is found for example in human breast cancer (MCF-7) cells (Ouadid-Ahidouch & Ahidouch, 2008; Ouadid-ahidouch *et al.*, 2004; Ouadid-Ahidouch *et al.*, 2001; Wonderlin *et al.*, 1995). Also, other voltage-gated ion-channels have been associated with cell cycle progression; the Kv4.1 channel is one other example (Kim *et al.*, 2010), as well as the hIK channel (chapter 2.2.2) (Bi et al., 2013; Faouzi et al., 2010; Ouadid-Ahidouch & Ahidouch, 2008; Ouadid-ahidouch et al., 2004; Tao et al., 2008; Yun et al., 2009)

In addition to their function in cell cycle control K^+-channel activity is also critical for cell volume regulation (Lang *et al.*, 2006; Sarkadi & Parker, 1991). The activity of channels allows the osmotic swelling of cells, a prerequisite for an increase in volume after cell division. Also, cell migration is strongly associated with changes in cell volume. The ability of channels to regulate the cell volume became also an important issue in the understanding of cell migration and invasion of tumor cells into the surrounding tissue. Here the aforementioned hIK channel often is delineated in this context (Cruse *et al.*, 2006; D'Alessandro *et al.*, 2013).

2.2.2. Calcium-activated potassium-channels: the hIK channel

Membrane hyperpolarization provides the electrochemical gradient for calcium influx (Kutchinsky *et al.*, 2003). The involvement of an elevation of cytosolic calcium during cell cycle progression has been reported for different cell types (Kahl, 2003; Lallet-Daher *et al.*, 2009; Machaca, 2010). Additionally, experimental data show a close connection between a rise in the cytosolic calcium concentration ($[Ca^{2+}]_{cyt}$) and a hyperpolarized membrane potential (Panner & Wurster, 2006). The complex dependency of Ca^{2+} fluxes, channel activity and regulatory mechanisms is depicted in a model in Fig. 2. Therefore calcium-gated potassium-channels can capture the function of a feed-back loop in this context. T-type Ca^{2+} channels are transient opening, low-voltage-dependent channels, which are activated at normal resting membrane potentials. The resulting increase in $[Ca^{2+}]_{cyt}$ has the consequence of the activation of Ca^{2+} activated K^+-channels. The activity of these K^+-channels and consequently the increased K^+ conductance hyperpolarizes the plasma membrane. In turn the T-type Ca^{2+} channels are inactive at this very hyperpolarized membrane potentials. Hence, both K^+ and Ca^{2+} cannels mediate $[Ca^{2+}]_{cyt}$ in a complex interplay (Capiod, 2013; Guéguinou *et al.*, 2014; Lacinova, 2005; Panner & Wurster, 2006).

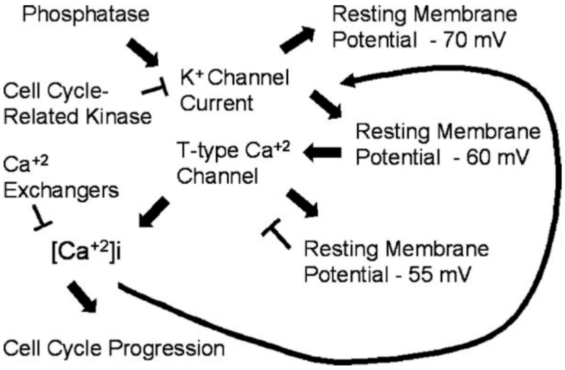
Phosphatase
Resting Membrane Potential - 70 mV
Cell Cycle-Related Kinase
K+ Channel Current
Resting Membrane Potential - 60 mV
Ca+2 Exchangers
T-type Ca+2 Channel
[Ca+2]i
Resting Membrane Potential - 55 mV
Cell Cycle Progression

Fig. 2 **Schematic model of the complex interplay between Ca^{2+} and K^+-channels in mediating cytosolic calcium concentrations.**

The activity of T-type calcium currents is controlled by the membrane potential, which is maintained by K^+-channels. At the transition from G1 to S phase the membrane potential becomes hyperpolarized due to K^+-channel activation. (Panner & Wurster, 2006)

The class of channels, which are involved in this regulatory network, can be divided into two subclasses with respect to their single channel conductance, their molecular phylogenetic relation, their pharmacology and their mechanism of calcium sensing (Wei *et al.*, 2005; Wulff & Köhler, 2013). One includes the voltage-dependent BK_{Ca}-channel, which has a large ("big") single-channel conductance of 200-250 pS and an intrinsic Ca^{2+} sensitive gating mechanism (Berkefeld *et al.*, 2010; Salkoff *et al.*, 2006). The second group includes the two historically defined groups of small-conductance (SK_{Ca}; 5-10 pS) and intermediate-conductance (IK_{Ca}; 20-40 pS) channels with a calcium sensitivity mediating calmodulin. Whereby not all of them are sensitive to Ca^{2+} (Wei *et al.*, 2005; Wulff & Köhler, 2013).

The main interest in this thesis is focusing on the voltage-independent hIK channel (human intermediate-conductance calcium-activated potassium-channel; $K_{Ca}3.1$, KCNN4; Ghanshani *et al.*, 1998). This channel has an intermediate single channel conductance in the range of 30 - 39 pS (Hoffman *et al.*, 2003; Ishii & Ishii, 1997; Jensen *et al.*, 2001; Logsdon, 1997).

The hIK channel consists of 427 amino acids and has the general structure of Shaker-like ion-channels. It is composed of four subunits each consisting of six transmembrane helices (Fig. 3) (Jensen *et al.*, 1998; Klein *et al.*, 2007). The loop between transmembrane domain V and VI has a canonical GYGD motif, which provides the structure for potassium selectivity. The calcium sensitivity is due to a calmodulin (CAM) binding site at the C-terminus of the channel (Morales *et al.*, 2013). The consecutively bound calcium sensor CAM couples channel activity to the cytosolic calcium concentration. Calcium binding enables the transition from a non-conducting to a conducting configuration (Keen *et al.*, 1999; Li *et al.*, 2009). A model of the hIK channel monomer with the important domains is presented in Fig. 3.

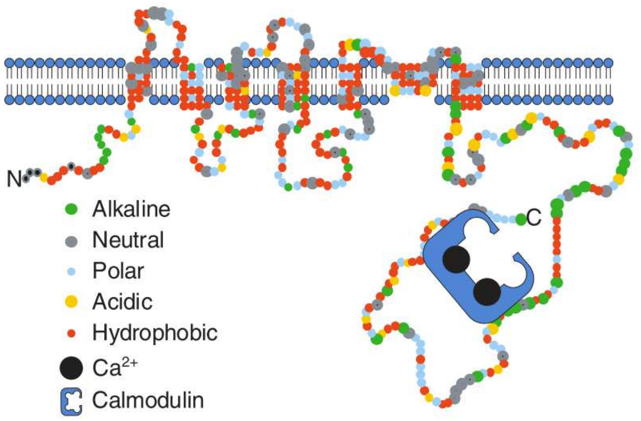

Fig. 3 **Structure of the hIK channel.**

Schematic illustration of the general structure and amino-acid composition of the hIK channel (human intermediate-conductance calcium-activated potassium-channel; $K_{Ca}3.1$, KCNN4). The channel is super composed of four subunits each consisting of six transmembrane domains. A consecutively associated calmodulin at the C-terminus of the protein mediates the calcium sensitivity of the voltage-insensitive K^+-channel. (Jensen *et al.*, 2002)

The hIK channel apparently has a wide spectrum of activities in cells. The channel is well characterized in the context of inflammatory effects like fibrosis and immune responses of lymphocytes, e.g. T-cell activation (Begenisich *et al.*, 2004; Berridge *et al.*, 2000; Bradding & Wulff, 2009; Feske *et al.*, 2013; Feske, 2007; Ghanshani *et al.*, 2000; Koshy *et al.*, 2013; Kuras *et al.*, 2012; Lewis, 2001; Nicolaou *et al.*, 2007; Panyi *et al.*, 2004; Shaw *et al.*, 2013). This include mast-cell (Cruse *et al.*, 2011) and fibrocyte (Cruse *et al.*, 2011) migration and diseases which are linked to immune responses like asthma (Bradding & Wulff, 2009), rheumatoid arthritis or psoriasis (Feske *et al.*, 2013).

It has further been shown by inhibition with specific blockers and by knockdown experiments that hIK channels regulate cell proliferation in mouse mesenchymal stem cells (MSCs) (Tao *et al.*, 2008), human dermal fibroblasts (Yun *et al.*, 2009) and breast cancer cells (Faouzi et al., 2010; Ouadid-Ahidouch & Ahidouch, 2008; Ouadid-ahidouch et al., 2004). Furthermore the involvement of hIK channels in migration of tumor cells like glioblastoma cells has been well established (D'Alessandro *et al.*, 2013; Schwab *et al.*, 2012). The multiple roles of hIK channels in important cell processes make the hIK channel an interesting target in cancer therapy.

2.3. Calcium

Calcium is an important second messenger in cells and involved in many signal pathways such as cell cycle control (Kahl, 2003), cell proliferation (Ay *et al.*, 2013), cell migration (Chen *et al.*, 2013b; Schwab *et al.*, 2006), cell division, apoptosis (Hanson *et al.*, 2004; Ichas & Mazat, 1998; Tantral *et al.*, 2004), or immune reactions (Qu *et al.*, 2011; Schwarz *et al.*, 2013; Shaw *et al.*, 2013). Consequently, a deregulation of the cytosolic Ca^{2+} homeostasis can be the cause of diseases like cancer. In the latter case Ca^{2+} signaling is particularly important in tumor proliferation and progression as well as in formation of metastasis (Chen *et al.*, 2013b; Liu *et al.*, 2011; Parkash & Asotra, 2010; Prevarskaya *et al.*, 2011).

In addition to the previous mentioned membrane hyperpolarization, proliferating cells also require calcium signals in order to enter and complete the S and M phase of the cell cycle (Roderick & Cook, 2008; Skelding *et al.*, 2011; Taylor, 2008). Therefore the intracellular calcium concentration is strongly regulated (Penner *et al.*, 1993) and a large number of channels, cellular regulators, Ca^{2+} buffer systems and other factors regulate and remodel Ca^{2+} homeostasis (Berridge *et al.*, 2003).

The calcium concentration in the cytoplasm ($[Ca^{2+}]_{cyt}$) is at rest only 100 nM; as a part of signaling cascades $[Ca^{2+}]_{cyt}$ can increase transiently to up to 1-10 µM (Clapham, 1995, 2007). The endoplasmic reticulum (ER) is in addition to the extracellular buffer the main cellular compartment for Ca^{2+} storage. Calcium concentrations in the ER can reach from high micromolar up to low milimolar concentrations (Corbett & Michalak, 2000). For a signal dependent increase in $[Ca^{2+}]_{cyt}$ specific channels in the plasma membrane, or in the ER membrane open and Ca^{2+} flows down its huge electrochemical gradient into the cytosol. To maintain the low resting $[Ca^{2+}]_{cyt}$ Ca^{2+} ions are either buffered by binding to Ca^{2+} binding proteins (Clapham, 1995, 2007), or the excess Ca^{2+} is transported together with potassium and / or sodium via antiporters (Clapham, 1995, 2007; Karlstad *et al.*, 2012; Roderick & Cook, 2008) against a concentration gradient to the extracellular medium. Furthermore Ca^{2+} is also actively transported by Ca^{2+} ATPases into the extracellular room or into the ER (Berridge *et al.*, 2003; Clapham, 1995, 2007; Karlstad *et al.*, 2012; Parkash & Asotra, 2010; Roderick & Cook, 2008; Vaca, 2010).

In non-excitable cells the refilling of internal Ca^{2+} stores in the ER occurs mainly via a mechanism called (STIM)/Orai-mediated store-operated calcium entry (SOCE) (Karlstad *et al.*, 2012; Lewis, 2011; Shen *et al.*, 2011; Targos *et al.*, 2005; Vaca, 2010). Calcium release-activated calcium (CRAC) channels, which belong to the so-called Orai-family and are localized at the plasma membrane, are activated when Ca^{2+} is released from intracellular stores (ER) in the frame of a signal cascade. The decrease of Ca^{2+} concentration in the ER triggers the accumulation of the ER Ca^{2+} sensor protein stromal interaction molecule (STIM1), which interacts with the Orai in the plasma membrane, enabling the refilling of internal Ca^{2+} stores in the ER. In addition, transient receptor potential (TRP) channels are modulators of $[Ca^{2+}]_{cyt}$, which have been associated with cell migration and cancer progression in the last decades (Fiorio Pla & Gkika, 2013). The aforementioned hIK channel is also connected with SOCE (Gao *et al.*, 2010; Millership *et al.*, 2011). It was demonstrated that hIK mediated hyperpolarization promotes the CRAC mediated rise of $[Ca^{2+}]_{cyt}$ followed by refilling of stores via SOCE (Ferreira & Schlichter, 2013). The K^+-channel regulated changes in the membrane potential, Ca^{2+} channels as the aforementioned T-type Ca^{2+} channels (Fig. 2) and CRAC channels, as well as the maintance of Ca^{2+} homeostasis and mediation of Ca^{2+} signaling are strongly connected (Capiod, 2013; Ferreira & Schlichter, 2013; Gao *et al.*, 2010; Guéguinou *et al.*, 2014; Lacinova, 2005; Millership *et al.*, 2011; Panner & Wurster, 2006).

2.4. Ionizing radiation

As the name indicates, ionizing radiation results in the ionizing of atoms when interacting with matter. This could occur via different physical effects: 1) the photoelectric effect, 2) the Compton effect, or 3) pair production. Ionizing radiation can be divided into two main classes namely dense and sparse ionizing radiation (Hall & Giaccia, 2006).

Dense ionizing radiation, like for example heavy-ion irradiation or α-particles, have a high energy deposition in a confined region. In contrast to this the energy deposition is randomly distributed with sparse ionizing radiation like photon irradiation (Scholz, 2003). The energy deposited in matter is termed dose (D; Gy = J/kg). To compare these different kinds of ionizing radiation the energy deposition per unit length is indicated as the so-called linear-energy transfer (LET; keV/µm). For a comparison of different types of radiation with respect to their impact on biological systems the concept of relative biological effectiveness (RBE) was implemented. The RBE value is obtained by dividing the radiation dose by a standard dose which elicits a defined biological endpoint (Okayasu, 2012).

2.4.1. Heavy-ion irradiation

Heavy-ions deposit most of their energy along their track through matter (Fig. 4). This results in a high number of ionization events along this track and only few ionizations in regions far away of the track due to secondary electrons; the so called δ-electrons. Heavy-ion irradiation is peculiar. During the travel of heavy-ions through matter, they loose energy and the velocity of the particles decreases. This results in a sharp rise in energy deposition at the end of their penetration range, the so called Bragg-peak (Nakamura *et al.*, 2010). This unique property of heavy-ion irradiation is currently used for cancer therapy approaches; because of the aforementioned penetration through matter heavy-ions spare the healthy tissue on the way to the tumor and have a strong destructive effect on the tumor (Hamada, 2009).

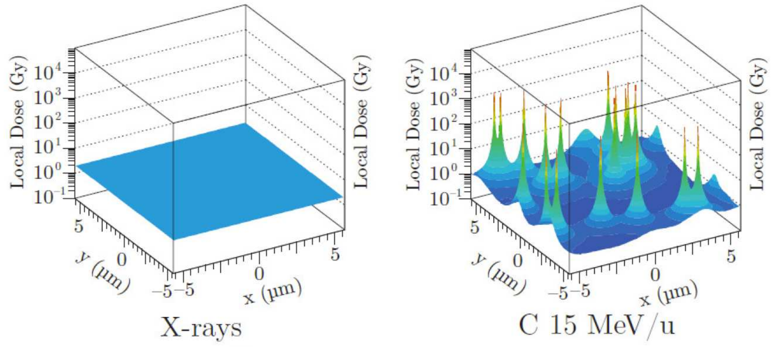

Fig. 4 **Dose distribution of X-rays and carbon-ions.**

The dose of photon irradiation like X-rays is homogeneous distributed, whereas carbon-ions with an energy of 15 MeV/u show local peaks with a high deposed energy around the ion-track. Both examples show a macroscopic dose of 2 Gy. (Scholz, 2003)

2.4.2. X-ray irradiation

Photon radiation, which is used for radiation research or therapy purpose, is Roentgen radiation also called X-rays. They are classified as a low-LET radiation (Okayasu, 2012). X-rays can be generated with a X-ray tube, where electrons from the cathode are accelerated in vacuum by the application of voltage. The accelerated electrons fly towards the anode and impinge on the tungsten surface. This generates X-rays, which are composed of the so-called Bremsstrahlung and characteristic lines. These lines have distinct energies, resulting from emission of electrons of the atom shells. The Bremsstrahlung strongly depends on the anode surface material and the acceleration energy. The energy of the generated photons is in the range of 100 eV and several MeV. For research and therapy purpose X-ray irradiation is filtered by aluminum or copper filters to eliminate softer, not tissue-penetrating, rays. The dose of X-rays on the target is in contrast to heavy-ion irradiation homogeneous distributed (Fig. 4).

2.4.3. Laser irradiation

In radiation research and here in particular when cells are imaged on a microscope, laser micro-irradiation becomes widely used to generate DNA damages (Dinant et al., 2007; Ferrando-May et al., 2013; Huang et al., 2013; Mortusewicz et al., 2008, 2006, 2005), The reason is that particle radiation with the microbeam-technique (Prise & Schettino, 2011) is not accessible for the majority of researchers. Laser micro-irradiation enables a distinct and directed damage in a defined region of the cell nucleus. In general the cellular DNA is needed to be sensitized with intercalating chemicals like Hoechst33258 or the incooperation of the thymidine analogue BrdU (Walter & Maximilians, 2003). But there are also studies were no sensitizers were used in this kind of application. The optical systems and laser wavelength used for this purpose are rather diverse. They reach from UV light to near infrared pulsed lasers (Botchway *et al.*, 2010). DNA damage is induced either via linear light absorption, or via non-linear absorption using ultra-short lasers pulses. As a consequence various types of DNA damage and repair-pathways are induced (Dinant *et al.*, 2007). An overview over the recent DNA repair studies using laser micro-irradiation to induce DNA lesions is reviewed in Ferrando-May *et al.* (2013).

The comparison of laser induced DNA damage with damage induced by X-rays or heavy-ion irradiation remains difficult. Nevertheless, Splinter and coworkers (2010) tried to compare the different types of treatment with respect to biological endpoints, e.g. DNA damage based on the foci numbers of irradiation induced repair protein recruitment. In these experiments the local dose equivalent in an irradiated mammalian nucleus was estimated to be 2 to 3 Gy by using a 337 nm pulsed nitrogen laser with a radiant exposure of 0.3 MJ/m^3 and sensitization of the DNA with BrdU incooperation (Splinter *et al.*, 2010). The results strongly depend on the used wavelength and laser energy. Still the data were overall in agreement with previously reported results concerning different biological endpoints. The estimated locally applied laser equivalent dose in the nuclear sub-volumes was in the range of several hundreds of Gy (Splinter *et al.*, 2010). Since DNA bases absorb only in the far UV (Voet *et al.*, 1963), it is speculated that solvated electrons and radicals are formed by photo-ionization events when a small volume is irradiated with a high photon density produced by a laser pulse (Ferrando-May *et al.*, 2013).

2.5. Reactive oxygen species

The initial events of ionizing radiation (excitation and ionization) are completed within 10^{-15} seconds, followed by a chemical thermal equilibrium of the produced species. The latter lasts ca. 10^{-12} seconds (Pouget & Mather, 2001); the timeline of these intermediate steps is shown in Fig. 5. The few hundred ROS molecules, which are generated in response to radiation by water radiolysis, are only a minor fraction compared to the large background of about 10^9 ROS/cell/day, which are generated in oxygen metabolism (Feinendegen & Toxicol, 2002). The variety of different radical species, which emerge from water radiolysis in cell free systems, was intensively measured and simulated in the past (Le Caër, 2011; Meesungnoen & Jay-Gerin, 2009; Roth & LaVerne, 2011; Wang *et al.*, 2010). The H_2O_2 yield for example was measured as a function of the radical scavenger concentration in aqueous solutions after high-energy heavy-ions irradiation. They demonstrated that the yields of H_2O_2 increased with LET (Wasselin-Trupin *et al.*, 2002).

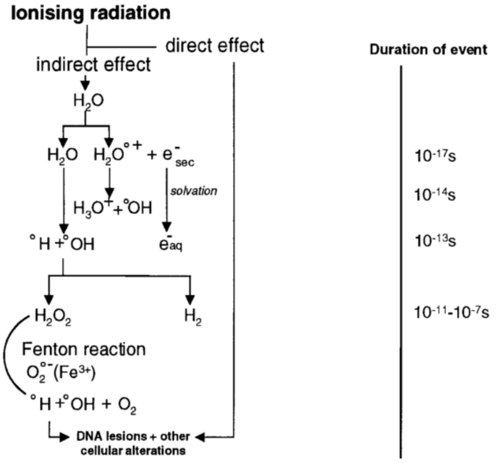

Fig. 5 **Timeline of the early effects of ionizing radiation.** The physical radiolysis of water occurs within the first femto seconds, followed by the chemical stage, where the generated reactive oxygen species further react with each other and are recombined. The longer living radicals formed by radical recombination like H_2O_2 can be transferred via the Fenton reaction into more reactive radicals, which can damage DNA and other cellular compartments in the order of nano seconds. (Pouget & Mather, 2001)

The aforementioned analyses have shown that radiolysis of water leads to a broad range of short living reactive oxygen species such as hydrated electrons (e^-_{aq}), hydroxyl radicals ($\cdot OH$), superoxide radicals ($O_2\cdot^-$) and hydrogen peroxide (H_2O_2). Hydrogen peroxide occupies a special role among them. Since H_2O_2 is not a radical, it is more stable and is able to diffuse until reacting with other molecules. In Monte-Carlo simulations the spatial distribution of different ROS after an ion traversal was simulated. Two exemplary results are depicted in Fig. 6. The H_2O_2 molecules were more persistent as e^-_{aq}.

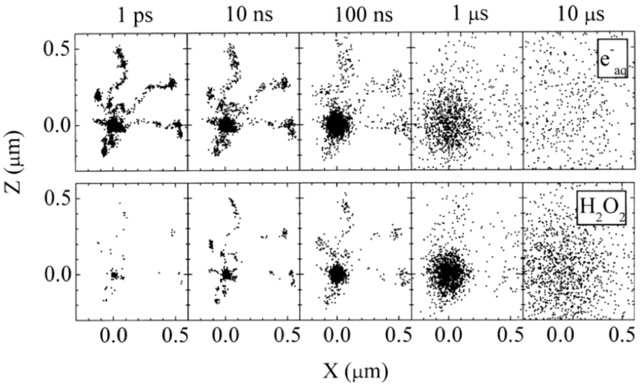

Fig. 6 **Simulation of the distribution of ROS after an ion traversal.**

Monte-Carlo simulation of the spatial distribution of the e^-_{aq} and H_2O_2 in liquid water after exposure to 24 meV $_4He^{2+}$ ions (LET approximately 26 keV/µm). The ion track is displayed in y-axis. In the early stage the distribution of e^-_{aq} is more dense than those of H_2O_2, but less persistent. (Muroya *et al.*, 2006)

Moreover, H_2O_2 is described to be a signaling molecule (Forman *et al.*, 2010; Rhee *et al.*, 2005; Stone & Yang, 2006) and a regulator of signal transduction cascades (Marinho *et al.*, 2014; Rojkind *et al.*, 2002; Stone & Yang, 2006; Veal *et al.*, 2007). Cytosolic concentrations in mammalian cells can reach from 1 nM up to the sub micromolar range for signaling purpose (Boveris & Cadenas, 2000; Freinbichler *et al.*, 2011). H_2O_2 has a dual role in the context as a second messenger. Whereas high intracellular concentrations (1-3 µM) are cell toxic and can therefore induce apoptosis (Antunes *et al.*, 2001; Nakagawa *et al.*, 2004) and at higher concentrations necrosis (Boveris & Cadenas, 2000; Valko *et al.*, 2006), it was shown in several studies that low concentrations of H_2O_2 enhance cell proliferation (Burdon *et al.*, 1989; Burdon & Rice-Evans, 1989; Liu *et al.*, 2002).

It was recently indicated that the diffusion of H_2O_2 through the cytoplasm is strongly limited. Consequently, it was demonstrated that H_2O_2 acts mostly locally in cells (Mishina *et al.*, 2011). The nonpolar H_2O_2 molecules are able to diffuse across biological membranes, moreover it was shown that H_2O_2 can enter cells from the exogenous medium via aquaporins (Bienert & Chaumont, 2014; Bienert *et al.*, 2007, 2006). But in spite of the good permeation through membranes it was depicted that endogenous produced H_2O_2 is more efficient to initiate cellular signal cascades than H_2O_2 from external source (Choi 2005). A concentration gradient across the membrane with a factor of about 10 was reported in older studies (Boveris & Cadenas, 2000), whereas recent studies with novel protein-based fluorescent reporters suggest that the concentration in the cytosol is 200-500 times lower than the external concentration; hence the membrane still is a significant diffusion barrier for H_2O_2 (Bilan *et al.*, 2013; Malinouski *et al.*, 2011).

Coming back to the relation between radicals and ionizing irradiation it must be mentioned that about 2000 ionizations per Gy per cell are produced by ionizing radiation (Mikkelsen & Wardman, 2003). It was estimated that only 1/3 of DNA damage from ionizing radiation is a direct result of an impact on the DNA (Azzam *et al.*, 2012). An important question in this context is how the few primary ionization events, which are generated by clinical relevant doses are amplified to activate signal cascades inside the cell. At this point it is worth recalling that the primary ionization events in the cytoplasm of a cell are insignificant compared to the amount of endogenous ROS, which are generated by cell metabolism. Little is known about how ionization of the cytoplasm effect cells and how these ionizations influence nuclear processes. One publication indicates that ROS are amplified via plasma membrane bound NADPH-oxidase after low dose irradiation with α-particles in a time window of 15-60 minutes after irradiation (Narayanan *et al.*, 1997).

It has been shown that biological reactions are not only depending on the primary ROS, which are generated as a direct result of IR. It was reported that after the initial formation of primary ROS secondary ROS molecules are generated in a time dependent manner several hours after irradiation in A549 cells (Ogura *et al.*, 2009). The source of this secondary produced ROS are mitochondria where ROS are amplified in a calcium dependent manner (Leach *et al.*, 2001; Ogura *et al.*, 2009; Valerie *et al.*, 2007). Changes in the calcium concentration lead to an increase in the mitochondrial membrane potential and an increased respiration, whereby ROS are generated per se by oxygen metabolism (Yamamori *et al.*, 2012).

The secondary generated ROS and especially long living species are also made responsible for a phenomena termed "bystander effects" (Azzam *et al.*, 2003). The latter describes a system in which a primary cell damage, e.g. DNA damage, is not confined to the cell which was directly hit by radiation. The primary stressed cell sends out signals to adjacent cell (Rzeszowska-Wolny *et al.*, 2009; Shao *et al.*, 2003) into the medium or via gap-junctions (Azzam *et al.*, 2003; Suzuki & Tsuruoka, 2004). These adjacent cells elicit the typical reactions, which are observed in the primary wounded cells.

2.6. Redox-buffering in cells

Cells have mechanisms to cope with redox stress. On the one hand enzymes like superoxide dismutase (SOD), or catalase are able to eliminate superoxide and hydrogen peroxide respectively (Slupphaug, 2003). On the other hand there is a large number of other factors like vitamins or thioles, which prevent the cell from further damage.

The thioredoxin system and the glutathione system are the two major thiol-dependend mechanisms, which maintain the cellular redox-state. Thioredoxins are small proteins with oxidoreductase activity. The catalytic reduction of substrates involves the formation of a disulfide bond that is subsequently reduced by NADPH (Veal *et al.*, 2007). Glutathione (L-γ-glutamyl-L-cysteinyl-glycine, GSH) on the other hand is kind of a tripeptide and is present in milimolar concentrations in the cell and therefore the most abundant thiol (Anderson, 1998; Circu & Aw, 2008; Dooley *et al.*, 2004; Rojkind *et al.*, 2002; Valko *et al.*, 2006). To preserve reductive conditions in the cytoplasm and the nucleus, the pool of both thioredoxins and glutathione is constantly reduced by specific enzymes. A recent study has shown that thioredoxin and glutathione are both acting as redox-buffers. Still both buffer systems have very distinct functions; they are not in a redox equilibrium and presumably act in different signaling cascades (Hansen *et al.*, 2006).

Here I would like to concentrate on the glutathione system. Glutathione has many cellular functions: On one hand it acts as an antioxidant via direct interaction with ROS, on the other hand it is the detoxification machinery of enzymes like glutathione peroxidases and glutathione-s-transferases (Filomeni *et al.*, 2002; Meyer & Hell, 2005; Morris *et al.*, 2014; Sies, 1999). Glutathione plays the principal role in the redox protection and cellular defense against H_2O_2, whereas catalase presumably contributes only minimal until GSH is depleted (Seo *et al.*, 2004). To maintain the intracellular redox environment glutathione is present in a larger variety in its reduced and biological active form (GSH). Under physiological conditions the reduced form GSH is 10-100-fold more abundant than the oxidized form (GSSG) (Filomeni *et al.*, 2002). It is still a matter of discussion weather there are different concentrations of GSH in the nucleus and in the cytoplasm. For A549 cells it was already shown that the nuclear and the cytoplasmic GSH pools are not in equilibrium (Cotgreave, 2003). Overall, it appears as if the nucleus is relatively more reducing than the cytoplasm (Hansen *et al.*, 2006).

The role of glutathione in the nucleus has been described recently, particularly in respect of high GSH levels in proliferating cells, like cancer cells (García-giménez *et al.*, 2013; Markovic *et al.*, 2007, 2010; Pallardó *et al.*, 2009; Schroeder *et al.*, 2007).

The cellular glutathione redox-state has been causally linked to several different targets like the anti-apoptotic protein BCL-2 (Voehringer, 1999), the central regulator of immunity, inflammation and cell survival transcription factor NF-κB (Bubici *et al.*, 2006; Filomeni *et al.*, 2002; Schreck *et al.*, 1992) and the transcription factor activator-protein-1 (AP-1) (Filomeni *et al.*, 2002). Also, the oxidation of cAMP-dependent protein kinase (PKA) (reviewed in Poole and Nelson, 2009) and the regulation of MAPK cascades, that are a major signal-pathway mediating tumor metastasis (Wu, 2006), are related to the glutathione redox-state.

2.7. Motivation

Here I want to uncover the general signal cascade, which connects primary events of IR and the activation of the human intermediate-conductance calcium-activated K^+-channel (hIK). First experimental data pointed out that calcium and ROS are involved in this radiation induced signal cascade. In the following experiments I want to detail the dynamics and spatial distribution of these two signaling molecules after IR stress, by using new generation of genetically encoded fluorescence reporters. This reporter enable the real-time detection of signal molecules like Ca^{2+} and ROS, as well there buffering, with a high temporal and spatial resolution. Furthermore, I want to link these cellular signals directly to the activation of the hIK channel and illustrate their impact to the electrophysiological properties of the cells.

3. Matherial and methodes

3.1. Chemicals

All chemicals were purchased from Biochrom AG (Berlin, Germany), Sigma-Aldrich GmbH (Taufkirchen, Germany), AppliChem GmbH (Darmstadt, Germany), Invitrogen (Karlsruhe, Germany), Merck (Darmstadt, Germany, Bio-Rad Laboratories GmbH (Muinch, Germany), Qiagen (Hilden, Germany) or Invitrogen (Karlsruhe, Germany) if not specified further.

Clotrimazole and Ionomycin were dissolved in DMSO and applied to the bath solution (chapter 3.4) or phosphate buffered saline (PBS; Sigma-Aldrich GmbH, Taufkirchen, Germany) in the concentrations mentioned in results. The final concentration of DMSO was less than 0.05 % (*v*/*v*).

Hydrogen peroxide (H_2O_2) solutions were always freshly prepared by serial dilution of H_2O_2 (30 %, Sigma-Aldrich GmbH, Taufkirchen, Germany) in the experimental solution or PBS buffer. The H_2O_2 concentration was occasionally measured at 240 nm, in order to control the stock solution and the dilution process.

3.2. Plasmids

The plasmids used in this work were kindly provided by:

- pHyPer-cyto (Evrogen): Ph.D. Alex Costa (Universitiy of Milan, Milan, Italy) (Belousov *et al.*, 2006; Mishina *et al.*, 2013)
- pSypHer-cyto (Evrogen): Ph.D. Vsevolod Belousov (Institute of Bioorganic Chemistry, Moscow, Russia) (Poburko *et al.*, 2011)
- YC3.60/pcDNA3: MD, Ph.D. Atsushi Miyawaki (RIKEN Brain Science Institute, Wako City, Japan) (Nagai *et al.*, 2001)
- pLPCX-Grx1-roGFP2: Prof. Dr. Andreas Meyer (University of Bonn, Germany) (Gutscher *et al.*, 2008)
- pEGFP-hK_{Ca}3.1: Ph.D. Heike Wulff (University of California, Davis, USA)

3.2.1. Plasmid amplification

Escherichia coli (*E. coli*) DH5α were prepared for transformation according the rubidiumchloride-method from Hanahan (1983) and stored at -80 °C. Frozen chemical competent DH5α were transformed with a 30 sec heat shock and plated after 1 h at 37 °C and 220 rpm in SOC media (20 % (*w*/*v*) trypton, 5 % (*w*/*v*) yeast extract, 10 mM NaCl, 2.5 mM KCl, 20 mM $MgCl_2$, 20 mM glucose, NaOH / pH 7.0) on LB-Agar plates (1.5 % (*w*/*v*) agar, 10 % (*w*/*v*) trypton, 10 % (*w*/*v*) NaCl, 5 % (*w*/*v*) yeast extract, NaOH / pH 7.5) containing kanamycin (50 µg/mL) or ampicillin (100 µg/mL) as selection marker. Single cones were picked and grown in LB-media (10 % (*w*/*v*) trypton, 10 % (*w*/*v*) NaCl, 5 % (*w*/*v*) yeast extract, NaOH / pH 7.5) containing ampicillin or kanamycin as selection markers at 37 °C over night. Plasmid DNA was extracted using the ZR Plasmid Miniprep™ Kit (Zymo-Research, Orange, Kalifornien, USA) or GenElute™ HP Plasmid Midiprep Kit (Sigma-Aldrich, Taufkirchen) according the manufactures protocol and the DNA concentration, as well as purity were estimated using NanoDrop® ND-1000 (UV-Vis Spectrophotometer; Thermo Fisher Scientific Inc., Waltham, MA, USA).

3.3. Cell culture

All experiments in this thesis were performed with HEK293 (human embryonic kidney 293) cells (Graham *et al.*, 1977; Jiang *et al.*, 2002) and A549 (adenocarcinomic human alveolar basal epithelial) cells (Giard *et al.*, 1973). Both cell lines were purchased from the Leibniz-Institut DSMZ (Deutsche Sammlung von Mikroorganismen und Zellkulturen GmbH) and maintained free of mycoplasmas as determined by a test from Minerva Biolabs, (Berlin, Germany).

Both adherent cell cultures were propagated in Dulbecco's Modified Eagle Medium (DMEM/ Ham's F-12, Biochrom AG, Berlin, Germany) media with stable glutamine supplied with 10 % (*v/v*) FCS (Sigma-Aldrich GmbH, Taufkirchen, Germany) and 1 % (*v/v*) penicilline/streptomycine (Sigma-Aldrich GmbH, Taufkirchen, Germany) respectively. Media for A549 cells was complemented with 1 % (*v/v*) NEAA (non-essential amino acids; Biochrom AG, Berlin, Germany) additionally. Both cell cultures were passaged twice a week using phosphate buffered saline (PBS; Sigma-Aldrich GmbH, Taufkirchen, Germany) for washing and 1 % (*v/v*) trypsin/EDTA solution (Sigma-Aldrich GmbH, Taufkirchen, Germany) or accutase (PAA, GE health care, Freiburg, Germany) for enzymatic detachment of the cells. The enzymatic activity of trypsin was stopped using cultivation media and the cells were transferred into new cell 25 cm^2 cell culture flasks. The cells were cultivated under standard conditions at 37 °C and 5 % CO_2.

Stock cultures were cryoconserved in FCS containing 10 % (*v/v*) DMSO and stored in liquid nitrogen. First experiments were done after the 5th passage after thawing.

3.3.1. Cell culture for microscopy

For microscopy cells were seeded on 25 mm round glass coverslips (No. 1.0). The coverslips were sterile flamed using pure ethanol. The cells were incubated at 37 °C with 5 % CO_2 until the cells reached a confluence of about 60 %. They were transiently transfected with TurboFect (Thermo Fisher Scientific Inc., Waltham, MA, USA), GeneJuice (Novagen, Merck KGaA, Darmstadt, Germany) or Lipofectamine (Life Technologies GmbH, Darmstadt, Germany) according the manufactures protocol.

For experiments at the X-ray microscopy setup the cells were seeded on 40 mm round glass coverslips (No. 1.5) and for heavy-ion experiments either on polycarbonate foil (18 mm diameter; 40 µm thickness) or 18 mm round glass coverslips (No. 0.0).

3.3.2. Cell culture for electrophysiological recordings

Since HEK293 cells obtain only few voltage-activated endogenous currents, which are well characterized (Jiang *et al.*, 2002), they were widely used as heterologous expression system for ion-channels in context of electrophysiological recordings. HEK293 cells were grown in 25 cm^2 cell culture flasks for one day and transfected with the plasmid pEGFP-hK_{Ca}3.1 and the transfection reagent Turbofect (Thermo Fisher Scientific Inc., Waltham, MA, USA) according manufactures protocol and measured one day after transfection. A549 cells were measured after two or three days of growth in 25 cm^2 cell culture flasks and incubation under the above mentioned standard conditions.

3.4. Patch clamp recordings

Patch clamp recordings were performed using a portable patch-clamp device (port-a-patch, Nanion, Munich, Germany), the EPC-9 amplifier (HEKA Electronics, Lambrecht, Germany) and PatchMaster software (HEKA, Lambrecht, Germany).

Confluent cells were measured two to three days after seeding. They were harvested according to the standard protocol (Brüggemann *et al.*, 2003; Fertig *et al.*, 2002). Cells were placed on 3-5 MΩ NPC-1® Chips (Nanion, Munich, Germany) and were measured in the whole-cell configuration. The sealing process was performed in solution containing 80 mM NaCl, 3 mM KCl, 10 mM $MgCl_2$, 35 mM $CaCl_2$, 10 mM HEPES/NaOH, pH 7.4. For normal recordings a buffer with 4 mM KCl, 140 mM NaCl, 1 mM $MgCl_2$, 2 mM $CaCl_2$, 5 mM Sorbitol, 10 mM HEPES /NaOH, pH 7.4 was used as an external bath solution. The intracellular solution contained 50 mM KCl, 10 mM NaCl, 60 mM K-Fluoride, 1 mM EGTA and 10 HEPES/KOH, pH 7.2. Some experiments were performed with an intracellular solution containing predefined free Ca^{2+} concentrations varying between 2 nM and 1 µM. The specific concentrations were calculated according to the formula available at "http://maxchelator.stanford.edu/CaMgATPEGTA-TS.htm" (Schoenmakers *et al.*, 1992), in order to obtain the desired amount of free Ca^{2+}.

The currents were measured at room temperature and provoked with a standard pulse protocol. The holding voltage was -20 mV for 200 ms followed by 800 ms long test pulses between -100 and +80 mV and finally a 200 ms pulse at -80 mV (Fig. 7 A). Additionally a voltage ramp protocol was performed with a pre and post holding voltage of -80 mV and a continuous ramp of 800 ms from -100 to + 100 mV, followed by a final 800 ms test pulse of +20 mV (Fig. 7 B).

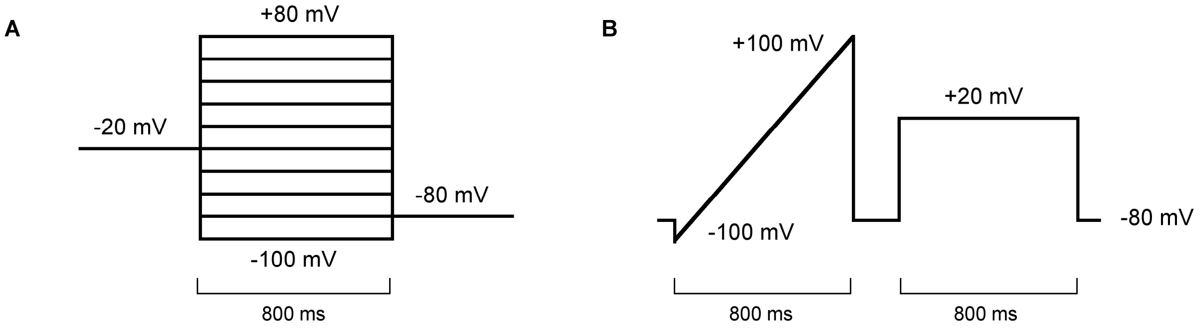

Fig. 7 **Pulse protocols used in this thesis to elicit currents in HEK293 and A549 cells.**

A standard pulse protocol with a holding voltage of -20 mV for 200 ms followed by 800 ms test pulses between -100 and + 80 mV in 20 mV steps, with a subsequent holding voltage of -80 mV (A). A ramp protocol from -100 to +100 mV over 800 ms followed by a +20 mV voltage step (B).

Data were analyzed using the Patchmaster, Fitmaster software (HEKA, Lambrecht, Germany) and Microsoft Excel. Instantaneous currents were received in the first 5% of the test voltage and the steady-state currents were sampled at the end (last 5%) of the test pulse. In order to normalize the currents to the cell size they were normalized (if mentioned) to the cellular capacitance. Graphing was performed using IGOR Pro software (WaveMetrics, Lake Oswego, OR).

3.5. Fluorescence microscopy

Single-cell imaging was performed at room temperature at a Leica confocal system TCS SP5 II with the software LAS AF Version 2.60 (Leica Microsystems CMS GmbH, Heidelberg). Images were acquired and UV-laser micro-irradiation was performed with a 40x (1,3 NA) oil- immersion objective.
A549 cells and HEK293 cells were grown on cover slips as described in (3.3.1). All measurements were made in PBS (Sigma-Aldrich GmbH, Taufkirchen, Germany), if not mentioned otherwise.

HyPer, SypHer and Grx1-roGFP2 were sequentially excited with a 405 nm diode and with an argon laser at 488 nm. Images (512 × 512 pixels in size) were acquired with a HyD detector at 500-550 nm. For HyPer and SypHer the background subtracted (selected ROIs at cell-free positions) ratio 488 nm / 405 nm is plotted for all experiments. For Grx1-roGFP2 the ratio was calculated by division of the background subtracted fluorescence intensity 405 nm / 488 nm.
The FRET based calcium sensor YC3.60 was excited at 458 nm with an argon laser. The emission of both CFP (465-500 nm) and YFP (520-570 nm) respectively was detected with a HyD detector simultaneously. The signals were plotted as the ratio of both emission intensities YFP / CFP and corrected for background fluorescence signals. For calcium imaging 5-6 positions were acquired per experiment without further zooming.

For laser micro-irradiation (m.i.) a continuous wave 405 nm diode laser was focused via a 40x (1,3 NA) oil-immersion objective. The power oft the laser beam was about 450 µW at the sample plane, which was measured by a UV dosimeter (Powermeter PM100D with S130C sensor; Thorlabs, Newton, New Jersey, USA). The laser beam was repeatedly scanned in the region of interest (ROI) with a pixel dwell time of 2.54 µsec. The resulting deposed laser energy in the ROI was obtained by varying the spot size of the ROI as well as the irradiation time. Predefined ROIs either in the cytoplasm or in the nucleus were exposed to 0.5 - 4.5 mJ/µm^2 of 405 nm UV-laser.

Image analysis was performed with the open source software FIJI (http://fiji.sc). The ratiometric images shown in the results have been created using FIJI and the look-up-table S-Pet after setting a threshold to avoid ratio-created artifacts. Data analysis was performed using FIJI and Microsoft Excel. Illustrations were accomplished using IGOR Pro software (WaveMetrics, Lake Oswego, OR).

3.6. Cell irradiation

Electrophysiological live-measurements in the X-ray tube (Isovolt160 Titan E, GE Sensing & Technologies, Ahrensburg, Germany) were performed as described in Roth (2013). The cells were irradiated with a voltage of 90 kV and 19 mA filtered by a 2 mm aluminum sheet. The dose rate was controlled by a dosimeter (DIADOS T11003 Diagnostikdosimeter) and the dose of 1 Gy was achieved by varying the distance and the duration of irradiation.

Live microscopic experiments were performed at the X-ray microscopy setup (GSI Helmholtzzentrum für Schwerionenforschung, Darmstadt, Germany). Imaging was performed with an Olympus IX71 using a 60x Optovar and the Andor oQ 1.10.5 software. The setup is equipped with an X-ray tube (Isovolt, GE Sensing & Technologies, Ahrensburg, Germany), operated at 35 kV and 80 mA (dose rate 32 Gy/min ± 10 %) or 35 kV and 20 mA (dose rate 8.6 Gy/min ± 10 %), filtered with a 0.5 mm aluminum sheet. The applied dose was controlled with a PTW D14 dosimeter (PTW, Freiburg, Germany).

Charged particle irradiation at the beamline-microscope (Jakob *et al.*, 2005) was performed at the Universal-Linear-Accelerator (UNILAC) facility (GSI Helmholtzzentrum für Schwerionenforschung, Darmstadt, Germany) using carbon-ions (C; 11.4 MeV/u, LET_{H2O} 170 keV/µm) or lead-ions (Pb; 4.7 MeV/u, LET_{H2O} 13500 keV/µm) and the same optical setup as for live X-ray experiments.

3.7. Matlab simulation

The simulation of H_2O_2 generation and buffering in chapter 6.1 was performed using Matlab (The MathWorks Inc., Natick, MA, USA) and the ordinary differential equation function solver (ODE45) (Anyigor & Afiukwa, 2013).

3.8. Statistical analysis

Data are expressed as means ± standard deviations of at least three different experiments (the number of experiments is indicated for each experiment). Significance was estimated by using the Student's t-test, either the paired Student's t-test if the same cell was measured before and after treatment or the unpaired t-test for population experiments. A value of $p < 0.05$ was considered as significant.

4. CHAPTER 1 - Activation of potassium-channels by ROS and calcium

In a preceding study it was shown that A549 cells, an epithelial adenocarcinoma cell line, exhibit an increased K^+ conductance and a consequent membrane hyperpolarization after irradiating cells with X-rays or high energy heavy-ion irradiation (Roth, 2013).

In this preceding work the hIK channel was identified with the help of channel blockers and by expression studies as the candidate channel, which is presumably activated by radiation (Roth, 2013). To further confirm the hypothesis that the hIK channel is a target for radiation this channel was here overexpressed in HEK293 cells, which display only a minor expression of this ion-channel under wildtype conditions (Roth, 2013). Furthermore it was tested if the same increase in K^+ conductance, which is observed in A549 cells by external applied H_2O_2 or internal perfusion with Ca^{2+} could be elicited in HEK293 expressing the hIK channel.

4.1. Activation of the hIK channel in A549 cells by ROS and calcium

The typical current response of an A549 cell could be divided into two kinetically different components, an instantaneous (I_{inst}) and a slow activating, time dependent (I_{td}) conductance (Fig. 8 C). Both conductances are carried by K^+ currents; this had been shown by measuring currents in buffers with different external K^+ concentrations and via canonical blockers of K^+-channels (Roth, 2013). These results were confirmed in the present study (data not shown).

The relative contribution of both current components to the total membrane conductance is very variable among different A549 cells. The general picture is that the overall conductance of cells with a negative reversal voltage, e.g. negative free running membrane potential, comprises a relative large instantaneous current component (Fig. 8); cells in which the slow activating conductance dominates show a more depolarized membrane voltage (Fig. 9).

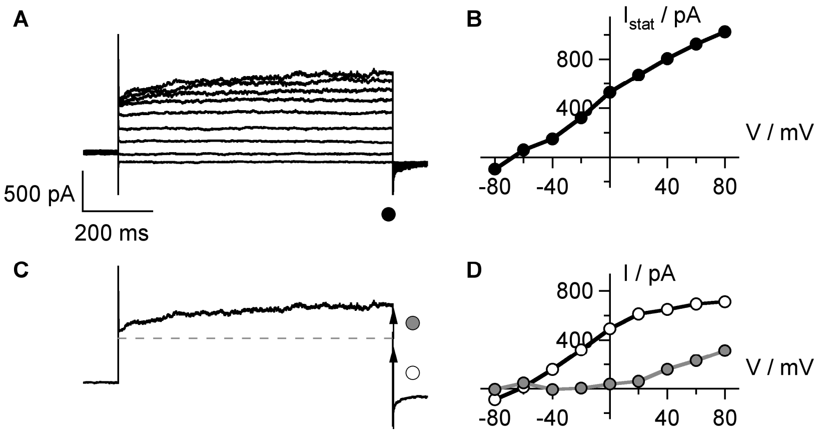

Fig. 8 **Representative current response of an A549 cell with a negative reversal potential.**

Current voltage relation of an exemplary A549 cell to a standard pulse protocol with test voltages between -80 and + 80 mV in 20 mV steps (A). The corresponding steady-state $I_{stat}V$ relation with a V_m of -60.2 mV is shown in B. The current can be decomposed into two kinetically different conductances; an instantaneous (I_{inst}) and a time dependent (I_{td}) current component (C). The contribution of each conductance to the steady-state current is shown in D.

It is well established that the free running membrane voltage (V_m) hyperpolarizes during the transition from G1 to S-phase (reviewed in Yang & Brackenbury; 2013). Since the A549 cells, which were used here, were not synchronized before electrophysiological measurements, it is possible that the differences in V_m presumably stem from cells in different stages of the cell cycle. In a large body of cells tested 74.6 % of the measured cells (n=59) had a depolarized V_m between +5 and -15 mV, whereas 25.4 % had a hyperpolarized V_m between -15 and -68 mV. A representative cell with a more depolarized V_m of -11.4 mV is illustrated in Fig. 9. The instantaneous current component I_{inst} is in general less prevalent in these cells compared to cells with a hyperpolarized V_m (Fig. 9 C).

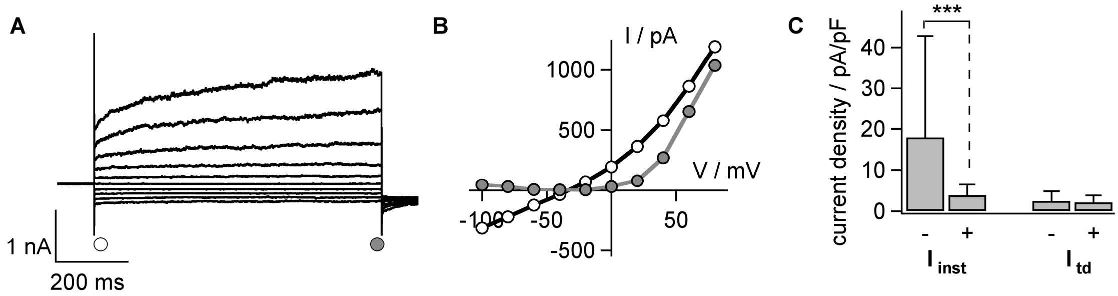

Fig. 9 **Representative current response of an A549 cell with a more depolarized membrane voltage.**

Current voltage relation of an exemplary A549 cell to a standard pulse protocol with test voltages between -100 and + 80 mV in 20 mV steps (A). The corresponding IV relation is shown in B. I_{inst} and I_{td} contributed nearly equal to the steady-state outward current of the cell. Cells with a hyperpolarized V_m (-68 to -15 mV; indicated with "-"; n=15) had a significant (*** $p < 0.001$) larger fraction of instantaneous current compared to cells with depolarized V_m (-15 to +5 mV; indicated with "+"; n=44) (C).

The ensemble of endogenous ion-channels in the epithelial lung cancer cells was already characterized in detail before (Roth, 2013). In this work the hIK channel was identified to be the most probable candidate for conducting the instantaneous current component. The influence of the hIK channel activator 1-Ebio and the inhibitors Clotrimazole and Tram-34 on I_{inst}, e.g. the hIK channel, was shown previously (Roth, 2013). The present data confirm previous results. The instantaneous conductance at +40 mV was blocked by 81 ± 33 % (3.3 ± 1.0 pA/pF) with Clotrimazole (Fig. 10), causing a depolarization by 18.6 ± 9.9 mV (n=3). Clotrimazole inhibits in the submicromolar concentrations used in this work exclusively the hIK channel (Pedarzani & Stocker, 2008; Wulff *et al.*, 2000, 2001).

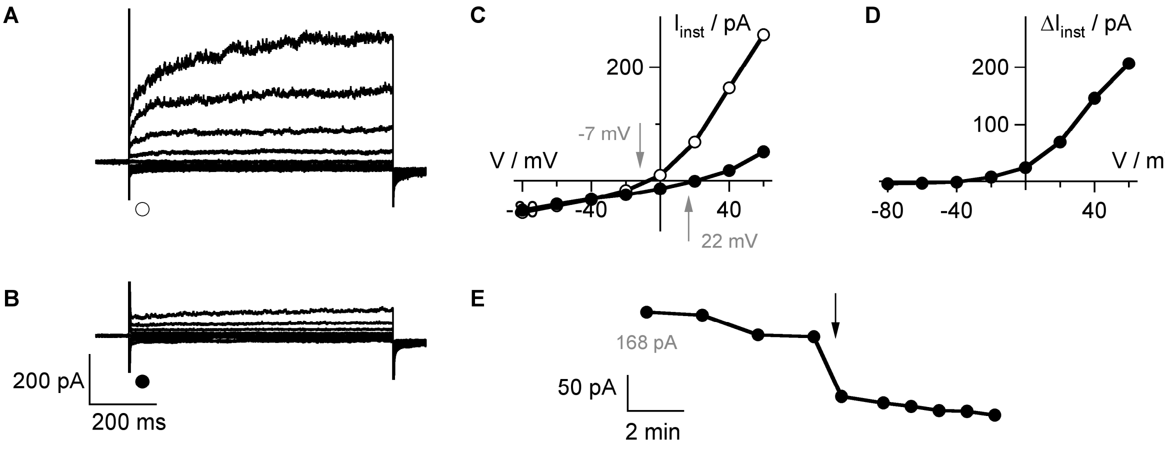

Fig. 10 **The instantaneous conductance is blocked with Clotrimazole.**

Current voltage relation of an exemplary A549 cell to a standard pulse protocol between -80 and +60 mV in 20 mV steps before (A) and after blocking with 300 nM CLT (B). The free running membrane voltage V_m depolarized by +29 mV as indicated with arrows in the $I_{inst}V$ relation in C. The inactivated current is displayed in D as a difference of the $I_{inst}V$ curves from C. The time course of CLT blocking of the instantaneous current at + 40 mV is illustrated in E; the time point of CLT addition is indicated with an arrow.

To analyze the calcium dependency of the instantaneous conductance in A549 cells, cells were either: 1) internally perfused with solutions of varying cytosolic calcium concentrations ($[Ca^{2+}]_{cyt}$) or 2) treated with the calcium ionophore Ionomycin in the bath solution.

After exchanging the internal solution from a solution with a cytosolic free Ca^{2+} concentration of 10 nM to one with 10 µM the instantaneous conductance increased. At a reference voltage of +20 mV the average increase in I_{inst} was on average 5.1 ± 3.2 pA/pF (n=9). As a consequence of the increase in I_{inst} the free running membrane voltage shifted on average by -8.1 ± 10.7 mV (n=9). The representative example in Fig. 11 A-C illustrates the Ca^{2+} induced increase of the instantaneous conductance, which is quasi linear in the voltage range between -80 and +20 mV and displayed a negative slope at high positive voltages (Fig. 11 C), which will be further delineated as typical hIK-like behavior. The fact that the $\Delta I_{inst}V$ relation has a reversal voltage close to the K^+ Nernst voltage confirms the K^+ nature of Ca^{2+} sensitive channel.

As a second approach A549 cells were treated with the calcium ionophore Ionomycin [1 µM] to obtain a rapid increase of $[Ca^{2+}]_{cyt}$ (Fig. 11 D-F). Upon addition of the ionophore the conductance increased at a reference voltage of +40 mV on average by 5.1 ± 1.5 pA/pF (n=7); concomitantly V_m shifted negative by -8.2 ± 6.7 mV (n=7). The results of these experiments and the fact that the activated conductance could be blocked with CLT support the fact that hIK channels indeed mediate the instantaneous conductance in A549 cells.

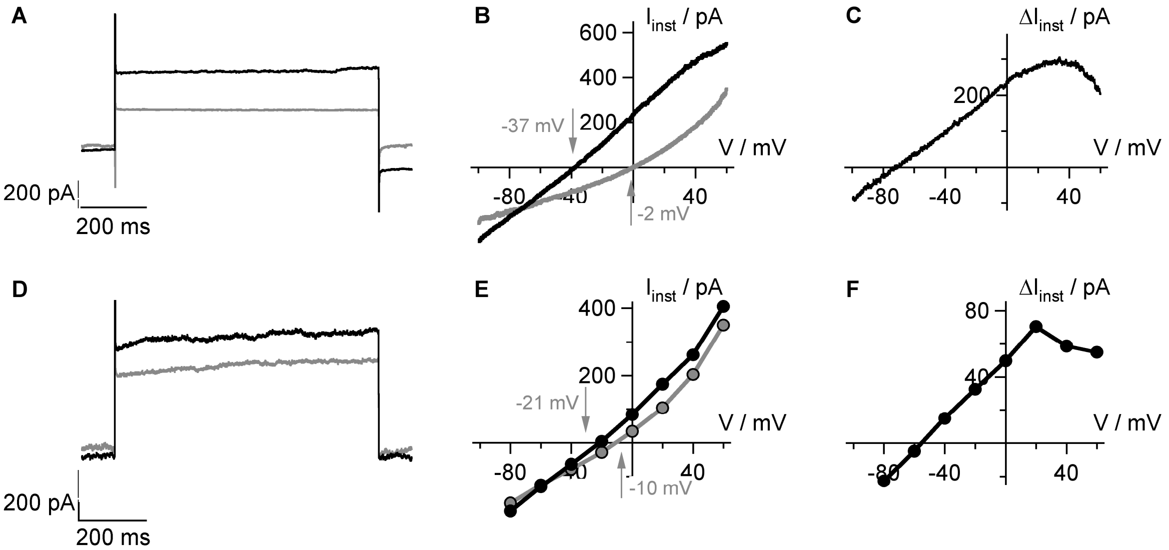

Fig. 11 **Calcium facilitates the activation of the instantaneous conductance in A549 cells.**

The instantaneous conductance increases quasi linear in the voltage range between -80 and +20 mV if $[Ca^{2+}]_{cyt}$ was raised either by a direct increase of the free calcium concentration or by treatment with the calcium ionophore Ionomycin. The representative current response to a +20 mV voltage step of an A549 cell with an internal free calcium concentration of 10 nM (grey) and after perfusion of the internal solution to 10 µM free calcium (black) is shown in A. The corresponding $I_{inst}V$ curve, obtained by a voltage ramp from -100 to +60 mV is shown in B. V_m shifts by -35 mV if $[Ca^{2+}]_{cyt}$ was elevated by the 1000-fold. The increase in conductance, as a difference of both curves from B is illustrated in C.

A similar increase to a +20 mV voltage step was generated if the cells were treated with the calcium ionophore Ionomycin [1µM] (D), where the grey curve represents the same cell before and the black curve after $[Ca^{2+}]_{cyt}$ was elevated. The cell was measured with a standard pulse protocol from -80 mV to +60 mV in 20 mV steps. The negative shift by -11 mV in V_m generated by activation of the instantaneous conductance is indicated with arrows in the corresponding $I_{inst}V$ curve (E). The $\Delta I_{inst}V$ curve in F was received by subtracting the $I_{insr}V$ curves from E. The cell in D-F was measured with an internal EGTA concentration of 1 mM.

It had been shown that ionizing radiation can activate potassium-channels in A549 cells (Kuo *et al.*, 1993). It was argued that most likely oxygen radicals (ROS) are a signal component in a signaling cascade, which connects the primary stress with channel activation. To test weather ROS are also able to activate hIK channels, the current voltage relations of A549 cells were recorded before and after addition of H_2O_2 to the external buffer.

Overall the response of A549 cells to H_2O_2 was very heterogeneous. From a total of 59 examined cells 35 % of these cells did not respond at all to H_2O_2 treatment. Most of the non-responding cells had a hyperpolarized free running membrane potential (Fig. 12 B) prior to H_2O_2 stimulation. In the remaining cells H_2O_2 stimulated an increase in membrane conductance. In the majority of these experiments the instantaneous current increased. Some other cells also showed an increase in the time dependent current (Fig. 12 A). Similar heterogeneous responses of the two conductances to ionizing irradiation were already observed in a previous work (Roth, 2013).

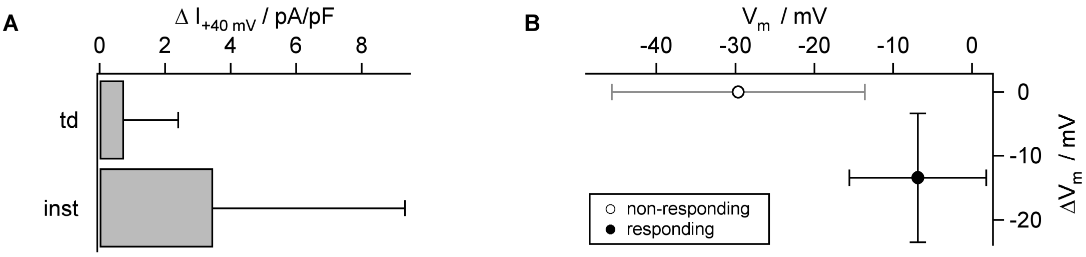

Fig. 12 **ROS mainly activate the instantaneous current component.**

Increase in current density at +40 mV in cells challenged with 0.3-3 µM H_2O_2. The currents were normalized to the membrane capacity in order to account for differences in cell size (A). The variability in the cellular response was large but on average the instantaneous current component increased more than the time dependent one. In a total of 59 cells tested only 65 % exhibited a response to all used concentrations (300 nm - 300 µM H_2O_2). Cells, which had a hyperpolarized membrane potential prior to H_2O_2 treatment, did on average show no response to the radical. Only cells with a depolarized voltage responded to H_2O_2 with a hyperpolarization (B).

Data from a representative A549 cell, which was responding to H_2O_2, is depicted in Fig. 13. They show that the cell exhibited a fast increase in conductance immediately after challenging the cell with 3 µM H_2O_2 (Fig. 13 F). In addition to the increase in instantaneous conductance (28 % at +40 mV), the free running membrane voltage shifted negative by -19.4 mV (Fig. 13 C). To extract information on the H_2O_2 activated conductance I calculated the difference $I_{inst}V$ relation by subtracting both $I_{inst}V$ relations in C. The respective data are plotted in Fig. 13 E. The $\Delta I_{inst}V$ relation illustrates the $I_{inst}V$ relation of the H_2O_2 induced current. Notably the $\Delta I_{inst}V$ relation displays the typical IV relation of hIK channels with a linear increase in conductance between -80 and +40 mV, a negative slope at positive voltages and a reversal voltage close to the K^+ equilibrium voltage (-86 mV).

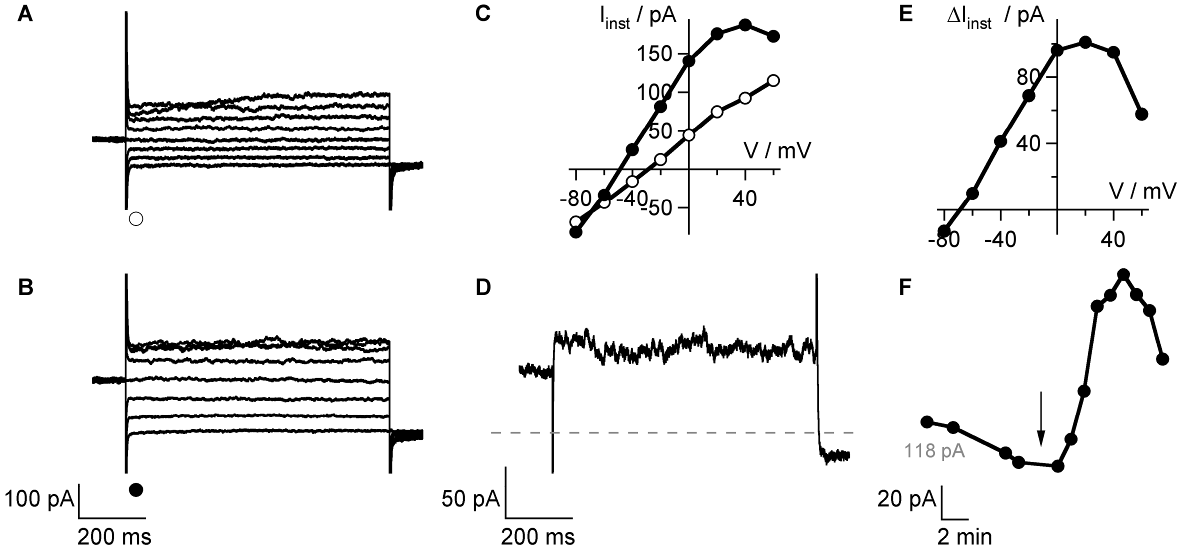

Fig. 13 **ROS mediated ion-channel activation in A549 cells.**

Current response of a representative A549 cell directly before (A) and 4 minutes after treatment with 3 µM external H_2O_2 (B). The $I_{inst}V$ relations of the data in A and B are shown in C. The V_m value shifted by -19.4 mV negative. The current difference analysis shows that mainly the instantaneous conductance is activated by H_2O_2. The difference current was obtained by subtracting the current response to +40 mV in presence of H_2O_2 from that in the absence (D). The $\Delta I_{inst}V$ relation in (E) displays the amount of activated conductance calculated by subtraction of the two $I_{inst}V$ curves in C. The time course of channel activation upon H_2O_2 treatment was very fast, with a maximal increase after 4 minutes (F).

In responding A549 cells the channel activity was enhanced even after challenging cells with low concentrations in the submicromolar range (Fig. 14 A); notably these concentrations are in the range of concentrations which can occur in the context of physiological situations in the cytosol of cells (Stone & Yang, 2006; Stone, 2004). The data indicate an unexpected negative correlation between the applied H_2O_2 concentrations and the effect on channel activation. Other than expected in typical does response relations the largest increase in current density was observed when challenging the cells with the lowest H_2O_2 concentrations. The opposite effect; e.g. an increase with higher H_2O_2 concentrations in the milimolar range, was shown by Roth (2013). The determined half maximal activation was shown to be 450 µM.

Nevertheless, the increase in conductance upon H_2O_2 treatment seems to depend strongly on the membrane voltage. The reaction to ROS was stronger in cells with a depolarized V_m (Fig. 14 B). This suggests that the amount of hIK channels, which could be activated by ROS is more critical than the concentration of ROS, e.g. H_2O_2. A negative V_m indicates that most of the expressed hIK channels were still active under the prevailing conditions (as shown in Fig. 9 C) and H_2O_2 had no further impact on the channel activity. Whereas cells with a more depolarized V_m (-15 to +5 mV) and a minor impact of the instantaneous conductance displayed an activation upon H_2O_2 treatment. This is in agreement with the observation that not all cells responded to H_2O_2 treatment (Fig. 12 B) as well as to ionizing radiation (Roth, 2013). The prevailing activity of hIK channels (correlating with a large impact of instantaneous current and a negative V_m) has therefore a major impact on the sensitivity of A549 cells to stimuli like ROS or ionizing radiation.

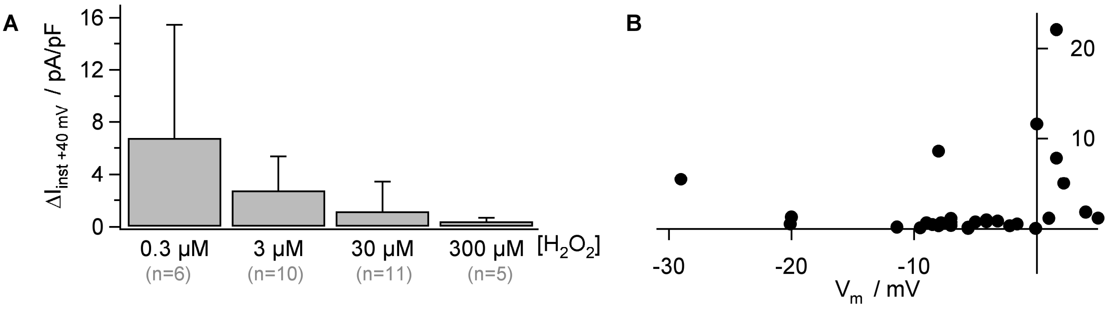

Fig. 14 **I_{inst} is activated with low physiological H_2O_2 concentrations and the activation is dependent on the membrane voltage.**

The increase in instantaneous current density to a voltage step of +40 mV of A549 cells challenged with different physiological concentrations of H_2O_2 indicates a negative correlation to the applied H_2O_2 concentration (A). The activation of instantaneous conductance, displayed as increase in current density to a voltage step of +40 mV was dependent on the membrane voltage (B).

To test if hIK channels contributed to the H_2O_2 stimulated conductance cells were treated after addition of H_2O_2 with the specific blocker Clotrimazole. The data in Fig. 15 show that this blocker was able to inhibit the H_2O_2 induced conductance. The difference curve in Fig. 15 C clearly reveals the typical hIK like $\Delta I_{inst}V$ relation, which is linear between -60 and +40 mV and decreases at positive voltages. The results of these experiments support the suggestion that hIK channels are activated by H_2O_2 treatment in the same manner as shown previously after ionizing radiation (Roth, 2013).

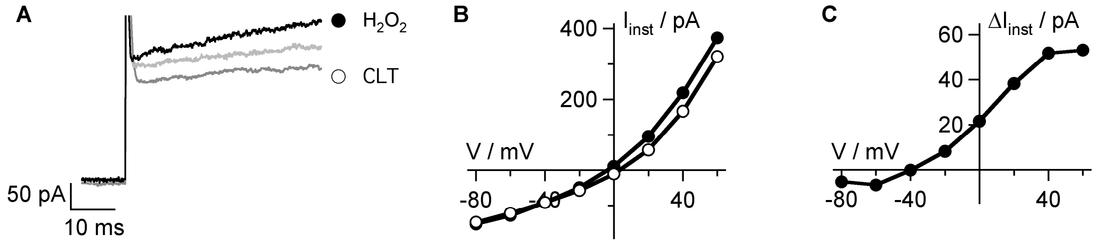

Fig. 15 **The inhibitor Clotrimazole blocks the H_2O_2 activated conductance in A549 cells.**

Current response of the same A549 cell to a pulse of +40 mV before (light grey), about 5 minutes after activation with 3 µM H_2O_2 (black) and after inhibition with 300 nM Clotrimazole (CLT; grey) (A). The corresponding I_{inst}V-curve of the H_2O_2 activated (filled symbols) and CLT inhibited (open symbols) current response are shown in B. The -3.2 mV negative shifted free running membrane voltage depolarized about +5.9 mV after CLT addition. The instantaneous current component was slightly elevated upon H_2O_2 treatment and reduced due to inhibition of hIK channels with CLT. The amount of blocked conductance upon CLT treatment is displayed in C calculated by subtracting both I_{inst}V curves from B.

4.2. Activation of heterologous expressed hIK channels in HEK293 cells by ROS, calcium and X-ray irradiation

To further examine the activation of the hIK channels, they were transiently overexpressed in HEK293 cells and analyzed by patch-clamp recordings. The currents of a representative control HEK293 cell and a HEK293 cell overexpressing hIK channels are illustrated in Fig. 16. HEK293 cells display only minor activity of endogenous ion-channels under the prevailing conditions (Fig. 16 A and B); these data are typical for the IV relations of wt HEK293 cells (Jiang *et al.*, 2002). Overexpression of the hIK channel generates a large instantaneous conductance, which is quasi linear over a voltage window from -80 to +40 mV (Fig. 16 D). Only at very positive voltages the conductance decreases. It has already been mentioned before that this behavior is typical for heterologous expressed hIK channels in HEK293 cells under the prevailing physiological conditions with high internal (110 mM) and low external (4 mM) potassium (Jensen *et al.*, 1998). The results of these experiments imply that the hIK channel is dominating the $I_{inst}V$ relation on HEK293 cells, which are overexpressing the hIK channel. The expression of this channel causes an increase in conductance at the resting membrane voltage with the result that V_m is in cells, which express the hIK channel negative shifted (compare Fig. 16 B and D).

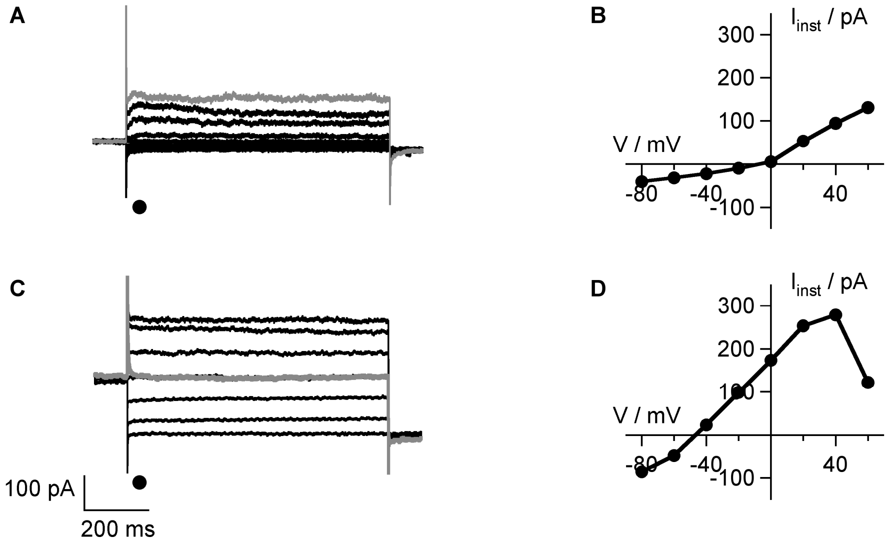

Fig. 16 **Representative current response of a HEK293 cell and a HEK293 cell overexpressing hIK channels.**

Current voltage relation of an exemplary HEK293 cell (A) and a HEK293 cell overexpressing the hIK channel (C) to a standard pulse protocol with test voltages between -80 and + 60 mV in 20 mV steps. The corresponding $I_{inst}V$ relations are shown in B and D respectively. The conductance at a voltage pulse of +60 mV is highlighted in grey. The endogenous currents of HEK293 cells are only minor and HEK293 cells are therefore a popular heterologous expression system for the characterization of ion-channels.

Both measurements were performed with an internal free calcium concentration of 10 nM.

In the next step I characterized the calcium dependency of the hIK channel in the heterologous expression system. The cytosolic concentration of Ca^{2+} ($[Ca^{2+}]_{cyt}$) was altered by an internal perfusion of the cytosol; the $I_{inst}V$ relations of the same HEK293 cell expressing hIK channels was recorded first with 10 nM $[Ca^{2+}]_{cyt}$ and then with 10 µM $[Ca^{2+}]_{cyt}$ (Fig. 17 A - C). The rise in $[Ca^{2+}]_{cyt}$ caused a strong (here 187 % at +20 mV) activation of hIK channels with the consequence that the membrane hyperpolarized by -45 mV. The same results were obtained in 3 similar measurements, causing a negative shift of V_m by -16.7 ± 16.4 mV (n=3) and an increase of the instantaneous current by 19.6 ± 15.7 pA/pF (n=3) at +40 mV.

In an alternative experiment $[Ca^{2+}]_{cyt}$ was increased by treating cells with the calcium ionophore Ionomycin [1 µM] (Fig. 17 D and E). The result of this experiment was similar to those reported from experiments in which $[Ca^{2+}]_{cyt}$ was directly increased by perfusion. The addition of the ionophore resulted in a strong increase in a conductance by 140 % at +20 mV, which was linear between -80 and + 40 mV and displayed a negative slope at high positive voltages.

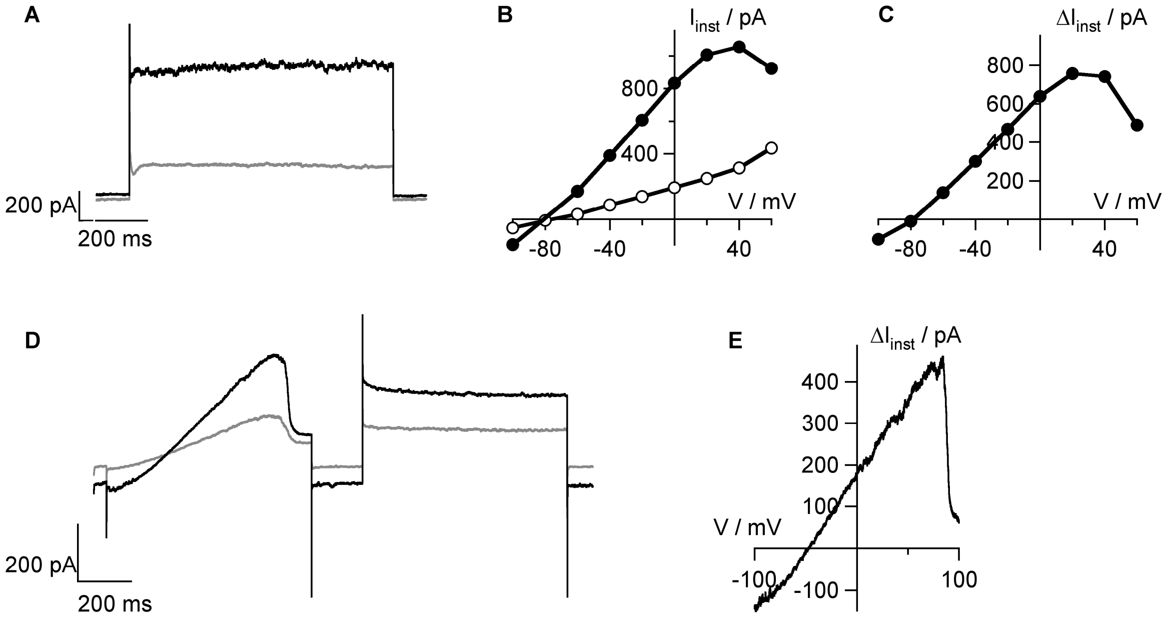

Fig. 17 **Elevation of $[Ca^{2+}]_{cyt}$ activates heterologous expressed hIK channels.**

HEK293 cells overexpressing the hIK channels were activated with an increase of $[Ca^{2+}]_{cyt}$ either by exchange of the internal solution (A) or by treatment with the calcium ionophore Ionomycin [1 µM] (D).

Changing the internal solution from a calcium concentration of 10 nM to 10 µM $[Ca^{2+}]_{cyt}$, activated overexpressed hIK channels. The current response to a +20 mV voltage step before (grey) and after (black) increasing of $[Ca^{2+}]_{cyt}$ is shown in A. The $I_{inst}V$ curves with 10 nM $[Ca^{2+}]_{cyt}$ (open symbols) and 10 µM $[Ca^{2+}]_{cyt}$ (filled symbols) are illustrated in B. The calcium-activated conductance is displayed in C as difference of the $I_{inst}V$ curves from B and reveals the typical linear increase in conductance between -80 and +40 mV, with a negative slope at high positive voltages.

A similar activation of hIK channels could be observed after treating HEK293 cells overexpressing hIK channels with the calcium ionophore Ionomycin [1µM]. The current response to a voltage ramp from -100 to +100 mV with a subsequent voltage step to +20 mV before (grey) and after treatment with 1 µM Ionomycin (black) is shown in D. The increase in conductance as difference of the measured voltage ramps before and after rise of the cytosolic calcium concentration is illustrated in E. The cell in D and E was measured with an internal free calcium concentration of 1 µM.

The hIK channel mediated conductance in HEK293 cells could be blocked with the inhibitor Clotrimazole (CLT) (Fig. 18). Challenging cells with 10 µM CLT caused a reduction of the conductance by about 76 % at +20 mV; as a result of the reduced conductance the cell depolarized by about +12 mV.

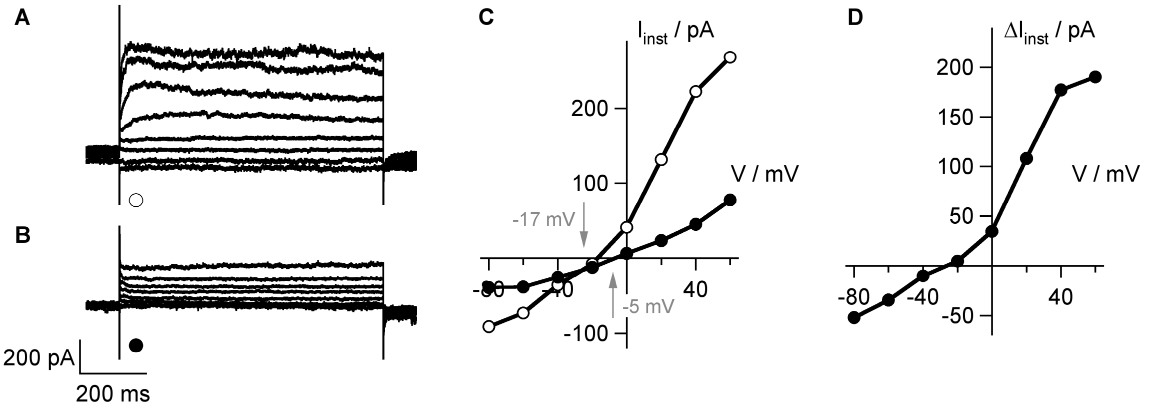

Fig. 18 **Clotrimazole blocks heterologous expressed hIK channels.**

Current traces of a HEK293 cells overexpressing the hIK channels to a voltage pulse protocol from -80 to +60 mV in 20 mV steps before (A) and after blockage with 10 µM Clotrimazole (CLT) (B). The corresponding $I_{inst}V$ relation is shown in C. The free running membrane voltage depolarized by +12 mV, as indicated with arrows. The blocked current is shown in D. The $\Delta I_{inst}V$ relation was obtained by subtraction of the $I_{inst}V$ relations from C. The cell was measured with an internal free calcium concentration of 100 nM.

In further experiments I attempted to elucidate the signal cascade by which reactive oxygen species and Ca^{2+} affect hIK activity. Treating HEK293 cells, which overexpress the hIK channel, with 300 µM H_2O_2 resulted in an increased K^+ conductance in the voltage range between -20 and +40 mV (Fig. 19 B). The mean increase in instantaneous current at a voltage pulse of +20 mV, which was evoked by 300 µM H_2O_2 was 5.7 ± 3.6 pA/pF (n=3); this increase in conductance caused a negative shift of V_m by -11 mV ± 2 mV (n=3). The conductance, which was stimulated by H_2O_2 could be inhibited by caesium. This is not a direct prove for a participation of hIK channels in the increase in conductance because Cs^+ is a general blocker of potassium-channels (Fig. 19 C). Still the results of these experiments support the view that H_2O_2 causes an increase in K^+ conductance. The fact that the latter conductance is mainly carried by hIK channels is underscored by experiments, in which wildtype HEK293 cells were treated with H_2O_2; these cells, which do not exhibit hIK activity, also exhibited not sensitivity to H_2O_2 (Fig. 19 E). Collectively the results of these experiments suggest that hIK channels are indeed a primary target of ROS stress in cells.

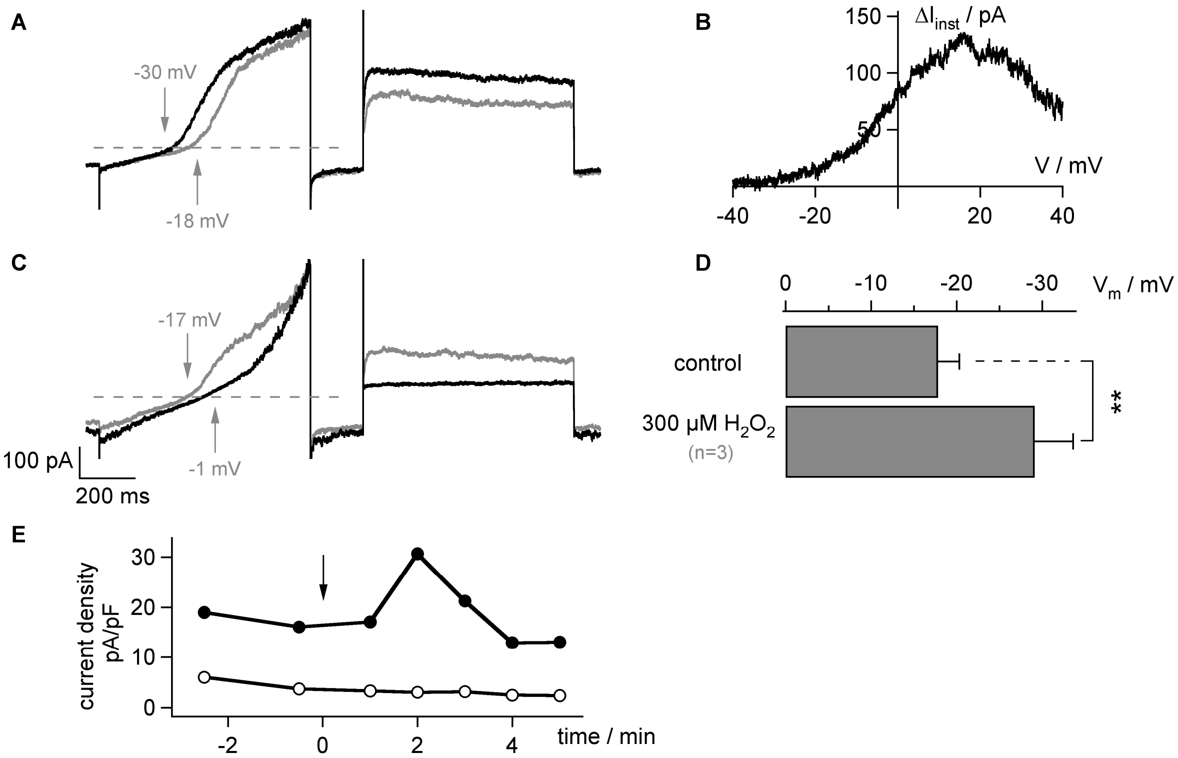

Fig. 19 **ROS mediated activation of overexpressed hIK channels.**

Representative current response of a HEK293 cell transiently overexpressing hIK channels before (grey) and after addition of 300 µM external H_2O_2 (A). The current response was recorded with a ramp protocol from -100 to +100 mV and a final voltage step to +20 mV. The free running membrane voltage hyperpolarized by -12 mV. The $\Delta I_{inst}V$-curve in B results from subtraction of the current recording directly before addition of H_2O_2 from the recording after external H_2O_2 was applied. The activated conductance was blocked with internal caesium (C), depolarizing the membrane by +16 mV (grey before and black after exchange of the internal solution). The shift in V_m upon challenging HEK293 cells overexpressing hIK channels with H_2O_2 by -11.3 ± 2.0 mV (n=3) was significant (** $p < 0.05$) (D). HEK293 wildtype cells (open symbols) showed no changes in current density, whereas the HEK293 cell which expresses hIK channels (filled symbols) elicited a maximal increase in current density 2 minutes after H_2O_2 was supplied to the external solution (E).

In the same line of arguments previous work suggested that the presence of hIK channels made cells sensitive to ionizing irradiation. After establishing now the current voltage relations of hIK channels in the heterologous expression system of HEK293 cells I examined the effect of X-ray irradiation on the conductance of these cells. Important to note is that previous experiments have shown that this treatment had no appreciable effect on the current voltage relations of wt HEK293 cells (Roth, 2013). The data in Fig. 20 show that irradiation of HEK293 cells, which overexpress the hIK channel indeed exhibited a radiation response. An increase in hIK channel activity, similar to that obtained after increasing $[Ca^{2+}]_{cyt}$ could be observed after irradiation with 1 Gy of X-ray irradiation. Fig. 20 A shows the current response of the same HEK293 cell, which expressed hIK channels, before and after irradiation. The difference $I_{inst}V$ relation, which shows the irradiation activated current, has the typical features of hIK channels e.g. the IV relation is linear over a voltage window from -60 to +40 mV, decreases at positive voltages and reverses close to the K^+ Nernst voltage. In similar experiments an activation of hIK channels by X-ray irradiation caused an average increase in the instantaneous current at a reference voltage of +20 mV by 1.5 ± 0.9 pA/pF (n=7); the concomitant negative shift of V_m was -6 mV ± 2 mV (n=7).

The time-course of the normalized current response before and after radiation stress indicates that the activation of hIK channels is a very early effect of ionizing radiation. An increase in conductance is already observed in a time window of 3-12 minutes after irradiation with 1 Gy of X-ray (Fig. 20 E). This observation is similar to the activation of potassium-channels in A549 cells after X-ray irradiation (Roth, 2013), indicating that a similar mechanism activates the hIK channels in both cell types.

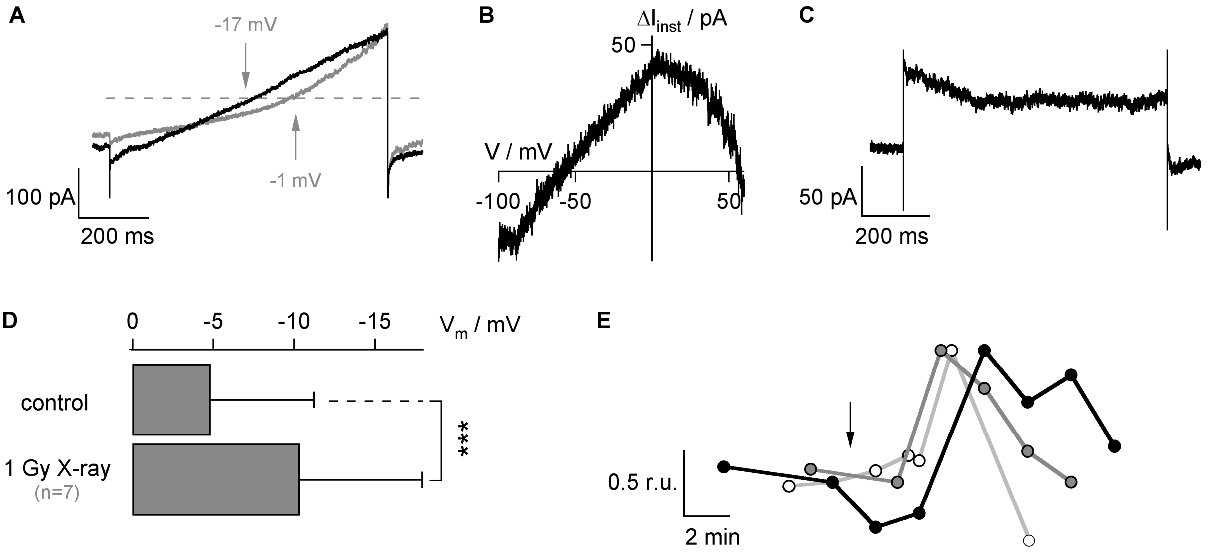

Fig. 20 **Activation of overexpressed hIK channels by irradiation with 1 Gy X-rays.**

Representative current response of a HEK293 cells overexpressing the hIK channel to a ramp protocol from -100 to +60 mV before (grey) and after (black) irradiation with 1 Gy X-rays (A). The shift of V_m by -16 mV is indicated with arrows. The increase in conductance as a difference of both is shown in B. The gained instantaneous conductance at a voltage step of +40 mV carried by the overexpressed hIK channel is illustrated in C.

The membrane voltage was significant hyperpolarized after irradiation by 1 Gy X-ray irradiation (*** $p < 0.001$; $n = 7$) (D). The time-course of radiation induced hIK channel activation is illustrated in E. The time-point of irradiation with 1 Gy of X-ray is indicated with an arrow. The mean current of a +20 mV pulse was normalized to the current directly before irradiation and the maximum after irradiation. The cells were measured with an internal EGTA concentration of 1 mM.

The degree of hIK activation by X-ray irradiation seems to depend on the level of hIK channel expression in HEK293 cells (Fig. 21 A). The general picture is the following: Cells which overexpress the hIK channel had a negative membrane potential and these cells exhibited a strong response to IR. Cells with a negative membrane voltage presumably expressed a larger amount of active hIK channels while cells with a more depolarized voltage expressed only a low amount of active hIK channels.

In A549 cells with a hyperpolarized membrane showed only a minor or no activation upon irradiation (Roth, 2013) and external applied ROS (Fig. 21 B). These data indicate that radiation cannot further augment the K^+ conductance in cells when a small number of endogenous hIK channels is already fully active in A549. In line with this argument radiation treatment was able to stimulate hIK activity in A549 cells, which exhibited a depolarized V_m e.g. a low hIK activity prior to the treatment. In this scenario the amount of endogenous expressed hIK channels and consequently the percentage of possibly activatable channels was limited (Fig. 21 B). Whereas the stimulating signal, e.g. an extension of $[Ca^{2+}]_{cyt}$ was the limiting factor in cells overexpressing hIK channels (Fig. 21 A).

Even though the results with HEK293 cells that heterologously expressed hIK channels are preliminary they support the view that hIK channels could be activated by ionizing radiation via ROS, e.g. H_2O_2 and Ca^{2+}.

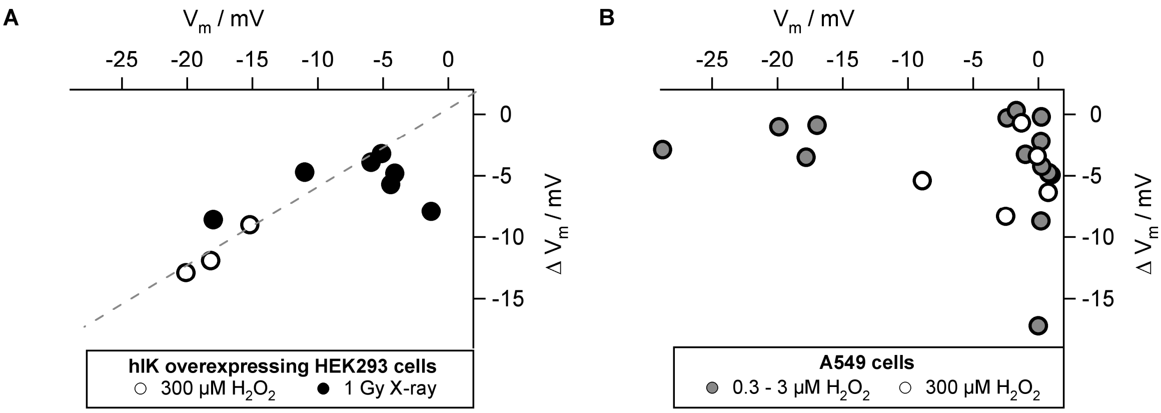

Fig. 21 **Radiation and ROS induced membrane hyperpolarization is dependent on the hIK channel activity.**

The scatter-plot illustrates the correlation of negative membrane voltage before treatment with H_2O_2 (open symbols) or X-ray irradiation (filled symbols) and the negative shift of the membrane voltage (ΔV_m) of HEK293 cells overexpressing the hIK channel (A).

A similar scatter-plot reveals that A549 cells became more hyperpolarized if their membrane voltage was depolarized before H_2O_2 treatment (B).

In summary the results of the electrophysiological experiments support the view that an elevation of H_2O_2 as well of $[Ca^{2+}]_{cyt}$ can mimic the effect of radiation in inducing hIK channel activity in cells, in which this channel is expressed. The sequence of events after irradiation presumably starts with an increase in ROS; it is reasonable to speculate that H_2O_2, a ROS with a long life time, is involved in this reaction. An elevation of ROS concentration activates endogenous hIK channels in A549 cells as well as heterologous expressed hIK channels in HEK293 cells. These data strongly support the view that cells, which express hIK channels, are sensitive to ionizing irradiation. This stress generates an elevated conductance of this K^+-channel with a consequent hyperpolarization of the cells. It is interesting to note that HEK293 cells, which are not sensitive to X-rays acquire a radio-sensitivity after expressing the hIK channel. This suggests that the events upstream of hIK channel activation including ROS generation and presumably $[Ca^{2+}]_{cyt}$ elevation are the same in A549 cells and HEK293 cells.

4.3. ROS stimulated increase of the cytosolic calcium concentration

Since the hIK channel is a calcium-activated ion-channel the most probable effect of radiation is not a direct effect of ROS on the channel protein. More likely is that radiation stress initiates a signal cascade, which finally leads to a raise in the cytosolic calcium concentration. To elucidate whether ROS are indeed able to trigger a calcium signal cascade, I expressed a calcium sensor in HEK293 and A549 cells and monitored the Ca^{2+} concentration in these cells before and after challenging them with external hydrogen peroxide.

As a Ca^{2+} sensor the genetically encoded FRET based calcium sensor YC3.60 was employed both in HEK293 and A549 cells. Cells expressing the chameleon sensor show only minor FRET efficiency under resting conditions in which the cytosolic calcium concentration ($[Ca^{2+}]_{cyt}$) is in the nanomolar range (Clapham, 1995, 2007). It is well established that $[Ca^{2+}]_{cyt}$ serves as a second messenger in cells and it can transiently raise up to 1000-fold in response to an appropriate stimulus.

To simulate a fast increase of $[Ca^{2+}]_{cyt}$ in HEK293 cells, which transiently overexpressed the chameleon sensor, they were challenged with the calcium ionophore Ionomycin [5 µM] (Fig. 22). Upon addition of the ionophore the FRET efficiency of the chameleon sensor increased dramatically. This is due to a conformational change of the linker between the CFP and the YFP fluorescent protein of the sensor, which is induced by calcium binding to the associated calmodulin (Miyawaki *et al.*, 2013; Nagai *et al.*, 2004; Whitaker, 2012). The increase in $[Ca^{2+}]_{cyt}$ was monitored as an increase in the ratio of the fluorescence intensities of YFP/CFP (Fig. 22 A). The ratio remained very stable (2.6 ± 0.4; n=140) during the time (here 60 min) over which cells were in a resting condition and exhibited a fast rise in response to Ionomycin treatment. The fluorescence ratio increased by a value of 11.8 ± 3.8 (n=140) after elevation of $[Ca^{2+}]_{cyt}$.

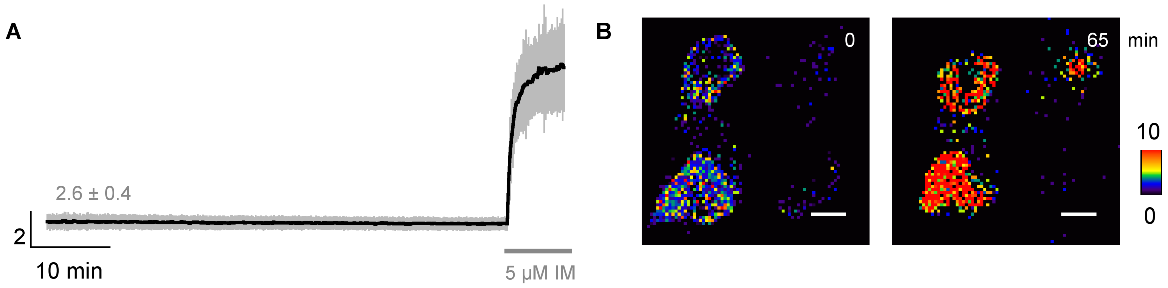

Fig. 22 **The calcium signal remains stable over a long time period.**

HEK293 cells expressing the FRET based calcium sensor YC3.60 were measured over a time period of about 60 minutes. The mean of YC3.60 ratio ± SD of 140 cells from a single experiment is shown in A and remained very stable over this time period (2.6 ± 0.4). The high amplitude at the end of the measurement was induced by treatment with 5 µM Ionomycin (IM). The calcium ionophore allows the adaption of the internal calcium concentration to the predefined external calcium concentration of 2 mM. The blue (=0) to red (=10) pseudocolored image of representative cells before and after treatment with 5 µM Ionomycin are illustrated in B (scale bar 10 µm).

To examine the impact of ROS on $[Ca^{2+}]_{cyt}$, HEK293 and A549 cells, which transiently expressed the chameleon sensor, were exposed to 200 µM H_2O_2 in the external buffer.

The typical response of the Ca^{2+} sensor to the ROS stress is shown in Fig. 23. In the present case HEK293 cells showed after a lag period of about 2 minutes a complex elevation of $[Ca^{2+}]_{cyt}$ (Fig. 23 A). In some cells $[Ca^{2+}]_{cyt}$ started to oscillate after ROS stimulation (Fig. 23 B). The maximal increase of $[Ca^{2+}]_{cyt}$ was observed 15.3 ± 7.9 minutes (n=140; N=5) after H_2O_2 was added to the external medium.

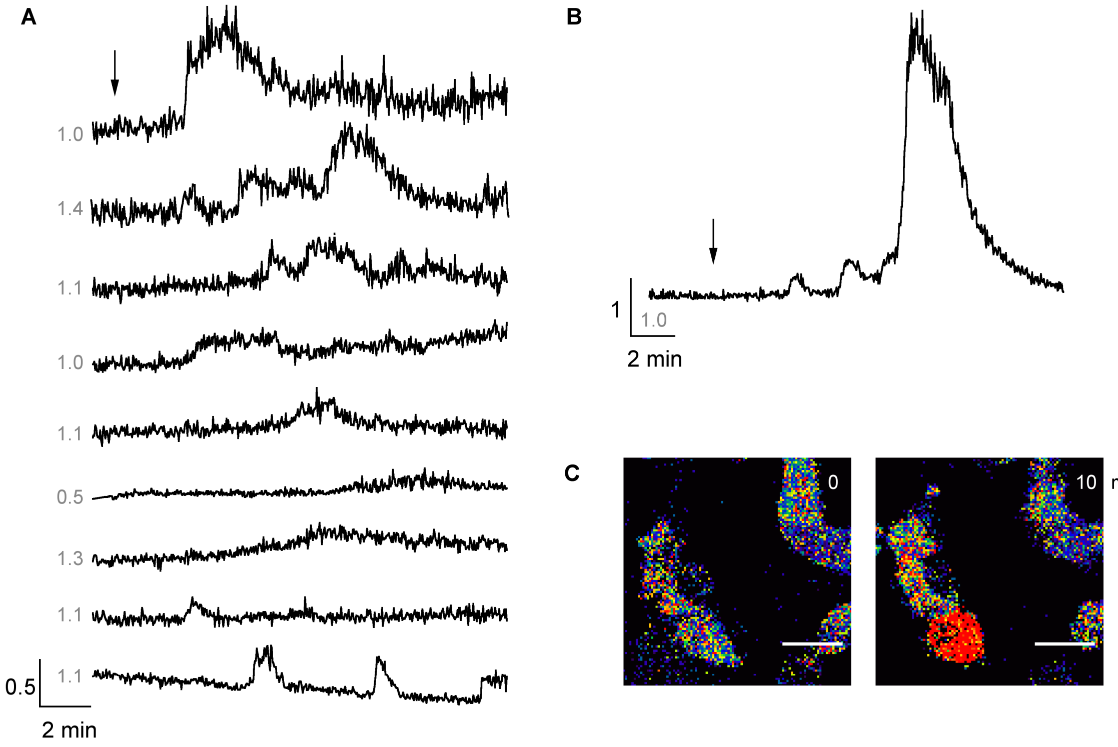

Fig. 23 **External applied ROS stimulate calcium signals in HEK293 cells.**

Exemplary single-cell responses of HEK293 cells transiently expressing the calcium sensor YC3.60 challenged with 200 µM external H_2O_2 (arrow) are displayed in A. The starting value of the $I_{YFP/CFP}$ ratio is indicated in grey. The cells showed increased calcium concentrations about 2 minutes after treatment. Some cells exhibited oscillations in $[Ca^{2+}]_{cyt}$ (B). The blue (=0) to red (=10) pseudocolored ratiometric images corresponding to the signal in (B) before and 10 minutes after H_2O_2 treatment (maximum) is shown in C (scale bar 10 µm). The cells were measured in solution with 2 mM $[Ca^{2+}]_{ext}$. The 10 illustrated representative single-cell responses are from 4 independent experiments.

Similar results were obtained with A549 cells. Also these cells responded about 2 minutes after treatment with external H_2O_2 with a significant increased $[Ca^{2+}]_{cyt}$ (Fig. 24). The maximal increase of $[Ca^{2+}]_{cyt}$ was observed 22.6 ± 7.6 minutes (n=60; N=3) after H_2O_2 was added to the external medium.

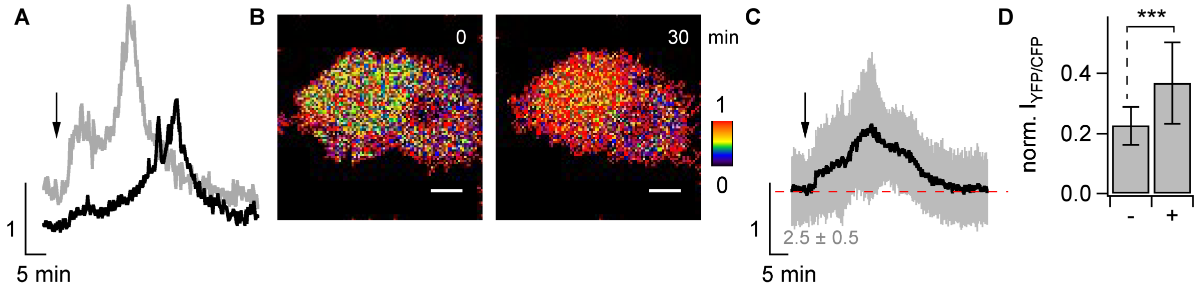

Fig. 24 **H_2O_2 stimulated increase of $[Ca^{2+}]_{cyt}$ in A549 cells.**

Ratiometric signal of two representative A549 cells transiently expressing the calcium sensor YC3.60 after treatment with 200 µM H_2O_2 (arrow). The cells exhibited after a short lag period an increase in $[Ca^{2+}]_{cyt}$ (A). The blue (=0) to red (=1) pseudocolored ratiometric images corresponding to the black graph before treatment and at the maximal response are shown in B (scale bar 10 µm). The mean ± SD of 9 cells is illustrated in C. The starting value of the $I_{YFP/CFP}$ ratio is indicated in grey. The cells exhibited already after 2 minutes a significant increase of $[Ca^{2+}]_{cyt}$ over baseline niveau. The maximal increase of $[Ca^{2+}]_{cyt}$ of these 9 cells was observed 20.6 ± 6.3 min (n=9) after addition of H_2O_2 to the external medium. The fluorescence intensity ratio of YFP/CFP before (-) and at the maximum after H_2O_2 (+) both normalized to $I_{YFP/CFP}$ after Ionomycin [5µM] treatment, exhibited a significant raise of $[Ca^{2+}]_{cyt}$ (*** $p < 0.001$; n=60 of 3 independent experiments) (D). The cells were measured in solution containing 2 mM $[Ca^{2+}]_{ext}$.

The analysis of calcium signals in HEK293 as well as in A549 cells reveals that low concentrations H_2O_2, which presumably resemble those in the cytosol of stressed cells, are able to elicit an increase in $[Ca^{2+}]_{cyt}$. The measured calcium responses were very diverse, ranging from only a slight elevation to recurring oscillations with large amplitudes. The general increase of $[Ca^{2+}]_{cyt}$ which starts to occur with a lag time of about 2 minutes after H_2O_2 was added to the external solution fits very well to the dynamics of hIK channel activation both endogenous in A549 and heterologous expressed in HEK293 cells. Also channel activation becomes apparent only after a lag time of about 2 min after challenging cells with H_2O_2 (Fig. 13 F). The results of these experiments strongly suggest a causal relation between ROS and hIK channel activation, which is mediated by a rise in $[Ca^{2+}]_{cyt}$.

5. CHAPTER 2 - Generation of ROS by UV-laser micro-irradiation

5.1. Establishing fluorescence based sensor proteins for *in vivo* monitoring of ROS and ROS buffering in cells after UV-laser micro-irradiation

The recent development of genetically encoded protein-based fluorescent-sensors opened a new avenue for the detection of radicals, which emerge in cells in response to stress. These protein sensors replace redox sensitive dyes like dichlorofluorescein derivatives, e.g. DCFDA (2'-7'-dichlorodihydrofluorescein diacetate), which have been used with mixed success to estimate the production of reactive oxygen species (ROS) *in vivo*. The new generation of genetically encoded fluorescence sensors overcome several of the disadvantages of the dyes. The reporter proteins can be targeted to cellular subcompartments via targeting sequences; they are also reversible and in the case of the sensor HyPer, which was used here, highly sensitive to only one ROS species e.g. H_2O_2 (Belousov *et al.*, 2006; Malinouski *et al.*, 2011; Markvicheva *et al.*, 2011). DCF derivatives in contrast are only slow oxidized by H_2O_2, which is one of the most relevant ROS (Mikkelsen & Wardman, 2003).

HyPer is a monomeric protein and senses hydrogen peroxide (H_2O_2) exclusively. It was constructed from Belousov *et al.* (2006) with a circular permutated YFP that is inserted into the well characterized regulatory domain of OxyR; a transcription factor from *E. coli* (Choi *et al.*, 2001; Kim *et al.*, 2002; Lee *et al.*, 2004). Exposure of HyPer to H_2O_2 leads to the formation of a disulfid bridge between Cys199 and Cys208 in the OxyR. This results in an increased fluorescence intensity for an excitation at 488 nm ($I_{488\ nm}$) and a decreased fluorescence intensity for excitation at 405 nm ($I_{405\ nm}$). Due to this opposite changes in fluorescence intensity at two different excitation wavelengths the corresponding ratio of the fluorescence intensity $I_{488nm\ /\ 405nm}$ increases upon oxidation of HyPer with H_2O_2. The data in Fig. 25 show a representative experiment in which the HyPer was expressed in HEK293 cells. When these cells were challenged with H_2O_2 in the bath solution the ratio of the HyPer reporter increased reporting an elevation of H_2O_2 in the cells.

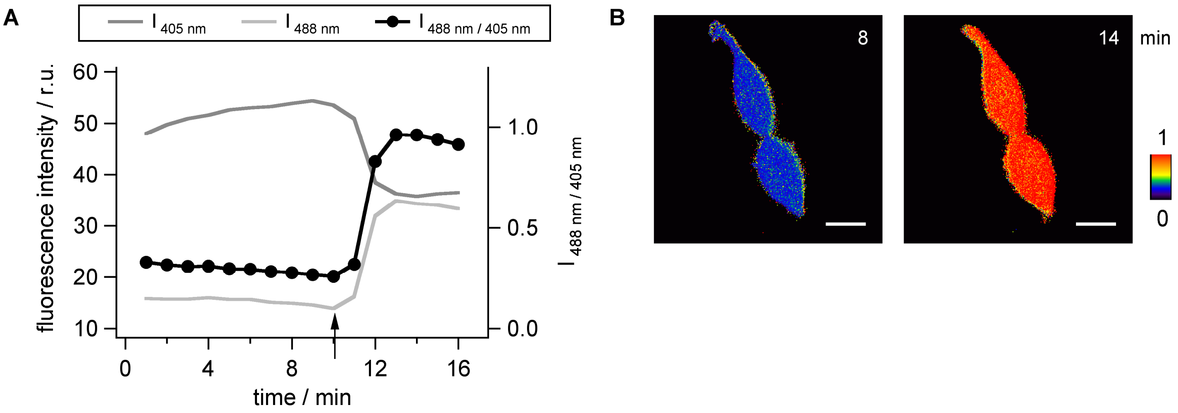

Fig. 25 **Fluorescence properties of the H_2O_2 sensor HyPer.**

HEK293 cells transiently expressing the ratiometric fluorescence sensor HyPer were monitored for 10 minutes before 50 µM H_2O_2 was added to the external solution. The background corrected fluorescence intensity at an excitation wavelength of 405 nm ($I_{405\ nm}$) decreased whereas the fluorescence intensity at an excitation wavelength of 488 nm ($I_{488\ nm}$) increased simultaneously (A). The fluorescence ratio, which was obtained by dividing $I_{488\ nm}$ / $I_{405\ nm}$ was increasing upon H_2O_2 treatment. The corresponding blue (=0) to red (=1) pseudocolored fluorescence images of two cells expressing the sensor before and after treatment with 50 µM H_2O_2 are shown in B (scale bar 10 µm).

Ratiometric sensors have several advantages in that they prevent many imaging artifacts, which are caused by bleaching of the sensor, concentration differences between cellular compartments or by the movement of the object (Lukyanov & Belousov, 2013). The ratio of the HyPer sensor is independent of the amount of protein, which is expressed in a cell. The data in Fig. 26 show that it is also very stable over long recording periods. The 12 examined cells displayed a mean $I_{488\ nm\ /\ 405\ nm}$ ratio of 0.35 ± 0.03 (n=133) in the monitored time of 30 minutes. This is a great advantage over DCF derivatives. A further problem associated with the DCF dye is that it generates by itself ROS during light exposure; this results in an artificial signal amplification. The HyPer sensor in contrast does not generate any artificial ROS upon exposure to light during image acquisition (Belousov *et al.*, 2006).

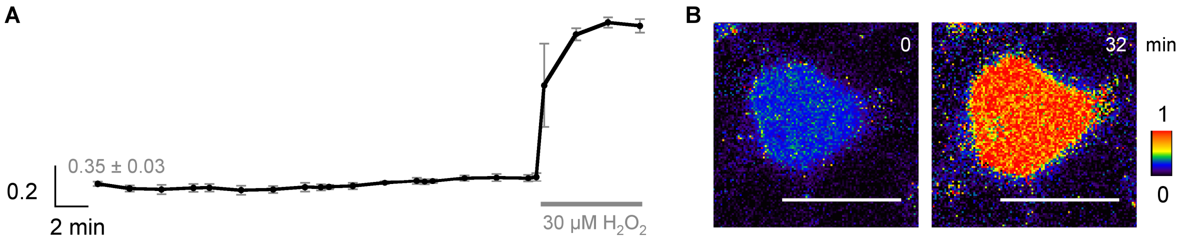

Fig. 26 **Stability of the ratiometric HyPer signal over long time recording.**

The ratio $I_{488\ nm}$ / $I_{405\ nm}$ of the HyPer protein expressed in HEK293 cells remained stable over more than 30 min of recording (n=7; 0.35 ± 0.03). Only after addition of 30 µM H_2O_2 to the external solution an increase in the ratio was obtained (A). Exemplary blue (=0) to red (=1) pseudocolored ratiometric images before and after addition of 30 µM H_2O_2 to the external solution are displayed in B (scale bar 10 µm). Experiments were performed as in Fig. 25.

To calibrate the HyPer signal the sensor was transiently expressed in HEK293 and A549 cells and the cells were then challenged with different concentrations of H_2O_2 in the bath medium. The representative data in Fig. 27 A and B show the fluorescence ratio of the HyPer sensor with different concentrations of H_2O_2 in the external buffer. The corresponding calibration curve shows the fluorescence ratio as a function of the external H_2O_2 concentration on a log-scale (Fig. 27 C).

The data were fitted with a sigmoidal function to obtain the concentration of H_2O_2 for a half-maximal (K_{ox}) increase in $I_{488\ nm\ /\ 405\ nm}$ ratio (equation 1). Here Δr_{min} and Δr_{max} are representing the minimal and maximal change in $I_{488\ nm\ /\ 405\ nm}$ ratio respectively.

$$f(x) = \Delta r_{min} + \left[\frac{(\Delta r_{max} - \Delta r_{min})}{\left(1+(\frac{x}{K_{ox}})^n\right)}\right] \qquad \textbf{equation 1}$$

If we assume that the concentration of the membrane permeable H_2O_2 is the same outside and inside of the cell we can estimate a K_{ox} of 31.3 µM. This value is much higher than the corresponding K_{ox} value, which was obtained when the purified HyPer was calibrated *in vitro*. The published data from the *in vitro* calibration report a dynamic range of the HyPer protein between 25 nM and 250 nM and a K_{ox} value of 160 nM (Belousov *et al.*, 2006). Hence, the K_{ox} value from *in vitro* calibrations is 200 times smaller than that of the present *in vivo* approach. The discrepancy between the *in vivo* and *in vitro* calibration may be explained by several factors. First it is not known if in our *in vivo* calibration the internal H_2O_2 concentration is indeed identical to the external calibration. Furthermore like in the case of many other reporters we must assume that the fluorescence properties of the protein are affected by cellular compounds and that the *in vitro* calibration cannot be directly used for a quantification of *in vivo* data. In a recent report the sensitivity of HyPer expressed in HEK293 cells was estimated to be between 1 and 50 μM H_2O_2 in experiments in which the cytosolic H_2O_2 concentration was altered by adding the redox molecule to the external solution of the cells (Malinouski *et al.*, 2011). Also in these experiments the sensitivity of HyPer to H_2O_2 was 200 to 500-fold lower in cells than in the *in vitro* experiment (Bilan *et al.*, 2013). Hence, the estimated K_{ox} value of 31.3 μM in the present experiments is in good agreement with the published dynamic properties of HyPer from *in vivo* calibrations.

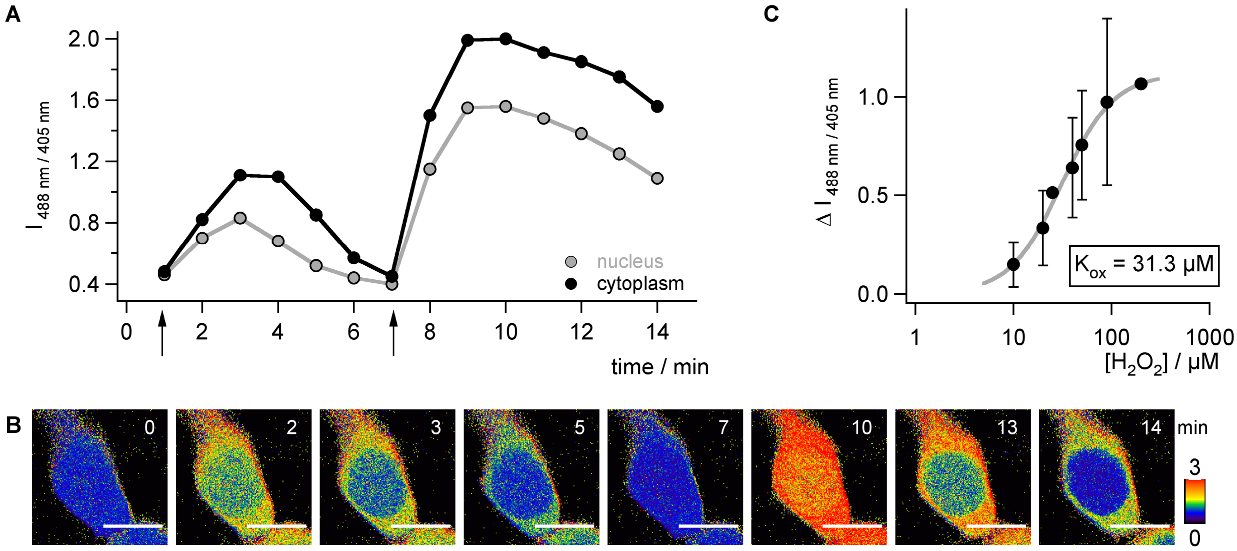

Fig. 27 ***In vivo* calibration of the ratiometric fluorescence sensor HyPer.**

Representing example of the $I_{488\ nm}$ / $I_{405\ nm}$ ratio from HyPer in HEK293 cell in the cytoplasm and in the nucleus under the influence of different concentrations of external H_2O_2 (A). The arrows indicate the time point where 20 μM (left arrow) and 100 μM (right arrow) were added to the external solution of the cells consecutively. The change in $I_{488\ nm}$ / $I_{405\ nm}$ ratio following H_2O_2 treatment is reversible; consecutive additions of H_2O_2 were made once the signal had decayed back to the resting level. In these experiments the magnitude of the signal excursion was depending the concentration of H_2O_2 added to the external buffer. The corresponding blue (=0) to red (=3) pseudocolored images of an exemplary cell are depicted in B (scale bar 10 μm). The data show that the cytoplasm exhibited a stronger signal than the nucleus and that the clearance of the signal form the nucleus was faster than from the cytosol. This suggests a faster buffering of H_2O_2 from the nucleus. The calibration curve of HyPer *in vivo* (n=1-7 ± SD) is shown in C. The H_2O_2 concentration in the external medium is plotted on a log-scale versus the measured increase in fluorescence ratio ($\Delta I_{488\ nm\ /\ 405\ nm}$). The data were fitted with a sigmoidal-function (equation 1). The concentration of H_2O_2 for half-maximal (K_{ox}) increase in $I_{488\ nm}$ / $I_{405\ nm}$ ratio was determined as 31.3 μM.

5.2. UV-laser micro-irradiation generates a rapid burst of H_2O_2 in the irradiated compartment

UV-laser micro-irradiation is widely used in radiation biology for creating distinct DNA double strand breaks and for analyzing the recruitment of repair proteins in living cells (Dinant et al., 2007; Ferrando-May et al., 2013; Huang et al., 2013; Mortusewicz et al., 2008, 2006, 2005). For this reason I examined the generation of ROS in cells following UV-laser micro-irradiation with a 405 nm laser at a CLSM setup. HEK293 and A549 cells, which transiently expressed HyPer, were challenged with UV-laser micro-irradiation at defined spots in the cell, e.g. the cytoplasm or the nucleus. An example of a cytoplasm micro-irradiation with 2 mJ/µm^2 of a HEK293 cell is depicted in Fig. 28. A rapid burst of H_2O_2 immediately after micro-irradiation was observed throughout the cytoplasm; a slight elevation of the H_2O_2 concentration also occurred in the nucleus. The same results were obtained with HEK293 cells and A549 cells. This implies that the response to the stress is a generic response of cells and not cell type specific.

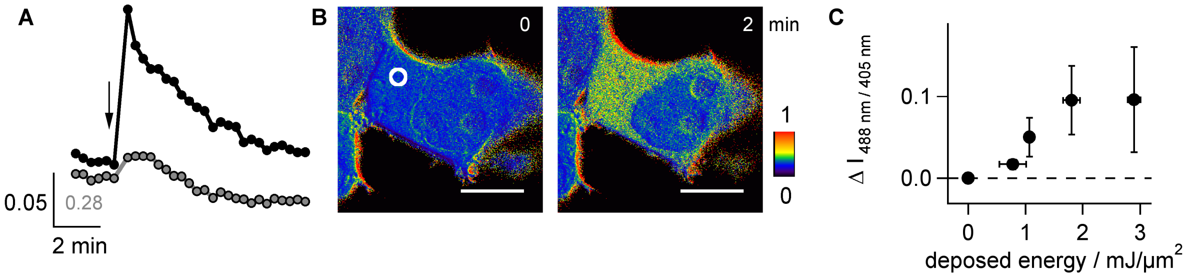

Fig. 28 **UV-laser micro-irradiation in HEK293 cells elicites the generation of H_2O_2.**

An exemplary HEK293 cell transiently expressing the H_2O_2 sensor HyPer was irradiated with a 405 nm laser (about 2 mJ/µm^2) in the cytoplasm. An elevated H_2O_2 concentration was observed in the cytoplasm (black); a slight elevation of the signal was also observed in the un-irradiated nucleus (grey) directly after irradiation (A). The starting value of the $I_{488\ nm\ /\ 405\ nm}$ ratio is indicated in grey. The corresponding blue (=0) to red (=1) pseudocolored images were taken before and after micro-irradiation (B) (scale bar 10 µm). The circle in the left image indicates the site of irradiation. The amount of H_2O_2, which was produced in the cytoplasm, was depending on the deposed laser energy (n≥4) (C).

In most of the cells the detected signals were clearly confined and only detected in the irradiated compartment e.g. either in the nucleus or the cytoplasm. Examples for defined compartment specific HyPer responses to local UV micro-irradiation are illustrated in Fig. 29 A and B. The ratiometric HyPer signal was immediately distributed homogeneously throughout the irradiated compartment. Using the aforementioned *in vivo* calibration (Fig. 27) I can estimate that an energy dose of 3 mJ/µm^2 generates in the exemplary A549 cells in Fig. 29 A and B a H_2O_2 concentration of 50 nM in the nucleus and about 25 nM in the cytoplasm. The same experiments were repeated in 80 single-cell experiments with irradiation of the cytoplasm and 21 experiments with nucleus irradiation with a range of laser energies. The mean elevation of the HyPer ratio in the nucleus and in the cytoplasm as a function of the laser energy, which was used to challenge the respective cell compartments is shown in Fig. 29 C. The results of these experiments show that a higher laser energy dose e.g. a higher UV stress is necessary to generate the same amount of H_2O_2 in the cytoplasm as in the nucleus. An increase in the HyPer ratio of 0.1 in Fig. 29 C corresponds to a treatment of cells with 8 µM external applied H_2O_2, if we use the *in vivo* calibration. If we use the *in vitro* calibration of HyPer this would translate into an internal H_2O_2 concentration of 40 nM; the latter is calculated on the assumption that the *in vivo* calibration underestimates the affinity of the sensor by a factor of 200.

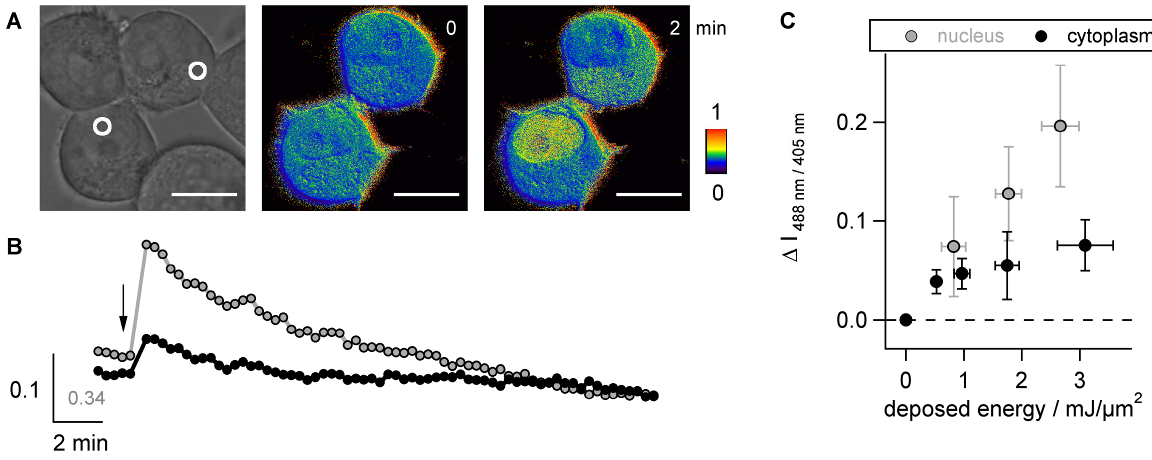

Fig. 29 **UV-laser micro-irradiation generates a rapid burst of H_2O_2 in the irradiated compartment.**

A549 cells transiently expressing the ratiometric fluorescence sensor HyPer were micro-irradiated with a 405 nm laser (3 mJ/μm^2) either in the nucleus or in the cytoplasm (circles in left image). The blue (=0) to red (=1) pseudocolored ratiometric images before and directly after micro-irradiation are shown in A. The starting value of the $I_{488\ nm\ /\ 405\ nm}$ ratio is indicated in grey and the onset of irradiation is indicated by arrow. The time course of H_2O_2 generation as well as the recovery of the signal is shown in B.

The irradiation elicited rise in H_2O_2 is shown by the rise in $I_{488\ nm}$/ $I_{405\ nm}$ ratio in C. The laser irradiation generated rises in H_2O_2 were in both compartments a function of the deposited energies. For the same energy doses of radiation stress the rise in H_2O_2 was higher in the nucleus (n≥4) than in the cytoplasm (n≥11).

To test whether the rise in the HyPer ratio after micro-irradiation is indeed due to H_2O_2 generation and not a photochemical artifact of the sensor protein, the same cells were first micro-irradiated with the 405 nm laser (3 mJ/μm^2) under normal experimental conditions in PBS and then treated with 6 mM N-acetylcysteine (NAC) (Fig. 30 A). Former studies revealed the prevention of DNA damage in presence of NAC after irradiation with UVA and visible light (Morley *et al.*, 2003). Indeed was the cell permeable antioxidant NAC capable to scavenge the irradiation generated raise in the HyPer ratio significantly. In further experiments cells were stimulated by UV micro-irradiation in the presence of 10 mM NAC in the bath solution. In this case UV-laser micro-irradiation had no perceivable effect on the HyPer ratio (Fig. 30 B).

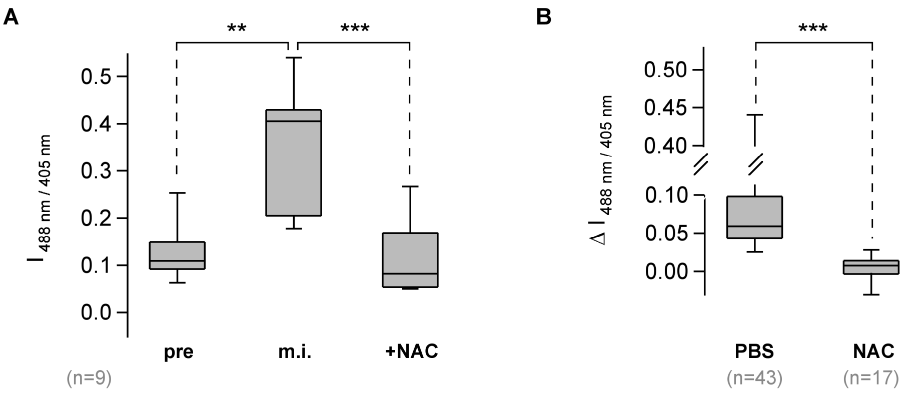

Fig. 30 **The ROS, which are elicited by laser micro-irradiation, are scavenged with the radical scavenger N-acetylcysteine.**

Ratio of Hyper in the same HEK293 cells before (pre), after micro-irradiation (m.i.) with 3 mJ/μm^2 from a 405 nm laser and after treating the same cells with 6 mM N-acetylcyteine (NAC) in the bath medium (+NAC) (A). The radiation generated ROS were scavenged by NAC. Cells were also measured either in standard PBS buffer (PBS) or in a PBS buffer containing 10 mM N-acetylcysteine (NAC). Micro-irradiation elicited in the latter case a significantly smaller increase in the HyPer ratio (B). (** $p < 0.05$; *** $p < 0.001$)

Since HyPer has like almost all GFP-like fluorescence proteins a pH sensitive tyrosine containing chromophore, it is necessary to perform control measurements, which test the contribution of pH changes to the HyPer signal (Belousov *et al.*, 2006; Bilan *et al.*, 2013; Ermakova *et al.*, 2014; Lukyanov & Belousov, 2013). For this purpose the H_2O_2 insensitive variant of HyPer the so called SypHer (Poburko *et al.*, 2011) was used. In SypHer the critical cysteine at position 199 of the OxyR is changed into a serine, creating a ratiometric fluorescence sensor with the same pH sensitivity like HyPer, but with no sensitivity to H_2O_2 (Fig. 31 A). The latter should only report the effect of UV-irradiation on the cellular pH.

Irradiating HEK293 cells, which transiently expressed SypHer, with the same dose of 405 nm laser (3 mJ/μm^2) resulted in no changes in fluorescence ratio. In contrast HEK293 cells expressing HyPer showed the expected increase in the HyPer ratio upon irradiation (Fig. 31 B). The results of these experiments strongly support the notion that the observed increase in fluorescence ratio after laser micro-irradiation could be affiliated to a generation of H_2O_2 in the irradiated compartment; any photoconversion of the sensor or non specific signals, which are related to excursions in the cellular pH do not contribute to the changes in fluorescence ratio following UV-irradiation.

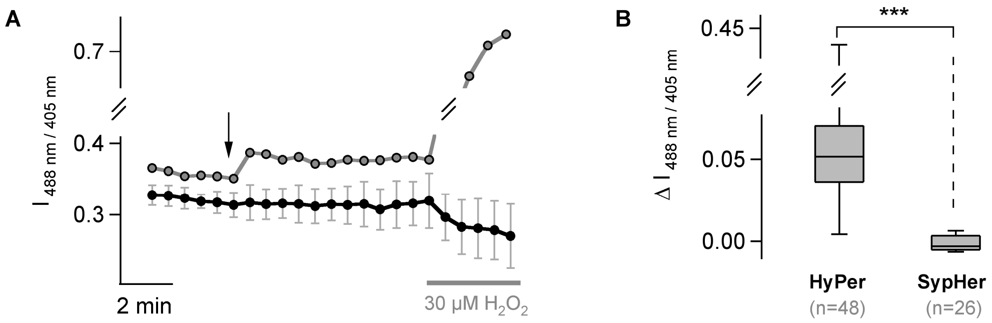

Fig. 31 **Laser micro-irradiation has no effect on the pH of the cytosol.**

HEK293 cells transiently expressing either HyPer (n=2) or a H_2O_2 insensitive cysteine mutant (C199S; SypHer; n=4 ± SD) were micro-irradiated with about 3 mJ/μm^2 of a 405 nm laser (arrow) and treated with 30 µM H_2O_2 in the bath medium afterwards (A). HE293 cells expressing HyPer displayed an increase in ratio after laser micro-irradiation, whereas the signal of the H_2O_2 insensitive mutant SypHer remained stable or decreased slightly. The H_2O_2 reporter HyPer exhibited after irradiation on average an increase in the $I_{488\ nm}$ / $I_{405\ nm}$ ration of 0.08 ± 0.095 (n=48); in contrast no significant change was observed if HEK293 cells expressing the cysteine mutant SypHer were irradiated with the same laser dose of 3 mJ/μm^2. (*** $p < 0.001$)

5.3. Cytoplasm and nucleus have different redox-buffering capacities

To further analyze the generation and processing of ROS after laser micro-irradiation I employed another ratiometric, protein-based fluorescence sensor. The sensor Grx1-roGFP2 consists of a redox-sensitive GFP variant (roGFP2; Cannon and Remington, 2006) fused to the human glutaredoxin1 (Grx1). The sensor allows an imaging of the glutathione redox-potential. Since glutathione is the main redox-buffer in cells the Grx1-roGFP2 signal provides an indirect measure of all ROS, which are generated during a stress and which are then buffered by glutathione (Gutscher *et al.*, 2008; Morgan *et al.*, 2011).

Test experiments showed that the application of H_2O_2 to the external solution induced a rapid and reversible response of the glutathione redox-potential sensor. While the fluorescence intensity at an excitation wavelength of 405 nm increased the fluorescence intensity at an excitation wavelength of 488 nm concomitant decreased. This resulted in a fast change in the ratio of this two wavelength ($I_{405\ nm}$ / $I_{488\ nm}$). The latter was obtained by dividing the fluorescence intensity at an excitation of 405 nm ($I_{405\ nm}$) and at 488 nm ($I_{488\ nm}$) (Fig. 32).

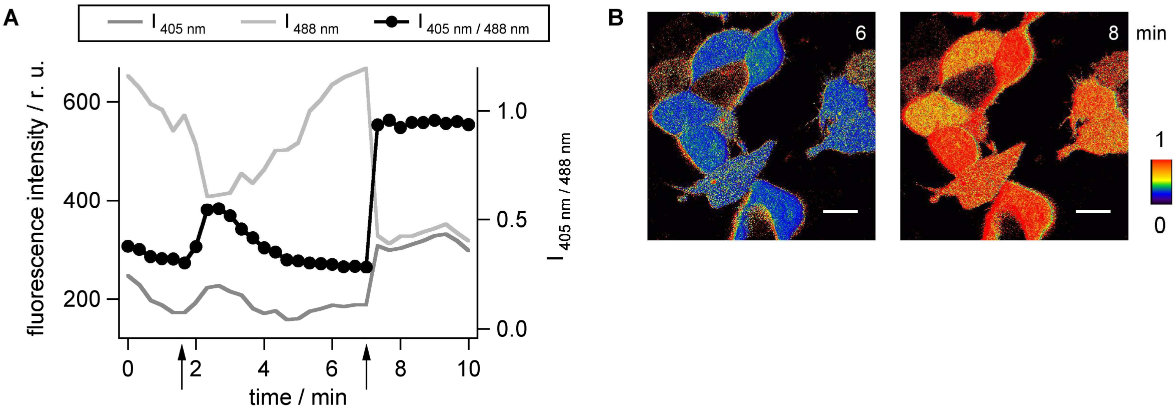

Fig. 32 **Fluorescence properties of the redox sensor Grx1-roGFP2.**

HEK293 cells transiently expressing the ratiometric fluorescence sensor Grx1-roGFP2 were treated first with 20 µM (left arrow) and then with 160 µM H_2O_2 (right arrow). The background corrected fluorescence intensity obtained with an excitation wavelength of 405 nm ($I_{405\ nm}$) increased and simultaneously the fluorescence intensity for an excitation wavelength of 488 nm ($I_{488\ nm}$) decreased (A). The calculated fluorescence ratio $I_{405\ nm\ /\ 488\ nm}$ therefore increased upon H_2O_2 treatment; the excursion of the signal was depending on the H_2O_2 concentration. The corresponding blue (=0) to red (=1) pseudocolored fluorescence images taken before and after treatment with 160 µM H_2O_2 are shown in B (scale bar 10 µm).

The ratiometric signal was stable over a long period of time. In the example shown in Fig. 33 the ratio was recorded over about 30 minutes in 12 cells under resting conditions without any appreciable changes in the ratio (0.36 ± 0.02; n=660) (Fig. 33). Only when the cells were treated with H_2O_2 the ratio of the sensor increased. The results of these experiments show that a loading of cells with ROS results in a buffering by glutathione throughout the cell. It has been reported that the sensor Grx1-roGFP2 is pH-insensitive under physiological conditions (Gutscher *et al.*, 2008; Lukyanov & Belousov, 2013; Roma *et al.*, 2012; Schwarzländer *et al.*, 2008). Hence, it was not necessary to perform further control experiments on unspecific side effects of the sensor.

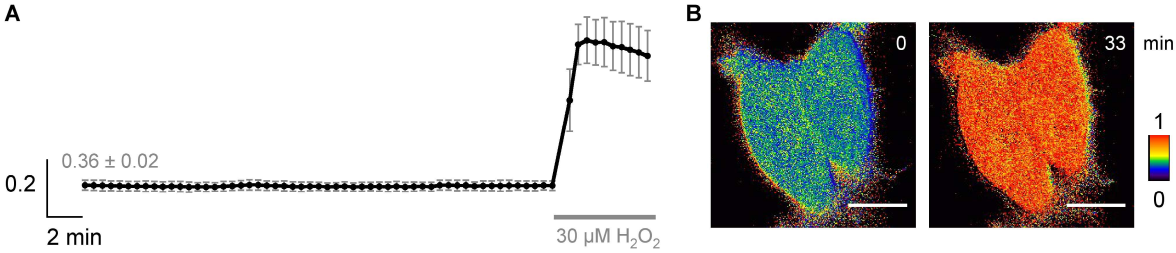

Fig. 33 **The ratiometric Grx1-roGFP2 signal is stable in long time recordings.**

The $I_{405\ nm}$ / $I_{488\ nm}$ ratio of glutathione redox-potential sensor Grx1-roGFP2 in HEK293 cells remained stable over 30 min of recording (n=12; 0.36 ± 0.02). Only after addition of 30 µM H_2O_2 to the external solution an increase in the ratio was obtained (A). Exemplary blue (=0) to red (=1) pseudocolored ratiometric images before and after addition of 30 µM H_2O_2 to the external solution are displayed in B (scale bar 10 µm).

In the following experiments HEK293 cells, which transiently expressed Grx1-roGFP2, were challenged with 405 nm laser micro-irradiation in the cytoplasm and in the nucleus. The overall protocol was the same, which was used in the context with the HyPer sensor. Micro-irradiation of cells in the cytoplasm surprisingly caused a dramatic increase in the fluorescence ratio in the nucleus. The half-time ($t_{1/2}$) of the regeneration of the GSH pool was determined by first fitting the decrease in $I_{405\ nm\ /\ 488\ nm}$ ratio with a single exponential function to determine the τ value and second calculating the $t_{1/2}$ value (equation 2). Here the r_{max} represents the $I_{405\ nm}$ / $I_{488\ nm}$ ratio at maximal response.

$$r(t) = r_{max} + A \cdot exp^{\left(\frac{-t}{\tau}\right)} \qquad \text{and} \qquad t_{1/2} = ln\,2 \cdot \tau \qquad \textbf{equation 2}$$

The increase in ratio ($\Delta I_{405\ nm}$ / $I_{488\ nm}$ 0.17 ± 0.11; n=15) in response to a deposed laser energy of 2.8 ± 1.0 mJ/µm² (n=15) was transient and decreased back to a resting value with a half time ($t_{1/2}$) of about 58.4 ± 18.0 sec (n=15). While the ratio increased in the nucleus the same parameter first decreased transiently in the cytoplasm before returning back to the resting value (Fig. 34). The same response of the Grx1-roGFP2 sensor in the nucleus and in the cytoplasm was obtained by repetitive irradiations. Only the amplitude of the excursions of the Grx1-roGFP2 ratio in nucleus was smaller in the second stimulation compared to the first one.

Another fraction of cells displayed additionally to the signal in the nucleus a rapid enhanced signal in the irradiated cytoplasm (Fig. 35 E and F). In other cells this cytosolic signal occurred with a delay (Fig. 36 A and B; cell 1).

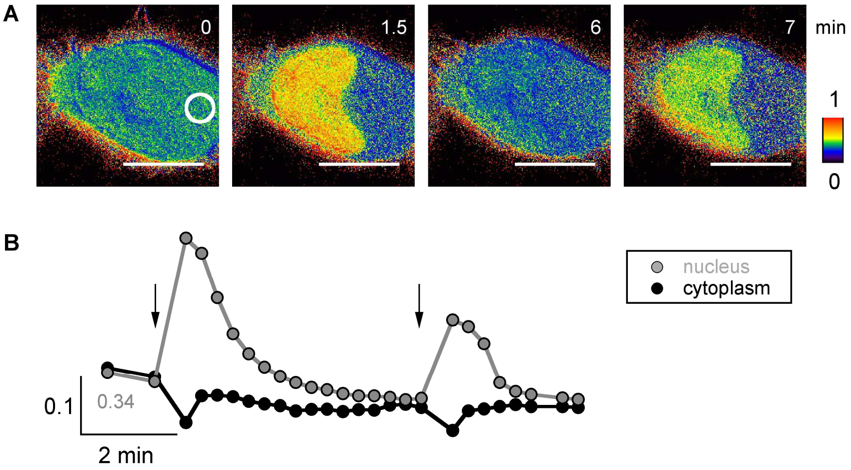

Fig. 34 **Repetitive micro-irradiation of the cytoplasm results in an increased glutathione-redox potential in the nucleus.**

A HEK293 cell transiently expressing the glutathione-redox sensor Grx1-roGFP2 was repeatedly irradiated with 2 mJ/µm² from the 405 nm laser line. The blue (=0) to red (=1) pseudocolored images in A correspond to time line in B (scale bar 10 µm). The circle in the first image in A indicates the region in which the cell was irradiated. The dynamics of the change in $I_{405\ nm}$ / $I_{488\ nm}$ ratio in the nucleus as well as in the cytoplasm are shown in B. The time points of micro-irradiation with 2 mJ/µm² are indicated with arrows and the starting value of the $I_{405\ nm\ /\ 488\ nm}$ ratio is indicated in grey.

The overall response of the cells to the laser micro-irradiation of the nucleus was rather diverse. A fraction of cells exhibited an increased glutathione redox-potential in the un-irradiated cytoplasm (Fig. 35 C and D), while this direct irradiation of the nucleus caused a Grx1-roGFP2 signal in the irradiated compartment in another fraction of cells (Fig. 35 A and B). In the latter cell fraction the increase in $I_{405\text{ nm}\ /\ 408\text{ nm}}$ ratio in the nucleus was identical to those cells where the nucleus signal occurred without irradiation of this compartment. According to this the same effect was provoked independent which compartment was irradiated with the same laser dose of 1 mJ/μm^2 (Fig. 36 C).

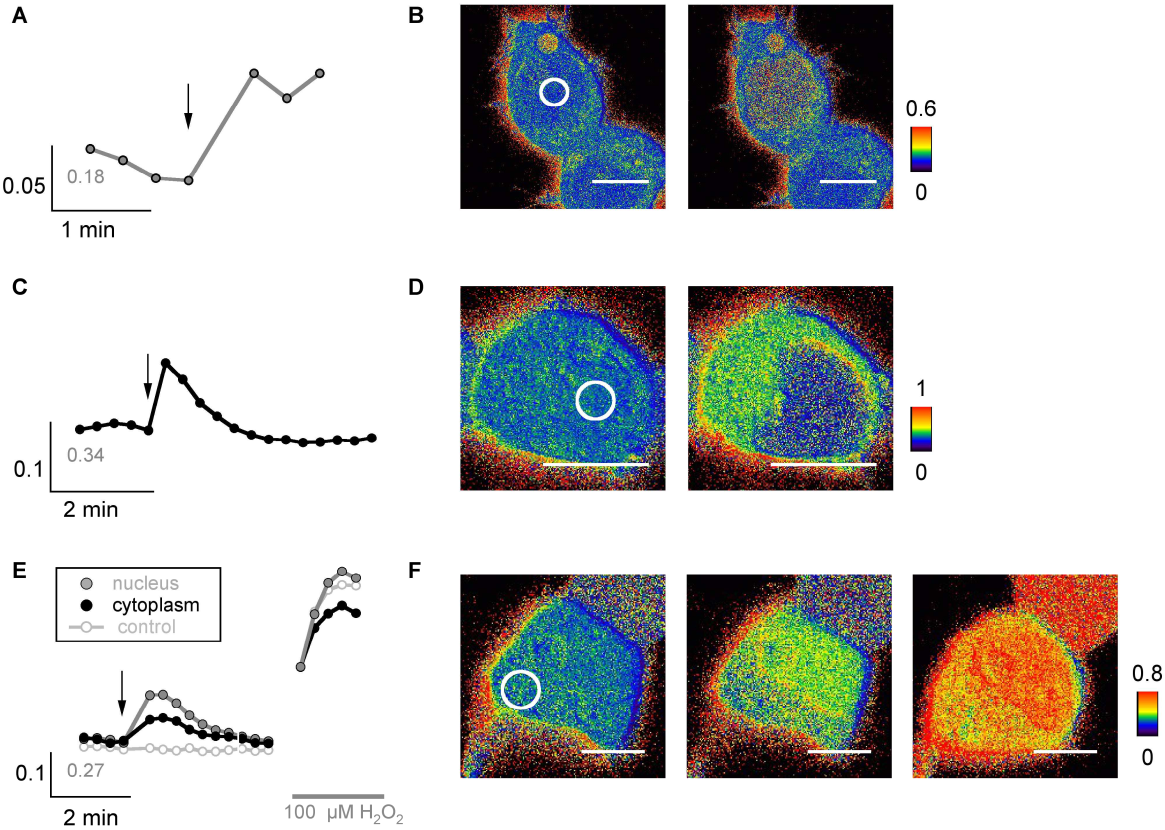

Fig. 35 **Selected examples of redox-buffering after laser micro-irradiation.**

HEK293 cells expressing the glutathione redox-sensor Grx1-roGFP2 were micro-irradiated either in the nucleus (A-D) or in the cytoplasm with a 405 nm laser. The values of the $I_{405\text{ nm}\ /\ 488\text{ nm}}$ ratio at the beginning of the time-course are indicated in grey. Some cells exhibited an increase in oxidized glutathione in the nucleus, after this compartment was irradiated (A+B), whereas other cells showed a higher signal in the un-irradiated cytoplasm (C+D). Irradiation of the cytoplasm resulted in a strong signal in the un-irradiated nucleus and a weaker signal in the irradiated cytoplasm (E+F). The graphs in A, C and E represent the change in $I_{405\text{ nm}\ /\ 488\text{ nm}}$ ratio in the nucleus (grey) or in the cytoplasm (black). The irradiation sites are marked in the corresponding blue (=0) to red (=0.6-1, as indicated next to the images) pseudocolored images in B, D and F (left image before m.i.; right image after m.i.; scale bar 10 µm). The cell in E and F was subsequently treated with 100 µM H_2O_2 in the external buffer to illustrate the different redox-buffer capacities.

The data in Fig. 32 and Fig. 33 already suggest that the redox-buffer capacity for H_2O_2 is the same in the nucleus and the cytosol; when H_2O_2 was added to the external solution the Grx1-roGFP2 signal increased in a uniform manner over the entire cell (Fig. 9). In an additional control experiment I nevertheless examined potential differences in the buffer capacity of the two compartments. For this purpose a cell was first irradiated in the cytosol. This resulted in the known rise of the signal in the nucleus (Fig. 36). After the signal had returned to the resting level the cell was challenged with 100 µM H_2O_2 in the external medium. This treatment caused an even signal increase throughout the entire cell in one case (cell 2) but a slightly higher signal in the nucleus in another case (cell 1). The comparison of the Grx1-roGFP2 responses to micro-irradiation and H_2O_2 treatment in the same cell suggests that the redox-buffer capacity for H_2O_2 is roughly the same in the nucleus and the cytoplasm. On the background of these data it can be speculated that UV micro-irradiation generates many other ROS and that the buffer capacity of the nucleus for these species is higher than in the cytoplasm.

But the even signal distribution after H_2O_2 treatment was not true for all examined cells (Fig. 35 E and F; Fig. 36 A and B cell 2). The diversity of different responses to micro-irradiation might give also a hind to differences in sensitivity to redox stress and differences in the glutathione pool during the cell cycle (García-giménez *et al.*, 2013; Markovic *et al.*, 2007, 2010; Pallardó *et al.*, 2009; Schroeder *et al.*, 2007).

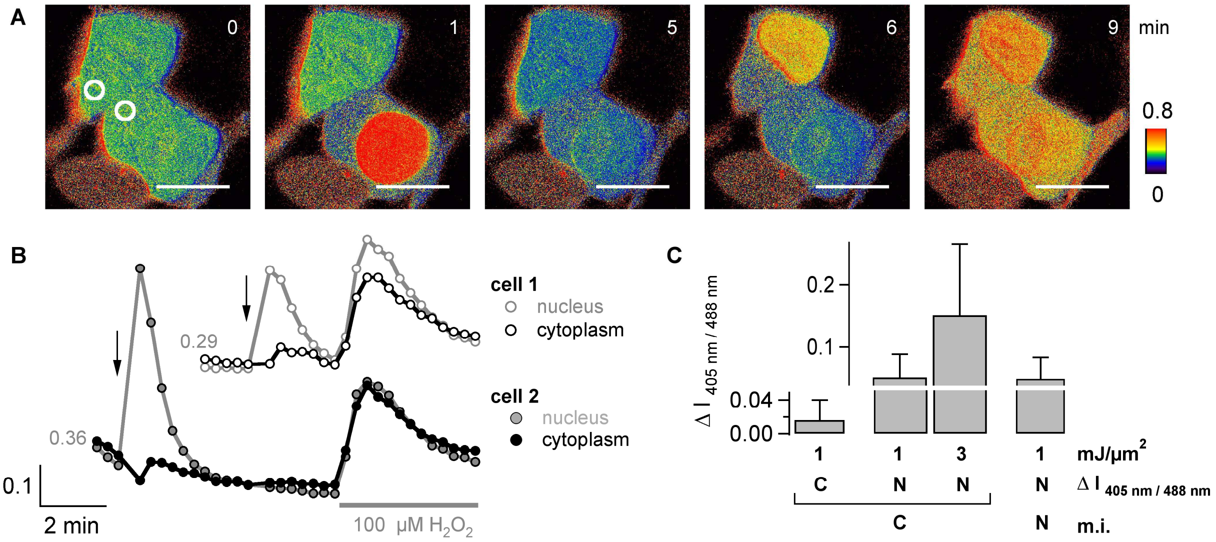

Fig. 36 **Cytoplasm and nucleus have different redox-buffering capacities.**

HEK293 cells transiently expressing the glutathione redox-potential sensor Grx1-roGFP2 were challenged with 405 nm laser micro-irradiation (3 mJ/µm^2) in the cytoplasm. This elicited a dramatic increase in the oxidized glutathione in the nucleus (grey) and a delayed increase in the cytoplasm in cell 1 (black). The values of the $I_{405\ nm\ /\ 488\ nm}$ ratio at the beginning of the time-course are indicated in grey. The blue (=0) to red (=0.8) pseudocolored fluorescence images in A (scale bar 10 µm) correspond to the data shown in B. The circles in the left image show the sites of irradiation. After treatment with 100 µM H_2O_2, which was applied to the external solution, both compartments showed a similar increase in oxidized glutathione (cell 2).

The increase in fluorescence ratio in the nucleus after irradiating the cytoplasm was depending on the deposed laser energy of either about 1 mJ/µm^2 or 3 mJ/µm^2 (C). A similar increase in oxidized glutathione in the nucleus (N $\Delta I_{405\ nm\ /\ 488\ nm}$) was obtained after micro-irradiation (m.i.) of either the nucleus (N) or the cytoplasm (C) with 1 mJ/µm^2.

I could show here that ROS, especially H_2O_2, are generated upon UV-laser micro-irradiation. The increase in H_2O_2 concentration could be reliably monitored with the protein-based HyPer sensor. The signal of HyPer was very stable under resting conditions and the recording procedure by itself caused no artificial ROS production. The control data also show that the signal, which follows micro-irradiation is H_2O_2 specific; it is not a photochemical artifact and it is also not caused by changes in the cellular pH. The UV light induced increase in ROS concentration was transient and lasted only several minutes before it returned to the resting level. This implies an efficient buffering of excess redox molecules in cells. By using the Grx1-roGFP2 reporter protein it was also possible to monitor the buffering of ROS via the glutathione system.

It was surprising to find that the reporter signals, which were elicited by the micro-irradiation stress, exhibited a compartment specificity. Irradiation of the cytosol caused a small cytosolic rise in the H_2O_2 concentration. The same kind of irradiation of the nucleus caused a much larger signal, which remained mostly confined to the nucleus. The results of these experiments in combination with data, which show that external H_2O_2 causes an even response over the entire cell suggests that irradiation elicits a short burst of ROS production. The H_2O_2 molecules presumably diffuse faster in the compartment in which they are generated than across the nuclear envelope. The experimental results with the Grx1-roGFP2 sensor cannot be explained on the basis of H_2O_2 production alone. The fact that this reporter exhibits an increased signal almost exclusively in the nucleus irrespectively on whether the micro-irradiation is focusing on the nucleus or on the cytosol suggests that redox species other than H_2O_2 are generated, which somehow escape the cytosolic buffer. They may quickly travel to the nucleus, were they are buffered by glutathione.

6. CHAPTER 3 - Real-time detection of ROS after X-ray and heavy-ion irradiation

6.1. Generation of reactive oxygen species after X-ray irradiation

The UV micro-irradiation approach has the advantage that the cells can be stimulated with high precision and subsequently monitored with a high spatial resolution. A disadvantage is the difficulty of defining the local dose of a UV-light treatment (Splinter *et al.*, 2010). A further difference between UV- and X-ray irradiation is that the former has a lower energy than X-rays. UV-light is unlike X-rays absorbed by different molecules; it is also not sufficiently strong for the radiolysis of water; hence UV- and X-ray may generate different responses in radicals in cells.

From an experimental point of view it is difficult to measure ROS immediately after irradiating cells with X-rays. For this reason ROS production was in the past mostly measured in the time frame of hours after irradiation stress (Korystov *et al.*, 2007; Ameziane-El-Hassani *et al.*, 2010; Narayanan *et al.*, 1997; Tominaga *et al.*, 2004; Ogura *et al.*, 2009; Hafer *et al.*, 2008 a;b) With these experimental limitations it is obvious that the ROS, which were detected in these studies, could not be the radicals, which were generated as primary response to radiation; the life time of radicals is much too short. The most probable explanation for the late ROS response to IR is a stress-induced release of ROS from mitochondria (Leach *et al.*, 2001; Ogura *et al.*, 2009; Valerie *et al.*, 2007; Yamamori *et al.*, 2012).

In addition to the question on the relevance of the late ROS signals to the primary stress response to radiation also the ROS measurements per se are a matter of controversial discussion in the literature. In one study ROS were measured after X-ray irradiation with a DCF (2'-7'-dichlorodihydrofluorescein diacetate) derivate; a chemical ROS dye. These data were criticized as potential artifacts because it appeared as if they may have originated from irradiating of the extracellular medium (Korystov *et al.*, 2007). The latter criticism does not exclude that IR generates ROS. Others could show a significant increase of ROS 20 minutes after irradiating cells 10 Gy of X-ray; in this study it was excluded that ROS from the cell culture medium contributed to the signal (Hafer *et al.*, 2008). As a resume it can be concluded here that the question on a generation of H_2O_2 after IR is not fully answered yet. Furthermore the contribution of ROS in the early phase of stress response to IR has for technical reasons never been examined.

To elucidate the generation of ROS, e.g. H_2O_2, I implemented both the HyPer sensor for a direct H_2O_2 detection as well as the Grx1-roGFP2 sensor for an indirect measure of radicals, which are buffered by glutathione. A custom build X-ray microscope at GSI (Helmholtzzentrum für Schwerionenforschung GmbH; Darmstadt; Germany) enabled for the first time a real-time monitoring of ROS in individual living cells after X-ray irradiation; the dynamics of ROS could be recorded with high spatial and temporal resolution.

HEK293 and A549 cells, which transiently expressed HyPer, were therefore challenged with X-ray irradiation and the fluorescence signal of the H_2O_2 sensor was monitored immediately after IR. An example for the irradiation of two HEK293 cells with 1 Gy of X-rays is shown in Fig. 37. Immediately after irradiation both cells showed a transient burst of H_2O_2 throughout the entire cell Fig. 37 A. In another subgroup of cells this increase in H_2O_2 lasted several minutes Fig. 37 C.

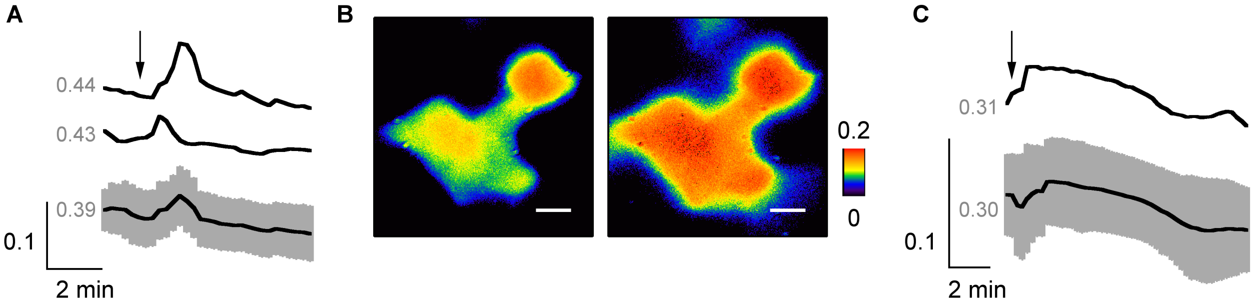

Fig. 37 **Reaction of HEK293 cells expressing HyPer to 1 Gy of X-ray irradiation.**

Two different types of reactions were observed in HEK293 cells, which transiently expressed the H_2O_2 sensor HyPer, after irradiation with 1 Gy X-rays (arrow). The values of the $I_{488\ nm\ /\ 405\ nm}$ ratio at the beginning are indicated in grey. Some cells responded with a transient burst of H_2O_2 (A), whereas the signal persisted several minutes in another sub-group of cells (C). The blue (=0) to red (=0.2) pseudocolored images taken before and after irradiation with 1 Gy of X-rays in B correspond to the data in the upper graph in A (scale bar 10 µm). The data in the lower panel of A and C are the mean ± SD from A n=11 and C n=4 cells from at least 2 independent experiments.

A rapid, transient burst of H_2O_2 immediately after irradiation with 1 Gy of X-rays was also observed in A549 cells (Fig. 38 A). The $I_{488\ nm\ /\ 405\ nm}$ ratio increased conspicuously above the resting values. The raise of the cytosolic H_2O_2 concentration after 5 Gy of X-ray irradiation was in the same range as that obtained by adding 30 µM H_2O_2 to the external solution (Fig. 38 B).

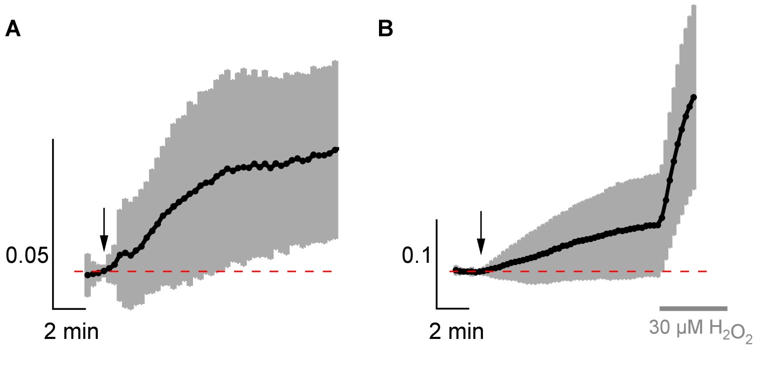

Fig. 38 **Generation of H_2O_2 in A549 cells after exposure to 1 Gy and 5 Gy of X-ray irradiation.**

A549 cells transiently expressing the H_2O_2 sensor HyPer were challenged with X-ray irradiation (arrow). The $I_{488\ nm\ /\ 405\ nm}$ ratio was normalized to the value directly before irradiation in order to correct for different starting values. The mean ± SD for a dose of 1 Gy (n=38; N=4) is displayed in A and the mean ± SD for a dose of 5 Gy (n=5; N=1) is displayed in B. The cells in B were subsequently treated with 30 µM external H_2O_2 in the buffer solution.

When the cells were irradiated with a high dose of X-rays (here 10 Gy) it was possible to monitor the kinetic of ROS generation. Three representative exemplary A549 cells, which were challenged with 10 Gy of X-ray irradiation, are shown in Fig. 39. The single-cell responses to the X-ray stress could be fitted with a single exponential function (equation 3), yielding a mean time-constant τ, of 4.2 ± 1.6 min (n=35; N=3). An exemplary fit with the corresponding data is shown in Fig. 39 E.

$$f(x) = y_0 + A \cdot exp^{\left(-\frac{(x-x_0)}{\tau}\right)}$$

equation 3

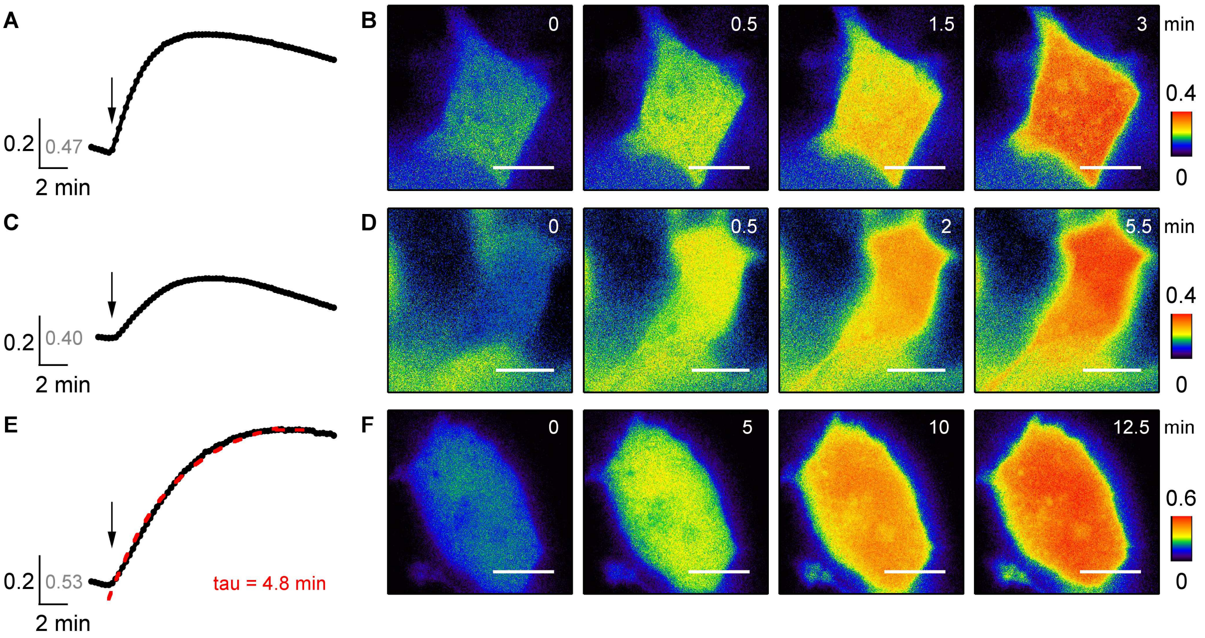

Fig. 39 **Generation of H_2O_2 in A549 cells after exposure to 10 Gy of X-rays.**

A549 cells expressing the HyPer reporter exhibited a slow progressive increase of H_2O_2 after challenging with 10 Gy of X-rays (arrow). The starting values of the $I_{488\ nm\ /\ 405\ nm}$ ratios are indicated in grey. The measured $I_{488\ nm\ /\ 405\ nm}$ ratio saturated about 3-10 minutes after irradiation before the signal started to decline. The traces in A, C and E show three representative single-cell responses to the irradiation stress. An exemplary single exponential fit (equation 3) to determine the time-constant τ is shown in E (red dashed line). The blue (=0) to red (=0.4 or 0.6) pseudocolored ratiometric images are displayed in B, D and F respectively (scale bar 10 µm).

As a second, indirect approach for monitoring the rise in ROS after X-ray stimulation the glutathione redox-sensor Grx1-roGFP2 was once more transiently expressed in A549 cells. These cells were then challenged with 10 Gy of X-ray and the fluorescence signal of the reporter was monitored. The exemplary data in Fig. 40 show that this treatment elicited a rapid response to the radiation stress through the cells. The radiation induced excursion of the fluorescence signal was again fitted with a single exponential function (equation 3), as exemplary shown in Fig. 40 E. This yields a time-constant τ of 0.9 ± 0.5 min (n=15; N=2). The maximal response of the sensor was already reached 1 minute after stimulation.

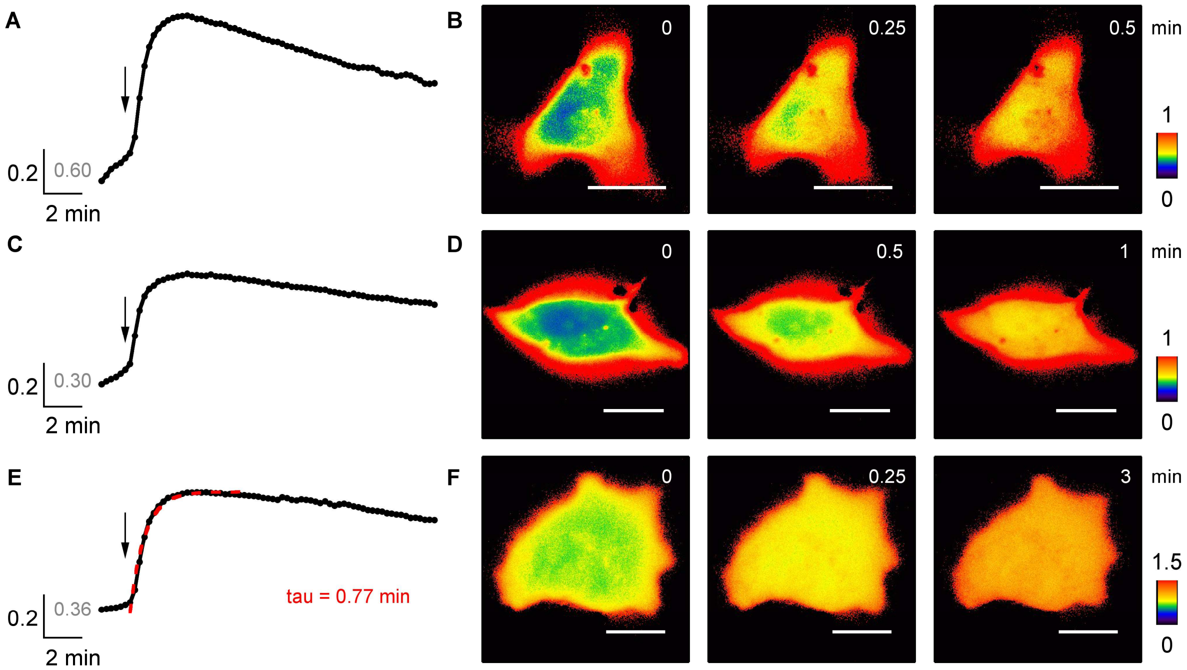

Fig. 40 **Rapid buffering of X-ray radiation generated ROS.**

Three exemplary A549 cells, which transiently expressed the glutathione redox-sensor Grx1-roGFP2, exhibited a rapid increase in $I_{405\ nm\ /\ 488\ nm}$ ratio after irradiation with 10 Gy of X-rays (arrow) (A, C and E). The starting values of the $I_{488\ nm\ /\ 405\ nm}$ ratio are indicated in grey. An exemplary single exponential fit (equation 3) to determine the time-constant τ is shown in E (red dashed line). The blue (=0) to red (=1 or 1.5) pseudocolored ratiometric images corresponding to the cellular responses from A, C and E are depicted in B, D and F respectively (scale bar 10 µm).

The increase in ratiometric fluorescence signals of the HyPer sensor and the Grx1-roGFP2 sensor in response to different doses X-ray irradiation are displayed in Fig. 41 A and B. The data underscore that any of the X-ray doses used for cell irradiation caused an increase in ROS. The data do not exhibit a clear-cut dose dependency. This may indicate that the response is already close to maximal with 1 Gy X-rays. It is also possible that the quality of the data is not sufficient for detecting such a dose dependency. The individual mean values have a very large variability; also the experiments with 5 Gy X-rays were only performed once for the HyPer sensor and twice for the Grx1-roGFP2 sensor.

The kinetic of ROS generation upon radiation stress for both sensors are depicted in Fig. 41 C and D. Every single-cell response was normalized to the ratio taken directly before radiation and to the maximal value after X-ray irradiation. In spite of the overall scatter of the data the plot shows that the HyPer signal increases much slower than the one from the glutathione-sensor. To quantify this observation the response of the raw data of each cell was fitted as exemplary shown in Fig. 39 E and Fig. 40 E with an exponential function to obtain the time-constant τ. A comparison of the time-constants from both sensors shows that they are significantly different; the GSSG signal increases on average approximately 5 times faster than the H_2O_2 signal (Fig. 41 E).

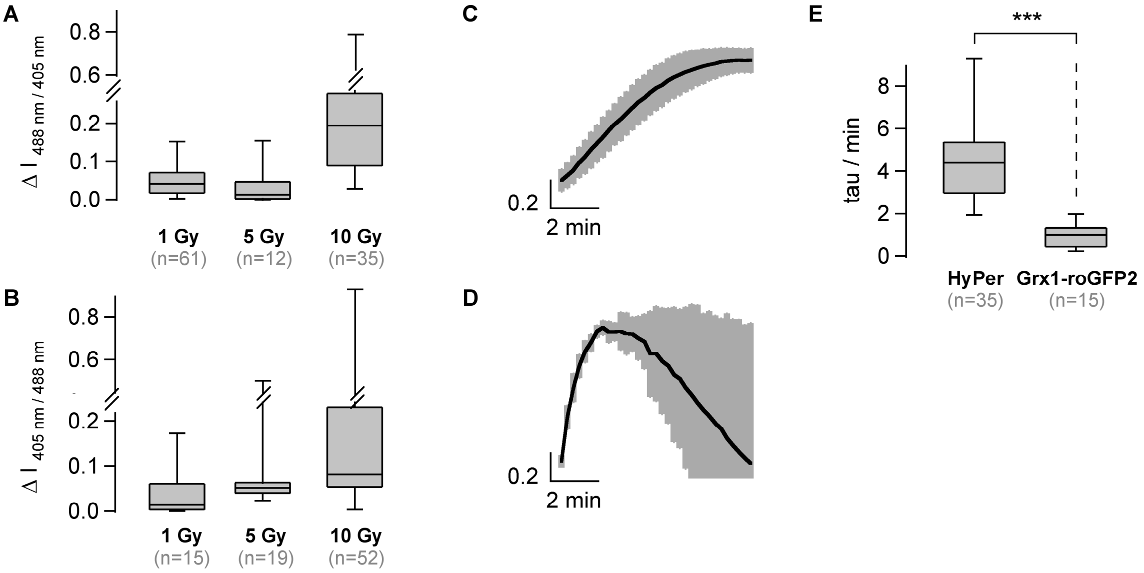

Fig. 41 **X-ray radiation induced ROS generation and buffering.**

The increase in ratiometric fluorescence signals of the reporter proteins of both, HEK293 and A549 cells, to IR stress with either 1 Gy, 5 Gy or 10 Gy X-rays is displayed as boxplots in A for the H_2O_2 sensor HyPer and in B for the glutathione sensor Grx1-roGFP2. The data were obtained from 3-6 independent experiments for the doses of 1 Gy and 10 Gy X-rays and from 1-2 independent experiments for 5 Gy of X-ray irradiation.

The kinetic of ROS generation in A549 cells was measured with HyPer (C; n=35; N=3) or Grx1-roGFP2 (D; n=15; N=2). Data were normalized to the minimal and maximal values of the respective ratios and shown as mean ± SD. All raw data from individual cells in C and D respectively were fitted with a single exponential function (equation 3) to obtain the time-constant τ, which is displayed in E for both ROS sensors (*** $p < 0.001$).

If we assume that the response time of the sensors to their respective signals is roughly the same this observation suggests that H_2O_2 rises after an oxidation of glutathione. A straight forward explanation for these data is that the initial rise in H_2O_2 concentration is dampened by the glutathione buffer in the cell. Only after the buffer capacity of the glutathione pool is exhausted H_2O_2 rises more strongly.

To test whether this explanation is feasible we simulated a simple two pool model in which we assume a constant glutathione (GSH) buffer concentration (dotted line) (Fig. 42 B). When a saturating burst of H_2O_2 was added to the system (arrow) the signal of the Grx1-roGFP2 sensor (grey), which represents the oxidized glutathione (GSSG), increases with a time-constant of 54 sec; this time-constant was estimated from the experimental data. The signal of the HyPer sensor (black), which represents the free, non-buffered H_2O_2 concentration in the system, increases much slower with a lag time and a time-constant of 252 sec. The time delay in this simple model is caused by the simplified assumption that only H_2O_2 is added to the system and oxidizes the GSH. In reality the cellular GSH pool is most likely oxidized by all kinds of ROS.

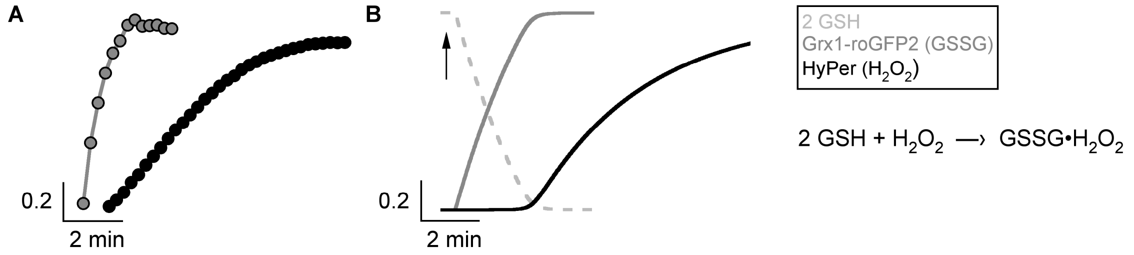

Fig. 42 **Simulation of the generation and buffering of H_2O_2.**

The normalized mean response of the H_2O_2 sensor HyPer (black) and the glutathione redox sensor Grx1-roGFP2 (grey) to 10 Gy of X-ray irradiation are displayed in A. The same dynamics of the two signals could be simulated in B with a kinetic model in which we assume that a saturating concentration of H_2O_2 was added to the system (arrow). The determined time-constants for Grx1-roGFP2 (54 sec) and HyPer (252 sec) from Fig. 41 were implemented to the simulation.

6.2. Generation of reactive oxygen species after heavy-ion irradiation

It has been mentioned in the introduction that sparsely irradiation by photons interacts differently with cells than irradiation with heavy-ions. To test whether ROS are also generated by heavy-ion particle irradiation cells expressing the HyPer reporter were measured at beamline microscope at UNILAC (GSI Helmholtzzentrum für Schwerionenforschung, Darmstadt, Germany). In these particular experiments cells were irradiated with lead- or carbon-ions. Exemplary responses of cells to lead irradiation (Pb; 4.7 MeV/u) are illustrated in Fig. 43 The data display that also this form of IR caused an increase in the HyPer signal implying a generation of H_2O_2. The increase in $I_{488\ nm\ /\ 405\ nm}$ ratio was again fitted by a single exponential function (equation 3) in order to determine the time-constant τ of H_2O_2 production. The curve fitting provided a mean time-constant τ of 1.3 ± 0.9 min (n=7; N=3) for the generation of H_2O_2 after heavy-ion irradiation.

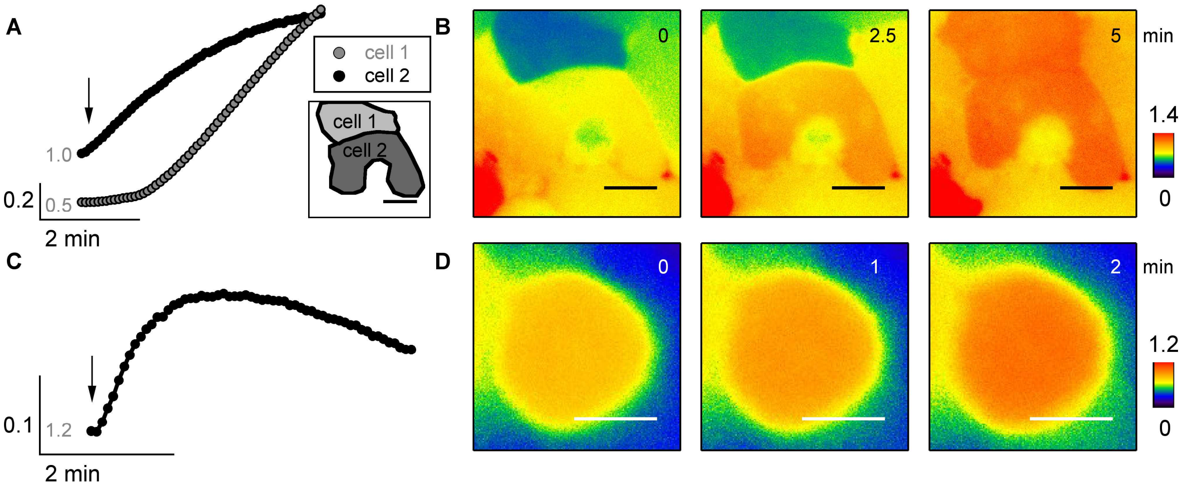

Fig. 43 **Generation of ROS after heavy-ion irradiation with Pb.**

HEK293 cells expressing the H_2O_2 reporter HyPer were irradiated with Pb (4.7 MeV/u) (arrow). They exhibited a fast increase in $I_{488\ nm\ /\ 405\ nm}$ ratio directly after irradiation, which indicates a rapid production of H_2O_2. The starting values of the $I_{488\ nm\ /\ 405\ nm}$ ratio are indicated in grey. The blue (=0) to red (=1.4 or 1.2) pseudocolored ratiometric images corresponding to A and C are displayed in B and D respectively (scale bar 10 µm).

The response of cells to carbon irradiation (C; 11.4 MeV/u) was rather variable. Only approximately 5 % out of 100 cells (N=3) irradiated with 10 Gy carbon-ions showed a response. The selected data in Fig. 44 nevertheless show that individual cells can respond to 10 Gy carbon irradiation (Fig. 44). The results of these experiments show that a generation of H_2O_2 after irradiation with heavy-ions is not obligatory; still cells are able to respond with an increase in the redox signal after irradiation stress. The pertinent question on why only a few cells showed a response to a high dose of carbon particle irradiation remains unanswered. Still the combined data from stimulations with lead- and carbon-ion irradiation demonstrate that also heavy-ion irradiation caused measurable elevations of H_2O_2 in cells.

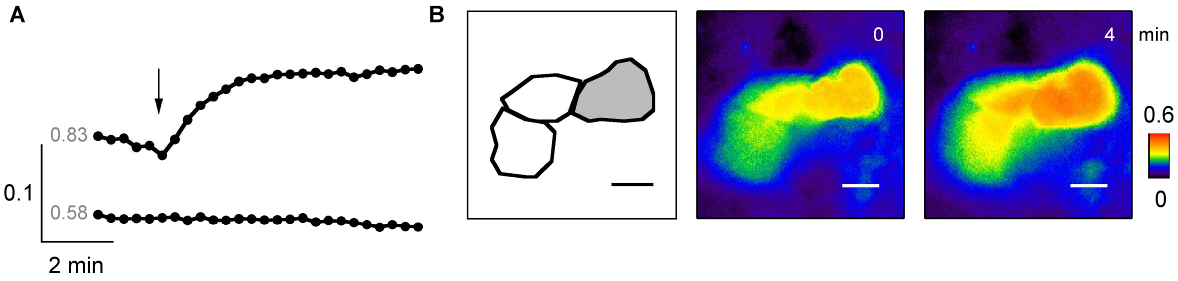

Fig. 44 **Generation of ROS after irradiation with carbon-ions.**

A549 cells expressing the H_2O_2 reporter HyPer were irradiated with carbon-ions (11.4 MeV/u) (arrow). Only few cells exhibited in this case an increase in $I_{488\ nm\ /\ 405\ nm}$ ratio after particle irradiation. This implies that a production of H_2O_2 is not mandatory after carbon-ion treatment. The time-course of the $I_{488\ nm\ /\ 405\ nm}$ ratio of a responding cell and a non-responding cell are shown in A; the starting values of the $I_{488\ nm\ /\ 405\ nm}$ ratio are indicated in grey. The blue (=0) to red (=0.6) pseudocolored ratiometric images before and at the maximal response after irradiation corresponding to the upper graph in A are shown in B (grey cell) (scale bar 10 µm).

In summary I could demonstrate and measure the real-time generation of ROS *in vivo* after X-ray irradiation as well as heavy-ion irradiation. This findings support the hypothesis that the amount of ROS, which are primarily produced after irradiation, are sufficient to trigger signal cascades that finally activate ion-channels. Already the effect of 1 Gy X-rays on the H_2O_2 concentration in cells was measurable with the HyPer reporter; and the analyses of higher doses of X-ray irradiation revealed new insights about the kinetics of primary ROS generation. Cells apparently have an active redox-buffer system; the operation of this buffer system can be monitored with the glutathione redox sensor Grx1-roGFP2. The experimental data and the simulation of the interplay between GSH, GSSG and H_2O_2 suggest, that the rise in H_2O_2 after IR stress is initially damped by the cellular redox-buffer. Only when the buffer is exhausted ROS increase strongly. The amount of H_2O_2, which is generated by IR stress, is sufficient to saturate the buffer and to cause a significant increase in the concentration of H_2O_2 in cells.

The results obtained by this experiments enable a new point of view on ROS induced signal cascades in cells, which were stressed by IR. The present data provide for the first time information on the very early events, which follow different qualities of ionizing radiation.

7. Discussion

The goal of this thesis was to elucidate the signal transduction cascade, which connects primary effects of ionizing irradiation in cells with the activation of the human intermediate-conductance calcium-activated potassium (hIK) channel. The main findings, which I report here, support a model according to which a pulse of ionizing radiation (IR) induces a rapid and transient burst of reactive oxygen species (ROS) not only in the nucleus but also in the cytoplasm. This elevation of ROS in the cytoplasm triggers a rise in the concentration of free Ca^{2+} in the cytosol (later termed as $[Ca^{2+}]_{cyt}$), which can lead to oscillations or a sustained raise of the cytosolic calcium concentration. The elevation of the second messenger Ca^{2+} is sufficient to activate the hIK channel. The latter causes an elevated potassium (K^+) conductance and a membrane hyperpolarization, a well known signal for cell cycle regulation. This working hypothesis is summarized in a sketch in Fig. 45.

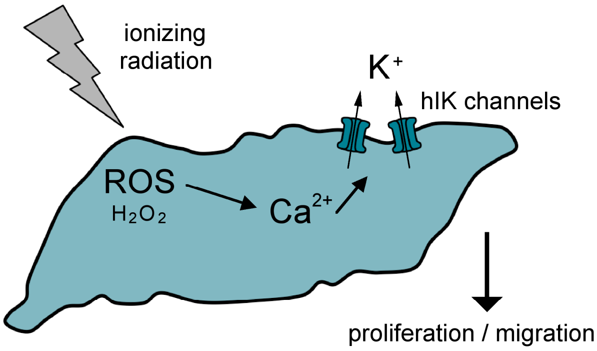

Fig. 45 **ROS and Ca^{2+} mediated signal cascade activating the hIK channel after ionizing radiation.**

The sketch summarizes the signal cascade, which was determined in this thesis, leading to the activation of hIK channels upon ionizing radiation (IR). IR induces a rapid burst of ROS in the cytoplasm. These ROS, especially the known signal molecule H_2O_2 stimulates a rise of the cytosolic calcium concentration, which subsequently activates intermediate-conductance calcium-activated K^+-channels. The membrane hyperpolarization is caused by an elevated K^+ conductance. The events, which are triggered by the hyperpolarization, affect cell differentiation.

7.1. Radiation, ROS and Ca^{2+} induced hIK channel activation and membrane hyperpolarization

After it had been discovered that ion-channels are involved in cell differentiation and that they have an impact on apoptosis, cell proliferation and cell migration, it became also apparent that they play a role in cancer development (Becchetti, 2011; Kunzelmann, 2005; Wang, 2004; Wonderlin & Strobl, 1996). Because of this importance of ion-channels in cell differentiation, also researchers in radiation biology addressed the question on whether IR has effects on ion-channel activity and if this may interfere with cell differentiation. Some isolated reports suggest that this is indeed the case. It was for example reported that the activity of voltage-gated Kv3.4-like channels had been induced in response to IR. This caused a G_2/M cell cycle arrest in K562 human erythroid leukemia cells (Palme *et al.*, 2013). Furthermore already in the early 90th it was found that γ-irradiation caused in A549 cells an activation of K^+-channels (Kuo *et al.*, 1993). With new methods, which are now available for recording channel activity with a high temporal resolution after IR stress and with information on the molecular nature of ion-channels in cells it was recently shown that X-rays, α-particles and heavy-ion irradiation trigger the activation of an interesting type of K^+-channels, namely the hIK channel in A549 cells. (Roth, 2013). The data show that the activation of this channel is a very early response to IR; it occurs within the first few minutes after irradiation. The fact that the hIK channel is the channel, which is responding to IR, was underscored with the help of channel blockers and by expression studies (Roth, 2013). The results of these experiments were confirmed in the present study by additional inhibition experiments with the specific hIK channel inhibitor Clotrimazole (CLT), which was used effectively at submicromolar concentrations (Pedarzani & Stocker, 2008; Wulff *et al.*, 2000, 2001).

The results of a previous study implied that only those cells, which functionally expressed hIK channels, were responding to IR with an increase in K^+ conductance. This hypothesis was confirmed in the present study. The hIK channel was therefore transiently expressed in HEK293 cells, e.g. cells, which are in their wildtype (wt) form insensitive to IR (Roth, 2013). The test experiments confirmed that the hIK channels were functionally expressed in these cells. The instantaneous current component of the transfected cells was blocked by the specific inhibitor CLT. Furthermore the typical hIK-like conductance could be activated in transfected HEK293 cells by increasing of the $[Ca^{2+}]_{cyt}$. This was achieved either by perfusing the internal solution or by adding the calcium ionophore Ionomycin to the bath solution. In both cases the rise in $[Ca^{2+}]_{cyt}$ augmented a hIK typical, quasi linear conductance in the voltage range between about -60 and +20 mV with a characteristic negative slope at high positive voltages. The results of these experiments confirmed that the hIK channel exhibits in HEK293 cells the same functional features as in native cell, which express this type of channel endogenously.

One major finding in the present study was that HEK293 cells, which are with respect to the membrane conductance in their wt form IR insensitive, become sensitive when they express the hIK channel. The data show that an irradiation of the transfected cells with 1 Gy X-rays caused an increase in the typical hIK conductance; the IR induced increase in conductance in these cells is the same as that induced by an elevation of $[Ca^{2+}]_{cyt}$. The results of these experiments underline, that the signal transduction upstream of the hIK channel is the same in HEK293 cells and A549 cell. The major difference between the IR sensitive A549 cells and the IR insensitive HEK293 cells is the presence or absence of hIK channels respectively in these two cell types.

Even though a direct redox regulation of ion-channels was described for instances for a K_{ATP} channel (Bao *et al.*, 2005) or for hERG channels (Bérubé *et al.*, 2001), there are no hinds in the literature for redox sensitive amino-acids in hIK channels. This suggests that the regulation of the hIK channel after IR stress is not direct. This view is supported by the finding that the channels only react after a short lag time; this implies a radiation induced signal cascade, which finally activates hIK channels. Kuo and coworkers (1993) already speculated about the impact of ROS in the context of radiation induced channel activation. The present data now show that the IR induced K^+ conductance in A549 cells was indeed also induced by a treatment of the cells with external applied H_2O_2. This H_2O_2 activated conductance was blocked by the hIK specific inhibitor CLT, indicating that the same channels are activated by ROS, IR and Ca^{2+} (Roth, 2013). A similar H_2O_2 induced activation of hIK channels was demonstrated in HEK293 cells, which overexpress these channels. The contribution of the hIK channels to the redox regulation in A549 cell is further supported by the finding that the same channel also activates when expressed heterologously in HEK293 cells quasi immediately after addition of H_2O_2 to the external solution; this reaction is the same of the hIK channel in A549 cells. Important for the focus of the present study is that HEK293 cells, which overexpressed hIK channels, are activated in a time window of 3-12 minutes after 1 Gy of X-ray irradiation. This kinetics of channel activation in response to IR is the same as in A549 cells, which natively express hIK channels (Roth, 2013). The results of these experiments support the hypothesis that the presence of hIK channels renders cells sensitivity to IR; they furthermore indicate that ROS are involved in this process.

The response of A549 cells to H_2O_2 was very heterogeneous and only 65 % of the cells exhibited a clear cut activation of the hIK channel after treatment with concentrations between 300 nM and up to 300 µM H_2O_2. A plot of the response to H_2O_2 as a function of the free running membrane potential (V_m) prior to the treatment indicates a causal relation between these parameters (Fig. 12 B). Most of the 35 % of cells, which were not responding to H_2O_2, had a hyperpolarized V_m. This suggests that these cells were proliferating (Wonderlin & Strobl, 1996). A similar fraction of A549 cells was also found to be insensitive to X-ray irradiation (Roth, 2013). The fraction of responding cells, which was found here, matches well with the estimate of 65 % of A549 cells in the resting state in an unsynchronized population, the latter was quantified by flow cytometric measurements (Roth, 2013). From the combination of these results it is reasonable to speculate that only resting A549 cells with a depolarized V_m and a low impact of the hIK channel to the instantaneous current component, are sensitive to externally applied ROS (H_2O_2) or IR induced ROS.

The previous finding that hIK channel activation by IR is reduced when the Ca^{2+} buffer concentration is increased has already indicated that $[Ca^{2+}]_{cyt}$ is involved in the signal cascade between IR and K^+ activation (Roth, 2013). I could here verify the anticipated changes in $[Ca^{2+}]_{cyt}$ in both HEK293 and A549 cells after treatment with external H_2O_2. Even though the calcium signals varied on a cell to cell basis, H_2O_2 robustly caused in almost all cells an increase in $[Ca^{2+}]_{cyt}$, which started after a short lag time; a maximal increase in $[Ca^{2+}]_{cyt}$ was seen after about 15 to 20 minutes of stimulation. The ability of low, supraphysiological levels of H_2O_2 to trigger a rise in $[Ca^{2+}]_{cyt}$ was already demonstrated previously. But in these studies neither the physiological relevance nor the mechanism, which is underlying this phenomenon were known (Stone & Yang, 2006).

For experimental reasons it was here not possible to analyze the response of $[Ca^{2+}]_{cyt}$ to IR e.g. X-rays or heavy-ions directly. Hence, we can only speculate that the ROS, which are generated in the cytoplasm in response to X-ray radiation will be sufficient to trigger an elevation of $[Ca^{2+}]_{cyt}$. A direct monitoring of $[Ca^{2+}]_{cyt}$ in response to X-ray or heavy-ion irradiation will be desirable in the future, because irradiation seems to stimulate $[Ca^{2+}]_{cyt}$ in some cells, but not in others (Chen *et al.*, 2013a; Du *et al.*, 2008; Szumiel *et al.*, 1990; Todd & Mikkelsen, 1994)

7.2. Real-time detection of ROS after ionizing radiation

A key topic of this thesis was the monitoring of changes in ROS following IR in real-time and with subcellular resolution. For an ionizing stimulation different types of radiation were employed: 1) 405 nm UV-laser micro-irradiation, 2) X-ray irradiation and 3) low-LET heavy-ion irradiation. To follow the dynamic changes in the concentration of ROS in cells after irradiation stress, the ROS species H_2O_2 was monitored with the fluorescence sensor protein HyPer. This sensor enables the detection of this single, long-lived ROS. H_2O_2 is interesting in the context of hIK channel activation, because H_2O_2 was able to enhance $[Ca^{2+}]_{cyt}$ as well as to activate hIK channels independent of the cell type. Following the generation of H_2O_2 after IR is also interesting in general terms, because it is already known to act as a signal molecule when it is present in physiological concentrations in the cell (Forman *et al.*, 2010; Marinho *et al.*, 2014; Rhee *et al.*, 2005; Rojkind *et al.*, 2002; Stone & Yang, 2006; Veal *et al.*, 2007).

The control experiments show that the HyPer sensor is indeed suitable for measuring H_2O_2 after IR stress. The sensor responds in a robust manner to an elevation of the cytosolic H_2O_2 concentration, which is achieved by adding the membrane permeable H_2O_2 to the bath medium of cells. As in the case of many other sensors the *in vivo* calibration of HyPer is not identical to the *in vitro* calibration of the sensor (Borzak *et al.*, 1990; Boyarsky *et al.*, 1988; Martinière *et al.*, 2013). The *in vivo* calibration provides a value for the half-maximal increase in $\Delta I_{488\ nm\ /\ 405\ nm}$ (K_{ox}) of 31.3 µM. This value is ca. 200 fold higher than the corresponding value from the *in vitro* calibration (Belousov *et al.*, 2006). The discrepancy between *in vivo* and *in vitro* calibration data in this study is in agreement with recent reports from the literature (Belousov *et al.*, 2006; Bilan *et al.*, 2013; Malinouski *et al.*, 2011). One mechanism, which presumably contributes to the difference between the two calibration methods, is the concentration difference between H_2O_2 in the bath and in the cell, which is caused by a reduced permeability of the membrane (Antunes & Cadenas, 2000; Cordeiro, 2014). A further factor, which contributes to the large difference between *in vivo* and *in vitro* calibration can be ascribed to the potent redox-buffer system in the cells (Marinho *et al.*, 2013). The present data show how the HyPer signal is first increasing and then decreasing after challenging cells with extracellular H_2O_2. These data underline that the intracellular concentration of H_2O_2 must be significantly lower than that in the external medium. An additional factor, which cannot be controlled by the experimenter, is that the fluorescence properties of GFP-based proteins could be sensitive to the milieu inside a cell. It is well established that the signal of GFP-based fluorescence proteins is influenced by the pH (Llopis *et al.*, 1998; Straight, 2007; Zou *et al.*, 2005). This pH sensitivity is also well known for the HyPer sensor (Belousov *et al.*, 2006; Bilan *et al.*, 2013; Ermakova *et al.*, 2014; Lukyanov & Belousov, 2013). At this point it is impossible to really translate the fluorescence signal of the HyPer sensor into accurate concentrations of H_2O_2 inside the cell. As a first approximation the *in vitro* calibration of the sensor can be used because there are good experimental reasons, which indicate that the *in vivo* calibration is an underestimation of the real affinity of the sensor to H_2O_2.

The lack of accuracy in the HyPer calibration can also be circumvent here by an indirect approach. The present experiments show that an application of 200 µM H_2O_2 to the external buffer solution causes a signal in the HyPer sensor, which is in the same order of magnitude as that which is generated by IR stress. The fact that 200 µM H_2O_2 in the external solution are also able to trigger a Ca^{2+} increase in cells and to activate hIK channels suggests that the same rise in H_2O_2, which is generated by IR will also elicit a rise in Ca^{2+}. If we consider the *in vitro* calibration as a basis of the quantification, we can conclude that the H_2O_2 concentration, which is required to induce a calcium signals in A549 and HEK293 cells, is about 1 µM inside the cell. This value is in the range of that described in the literature for signaling purpose of H_2O_2 (Boveris & Cadenas, 2000; Freinbichler *et al.*, 2011).

The present data provide for the first time an insight into ROS signals, which occur immediately after IR stress on a single-cell level. They demonstrate that 405 nm UV-laser micro-irradiation generates a rapid burst of H_2O_2 in the irradiated compartment independent of the type of cells, which was stressed. These data again confirm that the difference in sensitivity of different types of cells cannot be explained by a difference in the signal cascade upstream of the hIK channel. Both cell types respond in the same manner to the stress suggesting that the generation of H_2O_2 is a genuine response of cells to this kind of stress. The experiments show an increase in the HyPer $\Delta I_{488\ nm\ /\ 405\ nm}$ ratio of 0.1 after approximately 2 mJ/µm² of deposed laser-energy. This corresponds to a stress of cells with 8 µM of external H_2O_2. Using the *in vitro* calibration these data can be converted into an increase of the internal H_2O_2 concentration to 40 nM. The H_2O_2 concentration, which is induced in this manner, is in the same range as the previously mentioned H_2O_2 concentrations, which were necessary to induce calcium signals and to trigger ion-channel activation. It is worth mentioning again that the amount of H_2O_2, which was measured by HyPer, can only be used as an estimate, because HyPer competes with the powerful redox-buffer system in the cell (Meyer & Dick, 2010). However, since the reaction rate of HyPer is very fast (10^5 M^{-1} s^{-1}) (Bilan *et al.*, 2013) it is still reasonable to assume that the measured amounts of H_2O_2 is relatively close to that, which is required for signaling properties of H_2O_2.

In a previous study HaCaT keratinocytes were irradiated with UVA up to 4 J/cm² and ROS generation was measured with the chemical dye DCF. In this study a similar amount of ROS production was observed when the cells were treated with 10 mM external H_2O_2 for 90 minutes (Chignell & Sik, 2003). The laser energy, which was used in the latter study was 10.000 times smaller than the one used here. But it is difficult to compare micro-irradiation with whole-cell irradiation, since micro-irradiation causes a very high local in the irradiated subcompartment (Ferrando-May *et al.*, 2013) but no laser energy is deposed in the rest of the cell.
The UV micro-irradiation approach has the advantage that the cells can be stimulated with high precision and subsequently monitored with a high spatial resolution. A disadvantage is the difficulty of defining the local dose of a UV-light treatment (Splinter *et al.*, 2010). A further difference between UV- and X-ray irradiation is that the former has a lower energy than X-rays. UV-light is unlike X-rays absorbed by different molecules. It is presumably not sufficiently strong for the radiolysis of water and may produce different responses in radicals.

There are several reasons to believe that the rise in H_2O_2 concentration after a low dose of UV-irradiation is an overestimation of the real situation. It is well established that an illumination of the DCF dye with high-energy light causes an artificial production of ROS; the oxidation of DCFH to DCF is not reversible meaning that the DCF molecule accumulates over time. All this contributes to an overestimation of the real dynamics of H_2O_2 changes in cells. The application of DCF derivatives is altogether controversy discussed in the literature (Afzal *et al.*, 2003; Bonini *et al.*, 2006; Boulton *et al.*, 2011; Chen *et al.*, 2010; Karlsson *et al.*, 2010; LeBel *et al.*, 1992; Rota *et al.*, 1999). It is recommended to perform experiments in PBS rather than culture medium; this should avoid the generation of extracellular ROS (Boulton *et al.*, 2011), which can, after diffusion into the cell, contribute to the cellular signal. Furthermore it has also been proven that light irradiation of DCF results in an artificial ROS production independent of the presence of radicals. Hence, the data on ROS signals, which were measured with DCF derivatives, have to be considered with caution. The multiple control experiments in this study, which show that the HyPer sensor is very stable and not artificially corrupted by the stimulating conditions, underline that this protein-based sensor is the method of choice for measuring H_2O_2 concentrations in cells. One of the few disadvantages of the HyPer sensor is that it exhibits a sensitivity to pH (Belousov *et al.*, 2006; Bilan *et al.*, 2013; Ermakova *et al.*, 2014; Lukyanov & Belousov, 2013). The control experiments, in which I used a H_2O_2 insensitive variant of HyPer, show that the irradiation stress has no impact on the cellular pH. Hence, the HyPer signal that is generated by irradiation, is most likely the response of an elevation of H_2O_2. This conclusion is further supported by experiments in which the radical scavenger N-acetylcysteine (NAC) was able to suppress an increase in the HyPer signal after UV light stress.

An interesting observation in the present study was that the HyPer signal, which evolved in response to laser micro-irradiation was mostly confined to the irradiated compartment; the elevated HyPer signal was either in the nucleus or the cytoplasm depending on which compartment was irradiated. The data furthermore show that the same dose of laser light causes a much higher HyPer signal in the nucleus compared to the cytosol. These data are not that remarkable when we consider that the nucleus is much more tightly packed with IR absorbing molecules (e.g. DNA) than the cytosol. Even if the DNA bases do not absorb the light at the wavelength of 405 nm (Voet *et al.*, 1963), which was used here, it is still possible that DNA damage occurs when a small volume is irradiated with a high photon density (Ferrando-May *et al.*, 2013). The ROS molecules, which are formed in this primary photo-ionization event, can then recombine to H_2O_2. Moreover, endogenous sensitizers in the cytosol and in the nucleus can support the production of ROS under the influence of near UV-laser. Responses, which are elicited by UVA light are oxygen dependent, indicating that UVA mediated DNA damage is a secondary event due to oxidative stress (Girard *et al.*, 2011). But new observations summarized by Girard and coworkers (2011) strongly suggest that UVA photons are directly absorbed by the DNA and induce base damage; it appears as if the low energy of UVA is sufficient to directly excite DNA.

The origin of ROS in the cytosol in response to UV-irradiation is more difficult to explain. On the one hand the cytoplasm is fully packed with proteins, RNA molecules and other substances, which could act as target for ionization reactions like in the case of DNA in the nucleus. Some researchers also suggest that ROS are produced by irradiation of photosensitive chromophores in mitochondria by light in the range of 400-500 nm. In these studies ROS were measured, which leaked from the mitochondria. The ROS were in these cases measured with the aforementioned DCF dye; the dye signal could additionally be correlated with increased levels of calcium in the mitochondria after irradiation (Jou *et al.*, 2002, 2004; Peng & Jou, 2004). Other groups reported a similar generation of ROS, which originated from the mitochondria and which caused apoptosis, as a response to different qualities of light from the visible spectrum. The data from these studies collectively indicate that mitochondria could provide the source for ROS production following irradiation with UV or near UV light (Huang *et al.*, 2011; Wu *et al.*, 2007). The published data on ROS production in mitochondria can however not be directly compared to the present results. The aforementioned effects of an increase of ROS after laser irradiation occurred in most cases only about 1 hour after the stress. In the present study the ROS signal was detected immediately after irradiation. Also the ROS response to irradiation, which is shown here was only transient and lasted only a few minutes. Taken together the present data imply that the ROS, which are measured immediately after irradiation are not originating from mitochondria. This conclusion is further supported by additional experiments. The direct irradiation with 405 nm laser micro-irradiation of mitochondria, revealed similar changes in the HyPer $\Delta I_{488\ nm\ /\ 405\ nm}$ ratio as a random irradiation of the cytoplasm (data not shown).

It is known that glutathione modulates the free level of ROS after UVA irradiation (Tobi *et al.*, 2000). Furthermore glutathione it is the most abundant cellular thiol (Circu & Aw, 2008; Dooley *et al.*, 2004; Rojkind *et al.*, 2002; Valko *et al.*, 2006) and therefore one of the major defense mechanisms of cells to cope with redox-stress. On that account I employed another sensor (Grx1-roGFP2), which is measuring the glutathione redox-potential. If we assume that all types of ROS molecules will eventually be directly or indirectly buffered by glutathione the signal of the senor will report the sum of all ROS, which will end up in the buffer.

The data show that the redox-buffer is indeed responding to redox stress such as H_2O_2 treatment. Most surprising, however, was the observation that the fluorescence ratio for this sensor (Grx1-roGFP2) displayed after micro-irradiation a fast and distinct increase in the nucleus independently on the compartment, which was irradiated. Even after a robust irradiation of the cytosol with UV light the sensor lights up in the nucleus and only marginally in the cytoplasm. These results are difficult to interpret. One possible explanation would be that the redox-buffer capacity in the nucleus is higher than in the cytosol. Some evidence in support for this hypothesis comes from the finding that some cells had a higher extent of oxidized glutathione (GSSG) in the nucleus than in the cytosol after adding H_2O_2 to the external solution. Additional evidence comes from data with the HyPer sensor, which show that some cells are able to clear H_2O_2 faster from the nucleus than from the cytosol (Fig. 27 B). These data can be best explained if the HyPer signal decreases because the buffer regenerates the resting level of H_2O_2 (Belousov *et al.*, 2013; Meyer & Dick, 2010). These findings are in agreement with studies, which imply that the nucleus is more reducing than the cytoplasm and that this is a consequence of GSH (Cotgreave, 2003; Hansen *et al.*, 2006).

Since not all the cells, which were analyzed, displayed this behavior we have to assume that also other factors can be involved in the process of redox-buffering. One possibility is that the nuclear GSH pool may change during the cell cycle; this has been shown for proliferating cells (García-giménez *et al.*, 2013; Markovic *et al.*, 2007, 2010; Pallardó *et al.*, 2009; Schroeder *et al.*, 2007). The capacity to cope with redox stress, which changes with the cell cycle, may influence further signal pathways and stress responses.

Little was in the past known about the generation of primary ROS after X-ray irradiation in living cells. Only a few studies demonstrated an *in vivo* generation of ROS after IR. The ROS were in these studies mostly monitored in a time window between 20 minutes and up to several hours after X-ray IR (Ameziane-El-Hassani *et al.*, 2010; Hafer *et al.*, 2008; Iyer & Lehnert, 2002; Korystov *et al.*, 2007; Narayanan *et al.*, 1997; Ogura *et al.*, 2009; Tominaga *et al.*, 2004). These late ROS effects to X-ray irradiation were presumably triggered by release of ROS from mitochondria in response to this stress (Leach *et al.*, 2001; Ogura *et al.*, 2009; Valerie *et al.*, 2007; Yamamori *et al.*, 2012). In one case ROS were also measured with a population of cells within the first 3-5 min after X-ray irradiation and the data report an X-ray induced rise in cellular ROS (Leach *et al.*, 2001). But all of these studies used DCF dyes for measuring ROS and had to cope with the aforementioned disadvantages of the dye; this includes artificial signal amplification, a high cellular ROS background, no reversibility and accumulation of the signal over time.

Here it was possible to monitor for the first time with real-time recordings the development of ROS in living cells before and directly after irradiation. The data provide the kinetics and a good spatial resolution of this event on the level of single-cells. These measurements were made possible by a custom build X-ray microscope setup at GSI (Helmholtzzentrum für Schwerionenforschung, Darmstadt, Germany). This setup allows a real-time observation of cells before, during and after X-ray irradiation. By using again the HyPer sensor it was possible to observe measurable amounts of H_2O_2 production in cells even after 1 Gy of X-ray irradiation.

When cells were challenged with a higher dose of 10 Gy X-rays the HyPer signal was larger and showed a better signal to noise ratio. Form these data it was possible to extract the kinetics of the ROS production; the data reveal that H_2O_2 increases continuously with a maximal increase about 5 to10 minutes after IR. The same kind of measurements with the Grx1-roGFP2 sensor show that the latter signal also increases under the influence of X-ray stress; but the signal is about 5 times faster than the HyPer signal and precedes the latter. A reasonable speculation is that the high redox-buffer capacity of the cell prevents an initial rise in H_2O_2. Only when the buffer is exhausted H_2O_2 can increase in the cell. A simple simulation with a model, which considers an interplay of the redox-buffer and the dynamics of H_2O_2 evolution, and which uses the kinetic data from the experiments, confirmed that this scenario is reasonable. One important message of these data is that redox-buffering is very fast in cells and that the buffer can also be exhausted if the amount of ROS is high like under X-ray irradiation. The high redox-buffer capacity of cells also poses the question on how a low doses of radiation e.g. a dose below 1 Gy, can generate sufficient H_2O_2 for activating hIK channels. In a previous study it was found that even X-ray doses in the cGy range were able to stimulate activation of hIK channels (Roth, 2013). One possible explanation for the efficiency of X-rays to activate hIK channels even at low doses is that H_2O_2 acts most likely very locally in cells (Mishina *et al.*, 2011). These local effects may evade detection by the fluorescence sensors but may still be sufficient for initiating calcium signaling.

A summary of the present data and of data, which are concerned with the activation of the hIK channel, provide a detailed insight into the sequence of events and on a possible causal relation in the signal transduction cascade proposed in Fig. 45. The data in Fig. 46 B show that IR causes an immediate rise in ROS in the cell. These initial ROS are buffered by a glutathione redox-buffer system. When the buffer is exhausted, the concentration of ROS including that of H_2O_2 increases. This rise in H_2O_2 is directly followed by an increase in $[Ca^{2+}]_{cyt}$ (Fig. 46 A). Because of the Ca^{2+} sensitivity of the hIK channel the rise in Ca^{2+} falls together with an increase in the activation of hIK channels.

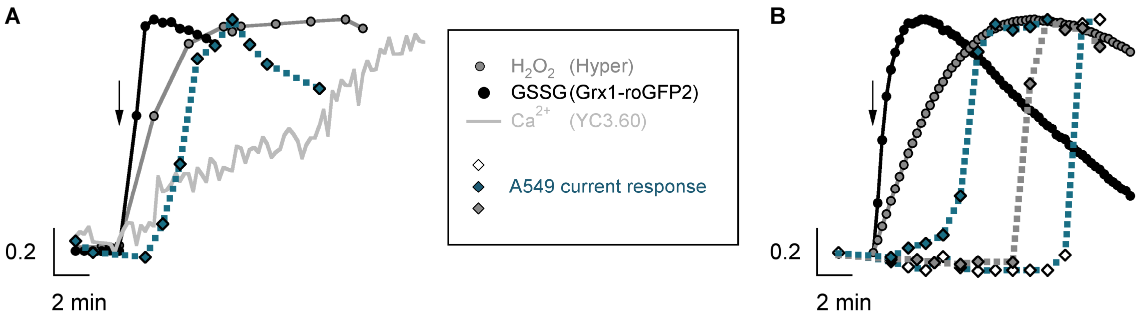

Fig. 46 **Time-course of ROS and Ca^{2+} signaling leading to an increased K^+ conductance of hIK channels.**

Summary of the main data of this thesis. The mean signals of the fluorescence sensors and the single-cell current response after treatment with H_2O_2 (A) or X-ray irradiation (B) were normalized to the value before treatment (=0) and their maximal increase (=1).

The A549 current responses after X-ray irradiation are from Roth (2013).

7.3. Cellular and physiological consequences of ionizing radiation induced hIK channel activation

The physiological impact of IR induced hIK channel activation was previously demonstrated: it occurred that low dose X-ray IR presumably stimulates cell proliferation and migration. At least in A549 cells IR does not induce apoptosis (Akino *et al.*, 2009; Roth, 2013). High doses on the other hand reduced migration and invasion (Akino *et al.*, 2009). Heavy-ion carbon irradiation had no stimulative effect on proliferation (Akino *et al.*, 2009). The latter data are in accordance with the observation that low-LET heavy-ion radiation (from the UNILAC at GSI) had no significant impact on the K^+ conductance in A549 cells (Roth, 2013). Here I could demonstrate that low-LET heavy-ion irradiation caused only in a minor fraction of cells an increase in the concentration of ROS. These data are in agreement with experiments, which show that heavy-ion irradiation had no impact on $[Ca^{2+}]_{cyt}$ in several cell lines (Du *et al.*, 2008). Collectively these data indicate significant differences between radiation qualities and here in particular between high- and low-LET heavy-ion irradiation.

Calcium-activated K^+-channels, especially hIK channels, are delineated to numerous functions in many different cell types. One interesting example regarding the impact of IR is their involvement in a mechanism called epithelial-mesenchymal transition (EMT), which is reported as a potential reason for the radio-resistance of cancer cells and as a cause of lung fibrosis; the latter is a negative side-effect of cancer radiotherapy (Gomez-Casal *et al.*, 2013; Gorowiec *et al.*, 2012; Jung *et al.*, 2007; Kargiotis *et al.*, 2010; Kim *et al.*, 2007; Wu, 2006; Zhou *et al.*, 2011). Furthermore hIK channels are well known for their role in lymphocyte activation (Fanger *et al.*, 1999; Jensen *et al.*, 2002; Tharp & Bowles, 2013) and it was previously demonstrated that low dose IR in the cGy range was able to stimulate hIK channels and therefore activate lymphocytes (Roth, 2013). These findings might have an impact on the understanding of the mechanisms of low dose radiation treatment or radon inhalation therapy; these are common therapeutical approaches in the treatment of inflammatory diseases.

Finally, the recent discovered role of hIK channels in migration of glioblastoma cells are of particular interest in context of IR induced channel activation (D'Alessandro *et al.*, 2013; Huber, 2013; Ruggieri *et al.*, 2012; Schwab *et al.*, 2012). Glioblastoma multiforme (GBM) is the most common and aggressive form of brain tumor; it is characterized by a rapid growth, a high invasitity, a high radio-resistance and in a high recurrence after radiotherapy (D'Alessandro *et al.*, 2013; Watkins & Sontheimer, 2012). Until now the mechanisms leading to the radio-resistance of GBM are poorly understood. The results presented here regarding the radiation sensitivity of hIK channels, might give new insights into the mechanism, which is leading to the high radio-resistance and invasitity of the tumor cells.

7.4. Conclusion

In summary this thesis elucidates a mechanism on how ionizing radiation induces the activation of intermediate-conductance calcium-activated K^+-channels independent of the cell type. The general signal cascade, which was uncovered, includes H_2O_2 and Ca^{2+} as mediating signal factors. I could monitor for the first time the generation of ROS in real-time after different qualities of ionizing radiation in single living cells. The data indicate differences between the redox-buffer capacities in nucleus and cytoplasm, which might influence any further signal pathway. Furthermore the present results indicate differences between different qualities of IR like X-ray irradiation and low-LET heavy-ion radiation. Heavy-ion irradiation affected only some cells in contrast to X-ray irradiation, where all cells exhibited a robust signal, indicating the generation of ROS.

The radiation induced increase in H_2O_2 in both nucleus and cytosol is capable to induce a rise of the cytosolic calcium concentration, which in turn activates hIK channels and hyperpolarizes cells. The stimulation of this signal cascade is a very early response to IR and the associated membrane hyperpolarization has an important physiological impact on cell proliferation and migration. Hence, it is reasonable to assume that the discovery of this primary signal cascade offers new insights in possible mechanisms, which lead to invasion and metastasis of tumors and cancer radio-resistance.

8. References

Afzal, M., Matsugo, S., Sasai, M., Xu, B., Aoyama, K., & Takeuchi, T. (2003). *Method to overcome photoreaction, a serious drawback to the use of dichlorofluorescin in evaluation of reactive oxygen species.* Biochem. Biophys. Res. Commun., 304(4): 619–24.

Akino, Y., Teshima, T., Kihara, A., Kodera-Suzumoto, Y., Inaoka, M., Higashiyama, S., Furusawa, Y., & Matsuura, N. (2009). *Carbon-ion beam irradiation effectively suppresses migration and invasion of human non-small-cell lung cancer cells.* Int. J. Radiat. Oncol. Biol. Phys., 75(2): 475–81.

Ameziane-El-Hassani, R., Boufraqech, M., Lagente-Chevallier, O., Weyemi, U., Talbot, M., Métivier, D., Courtin, F., Bidart, J.-M., El Mzibri, M., Schlumberger, M., & Dupuy, C. (2010). *Role of H_2O_2 in RET/PTC1 chromosomal rearrangement produced by ionizing radiation in human thyroid cells.* Cancer Res., 70(10): 4123–32.

Anderson, M. E. (1998). *Glutathione: an overview of biosynthesis and modulation.* Chem. Biol. Interact., 111-112: 1–14.

Antunes, F., & Cadenas, E. (2000). *Estimation of H_2O_2 gradients across biomembranes.* FEBS Lett., 475(2): 121–6.

Antunes, F., Cadenas, E., & Brunk, U. T. (2001). *Apoptosis induced by exposure to a low steady-state concentration of H_2O_2 is a consequence of lysosomal rupture.* Biochem. J., 356: 549–555.

Anyigor, C., & Afiukwa, J. (2013). *Application of matlab ordinary differential equation function solver (ode45) in modelling and simulation of batch reaction kinetics.* Am. J. Sci. Ind. Res., 4(3): 285–287.

Asher, V., Sowter, H., Shaw, R., Bali, A., & Khan, R. (2010). *Eag and HERG potassium channels as novel therapeutic targets in cancer.* World J. Surg. Oncol., 8(1): 113.

Asher, V., Warren, A., Shaw, R., Sowter, H., Bali, A., & Khan, R. (2011). *The role of Eag and HERG channels in cell proliferation and apoptotic cell death in SK-OV-3 ovarian cancer cell line.* Cancer Cell Int., 11(1): 6.

Ay, A.-S., Benzerdjerb, N., Sevestre, H., Ahidouch, A., & Ouadid-Ahidouch, H. (2013). *Orai3 constitutes a native store-operated calcium entry that regulates non small cell lung adenocarcinoma cell proliferation.* PLoS One, 8(9): e72889.

Azzam, E. I., de Toledo, S. M., & Little, J. B. (2003). *Oxidative metabolism, gap junctions and the ionizing radiation-induced bystander effect.* Oncogene, 22(45): 7050–7.

Azzam, E. I., Jay-Gerin, J.-P., & Pain, D. (2012). *Ionizing radiation-induced metabolic oxidative stress and prolonged cell injury.* Cancer Lett., 327(1-2): 48–60.

Bao, L., Avshalumov, M. V, & Rice, M. E. (2005). *Partial mitochondrial inhibition causes striatal dopamine release suppression and medium spiny neuron depolarization via H_2O_2 elevation, not ATP depletion.* J. Neurosci., 25(43): 10029–40.

Becchetti, A. (2011). *Ion channels and transporters in cancer. 1. Ion channels and cell proliferation in cancer.* Am. J. Cell Physiol., 301(2): C255–65.

Begenisich, T., Nakamoto, T., Ovitt, C. E., Nehrke, K., Brugnara, C., Alper, S. L., & Melvin, J. E. (2004). *Physiological roles of the intermediate conductance, $Ca2^{+}$-activated potassium channel Kcnn4.* J. Biol. Chem., 279(46): 47681–7.

Belousov, V. V, Fradkov, A. F., Lukyanov, K. A., Staroverov, D. B., Shakhbazov, K. S., Terskikh, A. V, & Lukyanov, S. (2006). *Genetically encoded fluorescent indicator for intracellular hydrogen peroxide.* Nat. Methods, 3(4): 281–286.

Belousov, V. V., Enikolopov, G. N., & Mishina, N. M. (2013). *Compartmentalization of ROS-mediated signal transduction.* Russ. J. Bioorganic Chem., 39(4): 341–355.

Berkefeld, H., Fakler, B., & Schulte, U. (2010). *Ca^{2+} -Activated K^{+} Channels: From Protein Complexes to Function.* Physiol. Rev., 90: 1437–1459.

Berridge, M. J., Bootman, M. D., & Roderick, H. L. (2003). *Calcium signalling: dynamics, homeostasis and remodelling.* Nat. Rev. Mol. Cell Biol., 4(7): 517–29.

Berridge, M. J., Lipp, P., & Bootman, M. D. (2000). *The versatility and universality of calcium signalling.* Nat. Rev. Mol. Cell Biol., 1: 11–21.

Bérubé, J., Caouette, D., & Daleau, P. (2001). *Hydrogen peroxide modifies the kinetics of HERG channel expressed in a mammalian cell line.* J. Pharmacol. Exp. Ther., 297(1): 96–102.

Bi, D., Toyama, K., Lemaître, V., Takai, J., Fan, F., Jenkins, D. P., Wulff, H., Gutterman, D. D., Park, F., & Miura, H. (2013). *The intermediate conductance calcium-activated potassium channel $K_{Ca}3.1$ regulates vascular smooth muscle cell proliferation via controlling calcium-dependent signaling.* J. Biol. Chem., 288(22): 15843–53.

Bienert, G. P., & Chaumont, F. (2014). *Aquaporin-facilitated transmembrane diffusion of hydrogen peroxide.* Biochim. Biophys. Acta, 1840(5): 1596–604.

Bienert, G. P., Møller, A. L. B., Kristiansen, K. a, Schulz, A., Møller, I. M., Schjoerring, J. K., & Jahn, T. P. (2007). *Specific aquaporins facilitate the diffusion of hydrogen peroxide across membranes.* J. Biol. Chem., 282(2): 1183–92.

Bienert, G. P., Schjoerring, J. K., & Jahn, T. P. (2006). *Membrane transport of hydrogen peroxide.* Biochim. Biophys. Acta, 1758(8): 994–1003.

Bilan, D. S., Pase, L., Joosen, L., Gorokhovatsky, A. Y., Ermakova, Y. G., Gadella, T. W. J., Grabher, C., Schultz, C., Lukyanov, S., & Belousov, V. V. (2013). *HyPer-3: a genetically encoded H_2O_2 probe with improved performance for ratiometric and fluorescence lifetime imaging.* ACS Chem. Biol., 8(3): 535–42.

Blackiston, D. J., Mclaughlin, K. A., & Levin, M. (2010). *Bioelectric controls of cell proliferation.* J. Cell Biol., 8(21): 3519–3528.

Bogin, O. (2004). *Ion Channels and Cancer An updated overview.* Modulator, (18): 16–18.

Bonini, M. G., Rota, C., Tomasi, A., & Mason, R. P. (2006). *The oxidation of 2',7'-dichlorofluorescin to reactive oxygen species□: a self-fulfilling prophesy?* Free Radic. Biol. Med., 40(6): 968–75.

Borowiec, A.-S., Hague, F., Gouilleux-Gruart, V., Lassoued, K., & Ouadid-Ahidouch, H. (2011). *Regulation of IGF-1-dependent cyclin D1 and E expression by hEag1 channels in MCF-7 cells: the critical role of hEag1 channels in G1 phase progression.* Biochim. Biophys. Acta, 1813(5): 723–30.

Borzak, S., Kelly, R. a, Krämer, B. K., Matoba, Y., Marsh, J. D., & Reers, M. (1990). *In situ calibration of fura-2 and BCECF fluorescence in adult rat ventricular myocytes.* Am. J. Physiol., 259: 973–81.

Botchway, S. W., Reynolds, P., Parker, A. W., & O'Neill, P. (2010). *Use of near infrared femtosecond lasers as sub-micron radiation microbeam for cell DNA damage and repair studies.* Mutat. Res., 704(1-3): 38–44.

Boulton, S., Anderson, A., Swalwell, H., Henderson, J. R., Manning, P., & Birch-Machin, M. A. (2011). *Implications of using the fluorescent probes, dihydrorhodamine 123 and 2',7'-dichlorodihydrofluorescein diacetate, for the detection of UVA-induced reactive oxygen species.* Free Radic. Res., 45(2): 139–46.

Boveris, A., & Cadenas, E. (2000). *Mitochondrial Production of Hydrogen Peroxide Regulation by Nitric Oxide and the Role of Ubisemiquinone.* IUBMB Life, 50: 245–250.

Boyarsky, G., Ganz, M. B., Sterzel, R. B., & Boron, W. F. (1988). *pH regulation in single glomerular mesangial cells. I. Acid extrusion in absence and presence of HCO3-.* Am. J. Physiol., 255: C844–56.

Bradding, P., & Wulff, H. (2009). *The K $^{+}$ channels K Ca 3.1 and K v 1.3 as novel targets for asthma therapy.* Br. J. Pharmacol., 157(8): 1330–1339.

Brüggemann, A., George, M., Klau, M., Beckler, M., Steindl, J., Behrends, J. C., & Fertig, N. (2003). *High Quality Ion Channel Analysis on a Chip with the NPC © Technology.* Assay Drug Dev. Technol., 1(5): 665–73.

Brüggemann, A., Stühmer, W., & Pardo, L. A. (1997). *Mitosis-promoting factor-mediated suppression of a cloned delayed rectifier potassium channel expressed in Xenopus oocytes.* Proc. Natl. Acad. Sci. U. S. A., 94(2): 537–42.

Bubici, C., Papa, S., Dean, K., & Franzoso, G. (2006). *Mutual cross-talk between reactive oxygen species and nuclear factor-kappa B: molecular basis and biological significance.* Oncogene, 25(51): 6731–48.

Burdon, R. H., Gill, V., & Rice-Evans, C. (1989). *Cell proliferation and oxidative stress . PubMed Commons.* Free Radic. Res. Commun., 7(3-6): 149–59.

Burdon, R. H., & Rice-Evans, C. (1989). *Free radicals and the regulation of mammalian cell proliferation.* Free Radic. Res. Commun., 6(6): 345–58.

Camacho, J. (2006). *Ether à go-go potassium channels and cancer.* Cancer Lett., 233(1): 1–9.

Cannon, M. B., & Remington, S. J. (2006). *Re-engineering redox-sensitive green fluorescent protein for improved response rate*, 45–57.

Capiod, T. (2013). *The need for calcium channels in cell proliferation.* Recent Pat. Anticancer. Drug Discov., 8(1): 4–17.

Celesia, G. G. (2001). *Disorders of membrane channels or channelopathies.* Clin. Neurophysiol., 112(1): 2–18.

Chen, H., Ye, H., Meng, D.-Q., Cai, P.-C., Chen, F., Zhu, L.-P., Tang, Q., Zhi-Xiong, L., Zhou, Q., Jin, Y., Xin, J.-B., Tao, X.-N., & Ma, W.-L. (2013)a. *Reactive Oxygen Species and X-Ray Disrupted Spontaneous [Ca^{2+}]i Oscillation in Alveolar Macrophages.* Radiat. Res., 179(4): 485–492.

Chen, Y.-T. Y.-F., Chiu, W.-T., & Shen, M.-R. (2013)b. *Remodeling of calcium signaling in tumor progression.* J. Biomed. Sci., 20: 23.

Chen, Zhong, Z., Xu, Z., Chen, L., & Wang, Y. (2010). *2',7'-Dichlorodihydrofluorescein as a fluorescent probe for reactive oxygen species measurement: Forty years of application and controversy.* Free Radic Res, 44(6): 587–604.

Chignell, C. F., & Sik, R. H. (2003). *A photochemical study of cells loaded with 2',7'-dichlorofluorescin: implications for the detection of reactive oxygen species generated during UVA irradiation.* Free Radic. Biol. Med., 34(8): 1029–1034.

Choi, H., Kim, S., Mukhopadhyay, P., Cho, S., Woo, J., Storz, G., & Ryu, S. E. (2001). *Structural basis of the redox switch in the OxyR transcription factor.* Cell, 105(1): 103–13.

Circu, M. L., & Aw, T. Y. (2008). *Glutathione and apoptosis.* Free Radic Res, 42(8): 689–706.

Clapham, D. E. (1995). *Calcium Signaling.* Cell, 80: 259–268.

Clapham, D. E. (2007). *Calcium signaling.* Cell, 131(6): 1047–58.

Corbett, E. F., & Michalak, M. (2000). *Calcium, a signaling molecule in the endoplasmic reticulum?* Trends Biochem. Sci., 25(7): 307–11.

Cordeiro, R. M. (2014). *Reactive oxygen species at phospholipid bilayers: Distribution, mobility and permeation.* Biochim. Biophys. Acta, 1838(1): 438–44.

Cotgreave, I. (2003). *Analytical developments in the assay of intra- and extracellular GSH homeostasis: specific protein S-glutathionylation , cellular GSH and mixed disulphide compartmentalisation and interstitial GSH redox balance.* Biofactors, 17(1-4): 269–77.

Cruse, G., Duffy, S. M., Brightling, C. E., & Bradding, P. (2006). *Functional K$_{Ca}$3.1 K$^+$ channels are required for human lung mast cell migration.* Thorax, 61(10): 880–5.

Cruse, G., Singh, S. R., Duffy, S. M., Doe, C., Saunders, R., Brightling, C. E., & Bradding, P. (2011). *Functional $K_{Ca}3.1$ K^+ channels are required for human fibrocyte migration.* J. Allergy Clin. Immunol., 128(6): 1303–1309.e2.

D'Alessandro, G., Catalano, M., Sciaccaluga, M., Chece, G., Cipriani, R., Rosito, M., Grimaldi, a, Lauro, C., Cantore, G., Santoro, a, Fioretti, B., Franciolini, F., Wulff, H., & Limatola, C. (2013). *$K_{Ca}3.1$ channels are involved in the infiltrative behavior of glioblastoma in vivo.* Cell Death Dis., 4: e773.

Deutsch, C., Price, M., Lee, S., King, V. F., & Garcia, M. L. (1991). *Characterization of High Affinity Binding Sites for Charybdotoxin in Human T Lymphocytes.* J. Biol. Chem., 266(6): 3668–3674.

Dinant, C., de Jager, M., Essers, J., van Cappellen, W. a, Kanaar, R., Houtsmuller, A. B., & Vermeulen, W. (2007). *Activation of multiple DNA repair pathways by sub-nuclear damage induction methods.* J. Cell Sci., 120: 2731–40.

Dooley, C. T., Dore, T. M., Hanson, G. T., Jackson, W. C., Remington, S. J., & Tsien, R. Y. (2004). *Imaging dynamic redox changes in mammalian cells with green fluorescent protein indicators.* J. Biol. Chem., 279(21): 22284–93.

Du, G., Fischer, B. E., Becker, G., Taucher-, G., Kraft, G., & Thiel, G. (2008). *The Absence of Early Calcium Response to Heavy Ion Irradiation in Mammalian Cells.* Radiat. Res., 170(3): 316–26.

Ermakova, Y. G., Bilan, D. S., Matlashov, M. E., Mishina, N. M., Markvicheva, K. N., Subach, O. M., Bogeski, I., Hoth, M., Enikolopov, G., & Belousov, V. V. (2014). *Red fluorescent genetically encoded indicator for intracellular hydrogen peroxide.* Submitt. Pap.

Fanger, C. M., Ghanshani, S., Logsdon, N. J., Rauer, H., Kalman, K., Zhou, J., Beckingham, K., Chandy, K. G., Cahalan, M. D., & Aiyar, J. (1999). *Calmodulin Mediates Calcium-dependent Activation of the Intermediate Conductance Channel, $IK_{Ca}1$.* J. Biol. Chem., 274(9): 5746–5754.

Faouzi, M., Chopin, V., Ahidouch, A., & Ouadid-Ahidouch, H. (2010). *Intermediate Ca^{2+}-sensitive K^+ channels are necessary for prolactin-induced proliferation in breast cancer cells.* J. Membr. Biol., 234(1): 47–56.

Feinendegen, L., & Toxicol, H. E. (2002). *Reactive oxygen species in cell responses to toxic agents.* Hum. Exp. Toxicol., 21(2): 85–90.

Felipe, A., Vicente, R., Villalonga, N., Roura-Ferrer, M., Martínez-Mármol, R., Solé, L., Ferreres, J. C., & Condom, E. (2006). *Potassium channels: new targets in cancer therapy.* Cancer Detect. Prev., 30(4): 375–85.

Ferrando-May, E., Tomas, M., Blumhardt, P., Stöckl, M., Fuchs, M., & Leitenstorfer, A. (2013). *Highlighting the DNA damage response with ultrashort laser pulses in the near infrared and kinetic modeling.* Front. Genet., 4: 135.

Ferreira, R., & Schlichter, L. C. (2013). *Selective activation of $K_{Ca}3.1$ and CRAC channels by P2Y2 receptors promotes Ca^{2+} signaling, store refilling and migration of rat microglial cells.* PLoS One, 8(4): e62345.

Fertig, N., Blick, R. H., & Behrends, J. C. (2002). *Whole cell patch clamp recording performed on a planar glass chip.* Biophys. J., 82(6): 3056–62.

Feske, S. (2007). *Calcium signalling in lymphocyte activation and disease.* Nat. Rev. Immunol., 7(9): 690–702.

Feske, S., Skolnik, E. Y., & Prakriya, M. (2013). *Ion channels and transporters in lymphocyte function and immunity.* Nat. Rev. Immunol., 12(7): 532–547.

Filomeni, G., Rotilio, G., & Ciriolo, M. R. (2002). *Cell signalling and the glutathione redox system.* Biochem. Pharmacol., 64(5-6): 1057–64.

Fiorio Pla, A., & Gkika, D. (2013). *Emerging role of TRP channels in cell migration: from tumor vascularization to metastasis.* Front. Physiol., 4: 311.

Forman, H. J., Maiorino, M., & Ursini, F. (2010). *Signaling functions of reactive oxygen species.* Biochemistry, 49(5): 835–42.

Freinbichler, W., Colivicchi, M. a, Stefanini, C., Bianchi, L., Ballini, C., Misini, B., Weinberger, P., Linert, W., Varešlija, D., Tipton, K. F., & Della Corte, L. (2011). *Highly reactive oxygen species: detection, formation, and possible functions.* Cell. Mol. Life Sci., 68(12): 2067–79.

Gao, Y., Hanley, P. J., Rinné, S., Zuzarte, M., & Daut, J. (2010). *Calcium-activated K^+ channel ($K_{Ca}3.1$) activity during Ca^{2+} store depletion and store-operated Ca^{2+} entry in human macrophages.* Cell Calcium, 48(1): 19–27.

García-Becerra, R., Díaz, L., Camacho, J., Barrera, D., Ordaz-Rosado, D., Morales, A., Ortiz, C. S., Avila, E., Bargallo, E., Arrecillas, M., Halhali, A., & Larrea, F. (2010). *Calcitriol inhibits Ether-à go-go potassium channel expression and cell proliferation in human breast cancer cells.* Exp. Cell Res., 316(3): 433–42.

García-giménez, J. L., Markovic, J., Dasí, F., Queval, G., Schnaubelt, D., Foyer, C. H., & Pallardó, F. V. (2013). *Nuclear glutathione.* Biochim. Biophys. Acta, 1830(5): 3304–3316.

Ghanshani, S., Coleman, M., Gustavsson, P., Wu, A. C., Gargus, J. J., Gutman, G. A., Dahl, N., Mohrenweiser, H., & Chandy, K. G. (1998). *Human Calcium-Activated Potassium Channel Gene KCNN4 Maps to Chromosome 19q13.2 in the Region Deleted in Diamond – Blackfan Anemia.* Genomics, 51: 160–161.

Ghanshani, S., Wulff, H., Miller, M. J., Rohm, H., Neben, A., Gutman, G. a, Cahalan, M. D., & Chandy, K. G. (2000). *Up-regulation of the $IK_{Ca}1$ potassium channel during T-cell activation. Molecular mechanism and functional consequences.* J. Biol. Chem., 275(47): 37137–49.

Giard, D. J., Aaronson, S. A., Todaro, G. J., Arnstein, P., Kersey, J. H., & Parks, W. P. (1973). *In Vitro Cultivation of Human Tumors: Establishment of Cell Lines Derived From a Series of Solid Tumors.* J Natl Cancer Inst, 51(5): 1417–1423.

Girard, P. M., Francesconi, S., Pozzebon, M., Graindorge, D., Rochette, P., Drouin, R., & Sage, E. (2011). *UVA-induced damage to DNA and proteins: direct versus indirect photochemical processes.* J. Phys. Conf. Ser., 261: 012002.

Gomez-Casal, R., Bhattacharya, C., Ganesh, N., Bailey, L., Basse, P., Gibson, M., Epperly, M., & Levina, V. (2013). *Non-small cell lung cancer cells survived ionizing radiation treatment display cancer stem cell and epithelial-mesenchymal transition phenotypes.* Mol. Cancer, 12(1): 94.

Gorowiec, M. R., Borthwick, L. A., Parker, S. M., Kirby, J. a, Saretzki, G. C., & Fisher, A. J. (2012). *Free Radical Biology & Medicine Free radical generation induces epithelial-to-mesenchymal transition in lung epithelium via a TGF- β 1-dependent mechanism.* Free Radic. Biol. Med., 52(6): 1024–1032.

Graham, F. L., Smiley, J., Russell, W. C., & Nairn, R. (1977). *Characteristics of a human cell line transformed by DNA from human adenovirus type 5.* J. Gen. Virol., 36(1): 59–74.

Guéguinou, M., Chantôme, A., Fromont, G., Bougnoux, P., Vandier, C., & Potier-Cartereau, M. (2014). *K_{Ca} and Ca^{2+} channels: The complex thought.* Biochim. Biophys. Acta.

Gutscher, M., Pauleau, A., Marty, L., Brach, T., Wabnitz, G. H., Samstag, Y., Meyer, A. J., & Dick, T. P. (2008). *Real-time imaging of the intracellular glutathione redox potential.* Nat. Methods, 5(6): 553–559.

Hafer, K., Konishi, T., & Schiestl, R. H. (2008). *Radiation-Induced Long-Lived Extracellular Radicals do not Contribute to Measurement of Intracellular Reactive Oxygen Species Using the Dichlorofluorescein Method.* BioOne, 169(4): 469–473.

Hall, E. J., & Giaccia, A. (2006). *Radiobiology for the radiologist* (p. 886). Lippincott Williams & Wilkins.

Hamada, N. (2009). *Recent Insights into the Biological Action of Heavy-Ion Radiation.* J. Radiat. Res., 50(1): 1–9.

Hanahan, D. (1983). *Studies on transformation of Escherichia coli with plasmids.* J. Mol. Biol., 166(4): 557–80.

Hansen, J. M., Go, Y.-M., & Jones, D. P. (2006). *Nuclear and mitochondrial compartmentation of oxidative stress and redox signaling.* Annu. Rev. Pharmacol. Toxicol., 46: 215–34.

Hanson, C. J., Bootman, M. D., & Roderick, H. L. (2004). *Cell signalling: IP3 receptors channel calcium into cell death.* Curr. Biol., 14(21): 933–5.

Hille, B. (2001). *Ion Channels of Excitable Membranes* (3rd editio.). Sinauer Associates Inc.

Hoffman, J. F., Joiner, W., Nehrke, K., Potapova, O., Foye, K., & Wickrema, A. (2003). *The hSK4 (KCNN4) isoform is the Ca^{2+}-activated K^{+}channel (Gardos channel) in human red blood cells.* Proc. Natl. Acad. Sci., 100(12): 7366–7371.

Huang, L., Wu, S., & Xing, D. (2011). *High fluence low-power laser irradiation induces apoptosis via inactivation of Akt/GSK3β signaling pathway.* J. Cell. Physiol., 226(3): 588–601.

Huang, Y.-Y., Chen, A. C.-H., Sharma, S. K., Wu, Q., & Hamblin, M. R. (2013). *Comparison of cellular responses induced by low level light in different cell types.* (M. R. Hamblin, R. W. Waynant, & J. Anders, Eds.)Proc. SPIE, 7552: 1–10.

Huber, S. M. (2013). *Oncochannels.* Cell Calcium, 53(4): 241–55.

Ichas, F., & Mazat, J. P. (1998). *From calcium signaling to cell death: two conformations for the mitochondrial permeability transition pore. Switching from low- to high-conductance state.* Biochim. Biophys. Acta, 1366(1-2): 33–50.

Ishii, T., & Ishii. (1997). *A human intermediate conductance calcium-activated.* Proc. Natl. Acad. Sci. USA, 94: 11651–11656.

Iyer, R., & Lehnert, B. E. (2002). *Low dose, low-LET ionizing radiation-induced radioadaptation and associated early responses in unirradiated cells.* Mutat. Res., 503(1-2): 1–9.

Jakob, B., Rudolph, J. H., Gueven, N., Lavin, M. F., & Taucher-Scholz, G. (2005). *Live cell imaging of heavy-ion-induced radiation responses by beamline.* Radiat. Res., 163(6): 681–90.

Jensen, B. S., Hertz, M., Christophersen, P., & Madsen, L. S. (2002). *The Ca^{2+}-activated K^+ channel of intermediate conductance:a possible target for immune suppression.* Expert Opin. Ther. Targets, 6(6): 623–36.

Jensen, B. S., Strøbæk, D., Christophersen, P., Jørgensen, T. D., Hansen, C., Silahtaroglu, A., Olesen, S., & Ahring, P. K. (1998). *Characterization of the cloned human intermediate-conductance Ca^{2+} -activated K^+ channel.* Am. J. Cell Physiol., 275: 848–856.

Jensen, B. S., Strøbaek, D., Olesen, S. P., Christophersen, P., & Strøbæk, D. (2001). *The Ca^{2+}-activated K^+ channel of intermediate conductance: a molecular target for novel treatments?* Curr. Drug Targets, 2(4): 401–22.

Jiang, B., Sun, X., Cao, K., & Wang, R. (2002). *Endogenous Kv channels in human embryonic kidney (HEK-293) cells.* Mol. Cell. Biochem., 238(1-2): 69–79.

Jou, M.-J., Jou, S.-B., Chen, H.-M., Lin, C.-H., & Peng, T.-I. (2002). *Critical Role of Mitochondrial Reactive Oxygen Species Formation in Visible Laser Irradiation-Induced Apoptosis in Rat Brain Astrocytes (RBA-1).* J. Biomed. Sci., 9: 507–516.

Jou, M.-J., Jou, S.-B., Guo, M.-J., Wu, H.-Y., & Peng, T.-I. (2004). *Mitochondrial Reactive Oxygen Species Generation and Calcium Increase Induced by Visible Light in Astrocytes.* Ann. N. Y. Acad. Sci., 1011(1): 45–56.

Jung, J.-W., Hwang, S.-Y., Hwang, J.-S., Oh, E.-S., Park, S., & Han, I.-O. (2007). *Ionising radiation induces changes associated with epithelial-mesenchymal transdifferentiation and increased cell motility of A549 lung epithelial cells.* Eur. J. Cancer, 43(7): 1214–24.

Kahl, C. R. (2003). *Regulation of Cell Cycle Progression by Calcium/Calmodulin-Dependent Pathways.* Endocr. Rev., 24(6): 719–736.

Kamosinska, B., Duszyk, M., Radomski, M. W., Radomski, A., & Man, S. F. (1997). *Nitric oxide activates chloride currents in human lung epithelial cells.* Am. J. Physiol., 272: 1098–104.

Kargiotis, O., Geka, A., Rao, J. S., & Kyritsis, A. P. (2010). *Effects of irradiation on tumor cell survival, invasion and angiogenesis.* J. Neurooncol., 100(3): 323–38.

Karlsson, M., Kurz, T., Brunk, U. T., Nilsson, S. E., & Frennesson, C. I. (2010). *What does the commonly used DCF test for oxidative stress really show?* Biochem. J., 428(2): 183–90.

Karlstad, J., Sun, Y., & Singh, B. B. (2012). *Ca^{2+} Signaling: An Outlook on the Characterization of Ca^{2+} Channels and Their Importance in Cellular Functions.* (M. S. Islam, Ed.)Adv Exp Med Biol., Advances in Experimental Medicine and Biology, 740: 143–157.

Keen, J. E., Khawaled, R., Farrens, D. L., Neelands, T., Rivard, A., Bond, C. T., Janowsky, A., Fakler, B., Adelman, J. P., & Maylie, J. (1999). *Domains responsible for constitutive and Ca^{2+}-dependent interactions between calmodulin and small conductance Ca^{2+}-activated potassium channels.* J. Neurosci., 19(20): 8830–8.

Kim, H.-J., Jang, H. S., Jeong, Y. A., Ryu, P. D., Kim, D.-Y., & Lee, S. Y. (2010). *Involvement of Kv4.1 K^+ Channels in Gastric Cancer Cell Proliferation.* Biol. Pharm. Bull., 33(10): 1754–1757.

Kim, J. H., Jang, Y. S., Eom, K.-S., Hwang, Y. Il, Kang, H. R., Jang, S. H., Kim, C. H., Park, Y. B., Lee, M. G., Hyun, I. G., Jung, K.-S., & Kim, D.-G. (2007). *Transforming Growth Factor $\beta 1$ Induces Epithelial-to-Mesenchymal Transition of A549 Cells.* J. Korean Med. Sci., 22(5): 898.

Kim, J.-B. (2014). *Channelopathies.* Korean J. Pediatr., 57(1): 1–18.

Kim, S. O., Merchant, K., Nudelman, R., Beyer, W. F., Keng, T., DeAngelo, J., Hausladen, A., & Stamler, J. S. (2002). *OxyR: a molecular code for redox-related signaling.* Cell, 109(3): 383–96.

Klein, H., Garneau, L., Banderali, U., Simoes, M., Parent, L., & Sauvé, R. (2007). *Structural determinants of the closed $K_{Ca}3.1$ channel pore in relation to channel gating: results from a substituted cysteine accessibility analysis.* J. Gen. Physiol., 129(4): 299–315.

Korystov, Y. N., Shaposhnikova, V. V, Korystova, A. F., Maksim, O., & Emel, M. O. (2007). *Detection of Reactive Oxygen Species Induced by Radiation in Cells Using the Dichlorofluorescein Assay Detection of Reactive Oxygen Species Induced by Radiation in Cells Using the Dichlorofluorescein Assay,* 168(2): 226–232.

Koshy, S., Wu, D., Hu, X., Tajhya, R. B., Huq, R., Khan, F. S., Pennington, M. W., Wulff, H., Yotnda, P., & Beeton, C. (2013). *Blocking $K_{Ca}3.1$ channels increases tumor cell killing by a subpopulation of human natural killer lymphocytes.* PLoS One, 8(10): e76740.

Kunzelmann, K. (2005). *Ion channels and cancer.* J. Membr. Biol., 205(3): 159–73.

Kuo, S. S., Saad, a H., Koong, a C., Hahn, G. M., & Giaccia, a J. (1993). *Potassium-channel activation in response to low doses of gamma-irradiation involves reactive oxygen intermediates in nonexcitatory cells.* Proc. Natl. Acad. Sci. U. S. A., 90(3): 908–12.

Kuras, Z., Yun, Y.-H., Chimote, A. a, Neumeier, L., & Conforti, L. (2012). *$K_{Ca}3.1$ and TRPM7 channels at the uropod regulate migration of activated human T cells.* PLoS One, 7(8): e43859.

Kutchinsky, J., Friis, S., Asmild, M., Taboryski, R., Pedersen, S., Vestergaard, R. K., Jacobsen, R. B., Krzywkowski, K., Schrøder, R. L., Ljungstrøm, T., Hélix, N., Sørensen, C. B., Bech, M., & Willumsen, N. J. (2003). *Characterization of Potassium Channel Modulators with QPatchTM Automated Patch-Clamp Technology System Characteristics and Performance.* Assay Drug Dev. Technol., 1(5): 685–693.

Lacinova, L. (2005). *Voltage-Dependent Calcium Channels.* Dissertation.

Lallet-Daher, H., Roudbaraki, M., Bavencoffe, A., Mariot, P., Gackière, F., Bidaux, G., Urbain, R., Gosset, P., Delcourt, P., Fleurisse, L., Slomianny, C., Dewailly, E., Mauroy, B., Bonnal, J. L., Skryma, R., & Prevarskaya, N. (2009). *Intermediate-conductance Ca^{2+}-activated K^+ channels ($IK_{Ca}1$) regulate human prostate cancer cell proliferation through a close control of calcium entry.* Oncogene, 28(15): 1792–806.

Lang, F., Shumilina, E., Ritter, M., Gulbins, E., Vereninov, A., & Huber, S. M. (2006). *Ion channels and cell volume in regulation of cell proliferation and apoptotic cell death.* Mech. Significance Cell Vol. Regul. Contrib Nephrol. Basel, Karger, 2006, vol 152, pp 142–160, 152: 142–160.

Lansu, K., & Gentile, S. (2013). *Potassium channel activation inhibits proliferation of breast cancer cells by activating a senescence program.* Cell Death Dis., 4(6): e652.

Le Caër, S. (2011). *Water Radiolysis: Influence of Oxide Surfaces on H2 Production under Ionizing Radiation.* Water, 3(4): 235–253.

Leach, J. K., Tuyle, G. Van, Lin, P., Schmidt-ullrich, R., & Mikkelsen, R. B. (2001). *Ionizing Radiation-induced, Mitochondria-dependent Generation of Reactive Oxygen/Nitrogen.* Cancer Res., 3894–3901.

Leanza, L., O'Reilly, P., Doyle, A., Venturini, E., Zoratti, M., Szegezdi, E., & Szabo, I. (2014). *Correlation between potassium channel expression and sensitivity to drug-induced cell death in tumor cell lines.* Curr. Pharm. Des., 20(2): 189–200.

LeBel, C. P., Ischiropoulos, H., & Bondy, S. C. (1992). *Evaluation of the probe 2',7'-dichlorofluorescin as an indicator of reactive oxygen species formation and oxidative stress.* Chem Res Toxicol, 5(2): 227–31.

Lee, C., Lee, S. M. S. C., Mukhopadhyay, P., Kim, S. J., Ahn, W.-S., Yu, M.-H., Storz, G., & Ryu, S. E. (2004). *Redox regulation of OxyR requires specific disulfide bond formation involving a rapid kinetic reaction path.* Nat. Struct. Mol. Biol., 11(12): 1179–85.

Lewis, R. S. (2001). *Calcium signaling mechanisms in T lymphocytes.* Annu. Rev. Immunol., 19: 497–521.

Lewis, R. S. (2011). *Store-operated calcium channels: New perspectives on mechanism and function.* Cold Spring Harb. Perspect. Biol., 3(12).

Li, W., Halling, D. B., Hall, A. W., & Aldrich, R. W. (2009). *EF hands at the N-lobe of calmodulin are required for both SK channel gating and stable SK-calmodulin interaction.* J. Gen. Physiol., 134(4): 281–93.

Liu, H., Hughes, J. D., Rollins, S., Chen, B., & Perkins, E. (2011). *Calcium entry via ORAI1 regulates glioblastoma cell proliferation and apoptosis.* Exp. Mol. Pathol., 91(3): 753–60.

Liu, S.-L., Lin, X., Shi, D.-Y., Cheng, J., Wu, C.-Q., & Zhang, Y.-D. (2002). *Reactive oxygen species stimulated human hepatoma cell proliferation via cross-talk between PI3-K/PKB and JNK signaling pathways.* Arch. Biochem. Biophys., 406(2): 173–82.

Llopis, J., McCaffery, J. M., Miyawaki, A., Farquhar, M. G., & Tsien, R. Y. (1998). *Measurement of cytosolic, mitochondrial, and Golgi pH in single living cells with green fluorescent proteins.* Proc. Natl. Acad. Sci. U. S. A., 95(12): 6803–8.

Logsdon, N. J. (1997). *A Novel Gene, $hK_{Ca}4$, Encodes the Calcium-activated Potassium Channel in Human T Lymphocytes.* J. Biol. Chem., 272(52): 32723–32726.

Lukyanov, K. A., & Belousov, V. V. (2013). *Genetically encoded fluorescent redox sensors.* Biochim. Biophys. Acta, 1840(2): 745–56.

Machaca, K. (2010). *Ca^{2+} signaling, genes and the cell cycle.* Cell Calcium, 48(5): 243–50.

Malinouski, M., Zhou, Y., Belousov, V. V, Hatfield, D. L., & Gladyshev, V. N. (2011). *Hydrogen peroxide probes directed to different cellular compartments.* PLoS One, 6(1): e14564.

Marinho, H. S., Cyrne, L., Cadenas, E., & Antunes, F. (2013). *The cellular steady-state of H_2O_2: latency concepts and gradients.* Methods Enzymol., 527: 3–19.

Marinho, H. S., Real, C., Cyrne, L., Soares, H., & Antunes, F. (2014). *Hydrogen peroxide sensing, signaling and regulation of transcription factors.* Redox Biol., 2: 535–562.

Markovic, J., Borrás, C., Sastre, J., Viña, J., Pallardó, V., Borra, C., Pallardo, F. V, Ortega, A., & Pallardó, F. V. (2007). *Glutathione is recruited into the nucleus in early phases of cell proliferation.* J. Biol. Chem., 282(28): 20416–24.

Markovic, J., García-Gimenez, J. L., Gimeno, A., Viña, J., & Pallardó, F. V. (2010). *Role of glutathione in cell nucleus.* Free Radic. Res., 44(7): 721–33.

Markvicheva, K. N., Bilan, D. S., Mishina, N. M., Gorokhovatsky, A. Y., Vinokurov, L. M., Lukyanov, S., & Belousov, V. V. (2011). *A genetically encoded sensor for H_2O_2 with expanded dynamic range.* Bioorg. Med. Chem., 19(3): 1079–84.

Martinière, A., Desbrosses, G., Sentenac, H., & Paris, N. (2013). *Development and properties of genetically encoded pH sensors in plants.* Front. Plant Sci., 4: 523.

Meesungnoen, J., & Jay-Gerin, J.-P. (2009). *High-LET Ion Radiolysis of Water: Oxygen Production in Tracks.* Radiat. Res., 171(3): 379–386.

Meyer, A. J., & Dick, T. P. (2010). *Fluorescent protein-based redox probes.* Antioxid. Redox Signal., 13(5): 621–50.

Meyer, A. J., & Hell, R. (2005). *Glutathione homeostasis and redox-regulation by sulfhydryl groups.* Photosynth. Res., 86(3): 435–57.

Mikkelsen, R. B., & Wardman, P. (2003). *Biological chemistry of reactive oxygen and nitrogen and radiation-induced signal transduction mechanisms.* Oncogene, 22(37): 5734–54.

Millership, J. E., Devor, D. C., Hamilton, K. L., Balut, C. M., Bruce, J. I. E., & Fearon, I. M. (2011). *Calcium-activated K^+ channels increase cell proliferation independent of K^+ conductance.* Am. J. Physiol. Cell Physiol., 300(4): 792–802.

Mishina, N. M., Markvicheva, K. N., Bilan, D. S., Matlashov, M. E., Shirmanova, M. V, Liebl, D., Schultz, C., Lukyanov, S., & Belousov, V. V. (2013). *Visualization of intracellular hydrogen peroxide with HyPer, a genetically encoded fluorescent probe.* Methods Enzymol., 526: 45–59.

Mishina, N. M., Tyurin-Kuzmin, P. a, Markvicheva, K. N., Vorotnikov, A. V, Tkachuk, V. a, Laketa, V., Schultz, C., Lukyanov, S., & Belousov, V. V. (2011). *Does cellular hydrogen peroxide diffuse or act locally?* Antioxid. Redox Signal., 14(1): 1–7.

Miyawaki, A., Nagai, T., & Mizuno, H. (2013). *Imaging intracellular free Ca^{2+} concentration using yellow cameleons.* Cold Spring Harb. Protoc., (11).

Morales, P., Garneau, L., Klein, H., Lavoie, M.-F., Parent, L., & Sauvé, R. (2013). *Contribution of the $K_{Ca}3.1$ channel-calmodulin interactions to the regulation of the $K_{Ca}3.1$ gating process.* J. Gen. Physiol., 142(1): 37–60.

Morgan, B., Sobotta, M. C., & Dick, T. P. (2011). *Measuring E(GSH) and H_2O_2 with roGFP2-based redox probes.* Free Radic. Biol. Med., 51(11): 1943–51.

Morley, N., Curnow, A., Salter, L., Campbell, S., & Gould, D. (2003). *N-acetyl-L-cysteine prevents DNA damage induced by UVA, UVB and visible radiation in human fibroblasts.* J. Photochem. Photobiol. B., 72(1-3): 55–60.

Morris, G., Anderson, G., Dean, O., Berk, M., Galecki, P., Martin-Subero, M., & Maes, M. (2014). *The Glutathione System: A New Drug Target in Neuroimmune Disorders.* Mol. Neurobiol.

Mortusewicz, O., Roth, W., Li, N., Cardoso, M. C., Meisterernst, M., & Leonhardt, H. (2008). *Recruitment of RNA polymerase II cofactor PC4 to DNA damage sites.* J. Cell Biol., 183(5): 769–76.

Mortusewicz, O., Rothbauer, U., Cardoso, M. C., & Leonhardt, H. (2006). *Differential recruitment of DNA Ligase I and III to DNA repair sites.* Nucleic Acids Res., 34(12): 3523–32.

Mortusewicz, O., Schermelleh, L., Walter, J., Cardoso, M. C., & Leonhardt, H. (2005). *Recruitment of DNA methyltransferase I to DNA repair sites.* Proc. Natl. Acad. Sci. U. S. A., 102(25): 8905–9.

Muroya, Y., Plante, I., Azzam, E. I., Meesungnoen, J., Katsumura, Y., & Jay-Gerin, J.-P. (2006). *High-LET Ion Radiolysis of Water: Visualization of the Formation and Evolution of Ion Tracks and Relevance to the Radiation-Induced Bystander Effect.* Radiat. Res., 165(4): 485–491.

Nagai, T., Sawano, a, Park, E. S., & Miyawaki, a. (2001). *Circularly permuted green fluorescent proteins engineered to sense* Ca^{2+}. Proc. Natl. Acad. Sci. U. S. A., 98(6): 3197–202.

Nagai, T., Yamada, S., Tominaga, T., Ichikawa, M., & Miyawaki, A. (2004). *Expanded dynamic range of fluorescent indicators for* Ca^{2+} *by circularly permuted yellow fluorescent proteins.* Proc. Natl. Acad. Sci. U. S. A., 101(29): 10554–9.

Nakagawa, H., Hasumi, K., Woo, J.-T., Nagai, K., & Wachi, M. (2004). *Generation of hydrogen peroxide primarily contributes to the induction of Fe(II)-dependent apoptosis in Jurkat cells by (-)-epigallocatechin gallate.* Carcinogenesis, 25(9): 1567–74.

Nakamura, K., Al., e t, & Group), (Particle Data. (2010). *Passage of particles through matter.* J. Phys., G(37): 075021.

Narayanan, P. K., Goodwin, E. H., & Lehnert, B. E. (1997). *Alpha particles initiate biological production of superoxide anions and hydrogen peroxide in human cells.* Cancer Res., 57(18): 3963–71.

Nicolaou, S. A., Neumeier, L., Peng, Y., Devor, D. C., & Conforti, L. (2007). *The* Ca^{2+}*-activated* K^{+} *channel* $K_{Ca}3.1$ *compartmentalizes in the immunological synapse of human T lymphocytes.* Am. J. Cell Physiol., 292(4): C1431–C1439.

Ogura, A., Oowada, S., Kon, Y., Hirayama, A., & Yasui, H. (2009). *Redox regulation in radiation-induced cytochrome c release from mitochondria of human lung carcinoma A549 cells.* Cancer Lett., 277(1): 64–71.

Okayasu, R. (2012). *Repair of DNA damage induced by accelerated heavy ions--a mini review.* Int. J. Cancer, 130(5): 991–1000.

Ouadid-Ahidouch, H., & Ahidouch, A. (2008). K^{+} *Channel Expression in Human Breast Cancer Cells□: Involvement in Cell Cycle Regulation and Carcinogenesis.* J Membr. Biol, 221(1): 1–6.

Ouadid-Ahidouch, H., & Ahidouch, A. (2013). K^{+} *channels and cell cycle progression in tumor cells.* Front. Physiol., 4: 220.

Ouadid-Ahidouch, H., Le Bourhis, X., Roudbaraki, M., Toilon, R., Delcourt, P., & Prevarskaya, N. (2001). *Changes in the* K^{+} *current-density of MCF-7 cells during progression through the cell cycle: possible involvement of a h-ether a-gogo* K^{+} *channel.* Recept. Channels, 7(5): 345–56.

Ouadid-ahidouch, H., Roudbaraki, M., Delcourt, P., Joury, N., & Prevarskaya, N. (2004). *Functional and molecular identification of intermediate-conductance* Ca^{2+}*-activated* K^{+} *channels in breast cancer cells: association with cell cycle progression.* Am. J. Cell Physiol., 287: C125–C134.

Ousingsawat, J. (2007). *Potassium Channels in Prostate and Colonic Cancer.* Dissertation.

Pallardó, F. V, Markovic, J., Luís, J., Viña, J., & García, J. L. (2009). *Role of nuclear glutathione as a key regulator of cell proliferation.* Mol. Aspects Med., 30(1-2): 77–85.

Palme, D., Misovic, M., Schmid, E., Klumpp, D., Salih, H. R., Rudner, J., & Huber, S. M. (2013). *Kv3.4 potassium channel-mediated electrosignaling controls cell cycle and survival of irradiated leukemia cells.* Pflugers Arch., 465(8): 1209–21.

Panner, A., & Wurster, R. D. (2006). *T-type calcium channels and tumor proliferation.* Cell Calcium, 40(2): 253–259.

Panyi, G., Varga, Z., & Gáspár, R. (2004). *Ion channels and lymphocyte activation.* Immunol. Lett., 92(1-2): 55–66.

Pardo, L. a. (2004). *Voltage-gated potassium channels in cell proliferation.* Physiology, 19: 285–92.

Pardo, L. a, Contreras-Jurado, C., Zientkowska, M., Alves, F., & Stühmer, W. (2005). *Role of voltage-gated potassium channels in cancer.* J. Membr. Biol., 205(3): 115–24.

Pardo, L. a, & Stühmer, W. (2008). *Eag1: an emerging oncological target.* Cancer Res., 68(6): 1611–3.

Pardo, L. a, & Sühmer, W. (2008). *Eag1 as a cancer target.* Expert Opin. Ther. Targets, 12(7): 837–43.

Parkash, J., & Asotra, K. (2010). *Calcium wave signaling in cancer cells.* Life Sci., 87(19-22): 587–95.

Patt, S., Preussat, K., Beetz, C., Kraft, R., Schrey, M., Kalff, R., Schönherr, K., & Heinemann, S. H. (2004). *Expression of ether à go-go potassium channels in human gliomas.* Neurosci. Lett., 368(3): 249–53.

Pedarzani, P., & Stocker, M. (2008). *Molecular and cellular basis of small--and intermediate-conductance, calcium-activated potassium channel function in the brain.* Cell. Mol. Life Sci., 65(20): 3196–217.

Peng, T.-I., & Jou, M.-J. (2004). *Mitochondrial Swelling and Generation of Reactive Oxygen Species Induced by Photoirradiation Are Heterogeneously Distributed.* Ann. N. Y. Acad. Sci., 1011(1): 112–122.

Penner, R., Fasolato, C., & Hoth, M. (1993). *Calcium influx and its control by calcium release.* Curr. Opin. Neurobiol., 3: 368–374.

Poburko, D., Santo-Domingo, J., & Demaurex, N. (2011). *Dynamic regulation of the mitochondrial proton gradient during cytosolic calcium elevations.* J. Biol. Chem., 286(13): 11672–84.

Poole, L. B., & Nelson, K. J. (2009). *Discovering mechanisms of signaling-mediated cysteine oxidation.* Curr. Opin. Chem. Biol., 12(1): 18–24.

Pouget, J., & Mather, S. J. (2001). *General aspects of the cellular response to low- and high-LET radiation.* Eur. J. Nucl. Med., 28(4).

Prevarskaya, N., Skryma, R., Bidaux, G., Flourakis, M., & Shuba, Y. (2007). *Ion channels in death and differentiation of prostate cancer cells.* Cell Death Differ., 14(7): 1295–304.

Prevarskaya, N., Skryma, R., & Shuba, Y. (2010). *Ion channels and the hallmarks of cancer.* Trends Mol. Med., 16(3): 107–21.

Prevarskaya, N., Skryma, R., & Shuba, Y. (2011). *Calcium in tumour metastasis: new roles for known actors.* Nat. Rev. Cancer, 11(8): 609–18.

Prise, K. M., & Schettino, G. (2011). *Microbeams in radiation biology: review and critical comparison.* Radiat. Prot. Dosimetry, 143(2-4): 335–9.

Qu, B., Al-Ansary, D., Kummerow, C., Hoth, M., & Schwarz, E. C. (2011). *ORAI-mediated calcium influx in T cell proliferation, apoptosis and tolerance.* Cell Calcium, 50(3): 261–9.

Rhee, S. G., Kang, S. W., Jeong, W., Chang, T.-S., Yang, K.-S., & Woo, H. A. (2005). *Intracellular messenger function of hydrogen peroxide and its regulation by peroxiredoxins.* Curr. Opin. Cell Biol., 17(2): 183–9.

Roderick, H. L., & Cook, S. J. (2008). *Ca^{2+} signalling checkpoints in cancer: remodelling Ca^{2+} for cancer cell proliferation and survival.* Nat. Rev. Cancer, 8(5): 361–75.

Rojkind, M., Domínguez-Rosales, J., Nieto, N., & Greenwel, P. (2002). *Role of hydrogen peroxide and oxidative stress.* Cell. Mol. Life Sci., 59: 1872–1891.

Roma, L. P., Duprez, J., Takahashi, H. K., Gilon, P., Wiederkehr, A., & Jonas, J.-C. (2012). *Dynamic measurements of mitochondrial hydrogen peroxide concentration and glutathione redox state in rat pancreatic β-cells using ratiometric fluorescent proteins: confounding effects of pH with HyPer but not roGFP1.* Biochem. J., 441(3): 971–8.

Rota, C., Chignell, C. F., & Mason, R. P. (1999). *Evidence for the free radical formation during the oxidation of 2'-7'-Dichlorofluorescein to the fluorescent dye 2'-7'-dichlorofluorescein by orseradish peroxidase: Possible impications for the oxidative stress measurements.* Free Radic. Biol. Med., 27(7/8): 873–881.

Roth, B. (2013). *Exposure to sparsely and densely ionizing irradiation results in an immediate activation of K^+ channels in A549 cells and in human peripheral blood lymphocytes.* Dissertation.

Roth, O., & LaVerne, J. a. (2011). *Effect of pH on H_2O_2 production in the radiolysis of water.* J. Phys. Chem. A, 115(5): 700–8.

Ruggieri, P., Mangino, G., Fioretti, B., Catacuzzeno, L., Puca, R., Ponti, D., Miscusi, M., Franciolini, F., Ragona, G., & Calogero, A. (2012). *The inhibition of $K_{Ca}3.1$ channels activity reduces cell motility in glioblastoma derived cancer stem cells.* PLoS One, 7(10): e47825.

Rzeszowska-Wolny, J., Przybyszewski, W. M., & Widel, M. (2009). *Ionizing radiation-induced bystander effects, potential targets for modulation of radiotherapy.* Eur. J. Pharmacol., 625(1-3): 156–64.

Salkoff, L., Butler, A., Ferreira, G., Santi, C., & Wei, A. (2006). *High-conductance potassium channels of the SLO family.* Nat. Rev. Neurosci., 7(12): 921–31.

Sarkadi, B., & Parker, J. C. (1991). *Activation of ion transport pathways by changes in cell volume.* Biochim. Biophys. Acta, 1071(4): 407–27.

Schoenmakers, T., Visser, G., Flik, G., & Theuvenet, A. (1992). *CHELATOR□: an improved method for computing metal ion concentrations in physiological solutions.* Biotechniques, 12(6): 870–879.

Scholz, M. (2003). *Effects of ion radiation on cells and tissues.* Radiat. Eff. Polym. Biol. Use, Adv. Polym. Sci., 162: 95–155.

Schreck, R., Albermann, K., & Baeuerle, P. (1992). *Nuclear factor kappa B□: an oxidative stress-responsive transcription factor of eukaryotic cells.* Free Radic. Res. Commun., 17(4): 221–37.

Schroeder, P., Popp, R., Wiegand, B., Altschmied, J., & Haendeler, J. (2007). *Nuclear redox-signaling is essential for apoptosis inhibition in endothelial cells-important role for nuclear thioredoxin-1.* Arterioscler. Thromb. Vasc. Biol., 27(11): 2325–31.

Schwab, A., Fabian, A., Hanley, P. J., & Stock, C. (2012). *Role of ion channels and transporters in cell migration.* Physiol. Rev., 92(4): 1865–913.

Schwab, A., Wulf, A., Schulz, C., Kessler, W., Nechyporuk-Zloy, V., Römer, M., Reinhardt, J., Weinhold, D., Dieterich, P., Stock, C., & Hebert, S. C. (2006). *Subcellular distribution of calcium-sensitive potassium channels (IK1) in migrating cells.* J. Cell. Physiol., 206(1): 86–94.

Schwarz, E. C., Qu, B., & Hoth, M. (2013). *Calcium, cancer and killing: the role of calcium in killing cancer cells by cytotoxic T lymphocytes and natural killer cells.* Biochim. Biophys. Acta, 1833(7): 1603–11.

Schwarzländer, M., Fricker, M. D., Müller, C., Marty, L., Brach, T., Novak, J., Sweetlove, L. J., Hell, R., & Meyer, a J. (2008). *Confocal imaging of glutathione redox potential in living plant cells.* J. Microsc., 231(2): 299–316.

Seo, Y. J., Lee, J. W., Lee, E. H., Lee, H. K., Kim, H. W., & Kim, Y.-H. (2004). *Role of glutathione in the adaptive tolerance to* H_2O_2. Free Radic. Biol. Med., 37(8): 1272–81.

Shao, C., Furusawa, Y., Kobayashi, Y., Funayama, T., & Wada, S. (2003). *Bystander effect induced by counted high-LET particles in confluent human fibroblasts: a mechanistic study.* FASEB J., 17(11): 1422–7.

Shaw, P. J., Qu, B., Hoth, M., & Feske, S. (2013). *Molecular regulation of CRAC channels and their role in lymphocyte function.* Cell. Mol. Life Sci., 70(15): 2637–56.

Shen, W.-W., Frieden, M., & Demaurex, N. (2011). *Remodelling of the endoplasmic reticulum during store-operated calcium entry.* Biol. Cell, 103(8): 365–80.

Sies, H. (1999). *Glutathione and its role in cellular functions.* Science (80-.)., 27(99): 916–921.

Skelding, K. a., Rostas, J. a. P., & Verrills, N. M. (2011). *Controlling the cell cycle: The role of calcium/calmodulin-stimulated protein kinases I and II.* Cell Cycle, 10(4): 631–639.

Slupphaug, G. (2003). *The interacting pathways for prevention and repair of oxidative DNA damage.* Mutat. Res. Mol. Mech. Mutagen., 531(1-2): 231–251.

Splinter, J., Jakob, B., Lang, M., Yano, K., Engelhardt, J., Hell, S. W., Chen, D. J., Durante, M., & Taucher-Scholz, G. (2010). *Biological dose estimation of UVA laser microirradiation utilizing charged particle-induced protein foci.* Mutagenesis, 25(3): 289–97.

Stone, J. R. (2004). *An assessment of proposed mechanisms for sensing hydrogen peroxide in mammalian systems.* Arch. Biochem. Biophys., 422(2): 119–24.

Stone, J. R., & Yang, S. (2006). *Hydrogen Peroxide: A Signaling Messenger.* Antioxid. Redox Signal., 8(3&4): 243–270.

Straight, A. F. (2007). *Fluorescent protein applications in microscopy.* Methods Cell Biol., 81(06): 93–113.

Sundelacruz, S., Levin, M., & Kaplan, D. L. (2009). *Role of membrane potential in the regulation of cell proliferation and differentiation.* Stem Cell Rev., 5(3): 231–46.

Suzuki, M., & Tsuruoka, C. (2004). *Heavy charged particles produce a bystander effect via cell-cell junctions.* Biol. Sci. Space., 18(4): 241–6.

Szumiel, I., Sochanowicz, B., & Buraczewska, I. (1990). *Ca^{2+} mobilization is related to the lethal effect of X-irradiation in L5178Y.* Int. J. Radiat. Biol., 58(1): 125–31.

Tantral, L., Malathi, K., Kohyama, S., Silane, M., Berenstein, A., & Jayaraman, T. (2004). *Intracellular calcium release is required for caspase-3 and -9 activation.* Cell Biochem. Funct., 22(1): 35–40.

Tao, R., Lau, C., Tse, H.-F., & Li, G. (2008). *Regulation of cell proliferation by intermediate-conductance Ca^{2+}-activated potassium and volume-sensitive chloride channels in mouse mesenchymal stem cells.* Am. J. Physiol. Cell Physiol., 295(5): C1409–16.

Targos, B., Barańska, J., & Pomorski, P. (2005). *Store-operated calcium entry in physiology and pathology of mammalian cells.* Acta Biochim. Pol., 52(2): 397–409.

Taylor, J.-T. (2008). *Calcium signaling and T-type calcium channels in cancer cell cycling.* World J. Gastroenterol., 14(32): 4984.

Tharp, D. L., & Bowles, D. K. (2013). *The Intermediate-Conductance Ca^{2+} -Activated K^+ Channel ($K_{Ca}3.1$) in Vascular Disease.* Cardiovasc. Hematol. Agents Med. Chem., 7(1).

Tobi, S. E., Paul, N., & McMillan, T. J. (2000). *Glutathione modulates the level of free radicals produced in UVA-irradiated cells.* J. Photobiol., 57: 102–112.

Todd, D. G., & Mikkelsen, R. B. (1994). *Ionizing radiation induces a transient increase in cytosolic free [Ca^{2+}] in human epithelial tumor cells.* Cancer Res., 54(19): 5224–30.

Tominaga, H., Kodama, S., Matsuda, N., Suzuki, K., & Watanabe, M. (2004). *Involvement of reactive oxygen species (ROS) in the induction of genetic instability by radiation.* J. Radiat. Res., 45(2): 181–8.

Vaca, L. (2010). *SOCIC: the store-operated calcium influx complex.* Cell Calcium, 47(3): 199–209.

Valerie, K., Yacoub, A., Hagan, M. P., Curiel, D. T., Fisher, P. B., Grant, S., & Dent, P. (2007). *Radiation-induced cell signaling: inside-out and outside-in.* Mol. Cancer Ther., 6(3): 789–801.

Valko, M., Rhodes, C. J., Moncol, J., Izakovic, M., & Mazur, M. (2006). *Free radicals, metals and antioxidants in oxidative stress-induced cancer.* Chem. Biol. Interact., 160(1): 1–40.

Veal, E. a, Day, A. M., & Morgan, B. a. (2007). *Hydrogen peroxide sensing and signaling.* Mol. Cell, 26(1): 1–14.

Voehringer, D. W. (1999). *BCL-2 and glutathione: alterations in cellular redox state that regulate apoptosis sensitivity.* Free Radic. Biol. Med., 27(9-10): 945–50.

Voet, D., Gratzer, W. B., Cox, R. a., & Doty, P. (1963). *Absorption spectra of nucleotides, polynucleotides, and nucleic acids in the far ultraviolet.* Biopolymers, 1(3): 193–208.

Walter, & Maximilians, L. (2003). *A new system for laser-UVA-microirradiation of living cells.* J. Microsc., 209(2): 71–75.

Wang, W., Yu, Z., & Su, W. (2010). *Ion irradiation and biomolecular radiation damage II. Indirect effect.* Phys. - Biol. Phys.

Wang, Z. (2004). *Roles of K^+ channels in regulating tumour cell proliferation and apoptosis.* Pflügers Arch. Eur. J. Physiol., 448(3): 274–86.

Wasselin-Trupin, V., Baldacchino, G., Bouffard, S., & Hickel, B. (2002). *Hydrogen peroxide yields in water radiolysis by high-energy ion beams at constant LET.* Radiat. Phys. Chem., 65: 53–61.

Watkins, S., & Sontheimer, H. (2012). *Unique biology of gliomas: challenges and opportunities.* Trends Neurosci., 35(9): 546–556.

Wei, A. D., Gutman, G. A., Aldrich, R., Chandy, K. G., Grissmer, S., & Wulff, H. (2005). *International Union of Pharmacology. LII. Nomenclature and Molecular Relationships of Calcium-Activated Potassium Channels.* Pharmacol. Rev., 57(4): 463–472.

Whitaker, M. (2012). *Genetically-encoded probes for measurement of intracellular calcium.* Methods Cell Biol.

Wonderlin, W. F., & Strobl, J. S. (1996). *Potassium Channels, Proliferation and G1 Progression.* Membr. Biol., 107: 91–107.

Wonderlin, W. F., Woodfork, K. a, & Strobl, J. S. (1995). *Changes in membrane potential during the progression of MCF-7 human mammary tumor cells through the cell cycle.* J. Cell. Physiol., 165(1): 177–85.

Wu, S., Xing, D., Wang, F., Chen, T., & Chen, W. R. (2007). *Mechanistic study of apoptosis induced by high-fluence low-power laser irradiation using fluorescence imaging techniques.* J Biomed Opt, 12(6).

Wu, W.-S. (2006). *The signaling mechanism of ROS in tumor progression.* Cancer Metastasis Rev., 25(4): 695–705.

Wulff, H., Gutman, G. A., Cahalan, M. D., & Chandy, K. G. (2001). *Delineation of the Clotrimazole / TRAM-34 Binding Site on the Intermediate Conductance Calcium-activated Potassium Channel, $IK_{Ca}1$.* J. Biol. Chem., 276(34): 32040–32045.

Wulff, H., & Köhler, R. (2013). *Endothelial Small- and Intermediate-Conductance K_{Ca} Channels: An Update on Their Pharmacology and Usefulness as Cardiovascular Targets.* J. Cardiovasc. Pharmacol., 61(2): 102–112.

Wulff, H., Miller, M. J., Hansel, W., Grissmer, S., Cahalan, M. D., & Chandy, K. G. (2000). *Design of a potent and selective inhibitor of the intermediate-conductance Ca^{2+}-activated K^+ channel, $IK_{Ca}1$: a potential immunosuppressant.* Proc. Natl. Acad. Sci. U. S. A., 97(14): 8151–6.

Yamamori, T., Yasui, H., Yamazumi, M., Wada, Y., Nakamura, Y., Nakamura, H., & Inanami, O. (2012). *Ionizing radiation induces mitochondrial reactive oxygen species production accompanied by upregulation of mitochondrial electron transport chain function and mitochondrial content under control of the cell cycle checkpoint.* Free Radic. Biol. Med., 53(2): 260–70.

Yang, M., & Brackenbury, W. J. (2013). *Membrane potential and cancer progression.* Front. Physiol., 4: 185.

Yun, J., Park, H., Ko, J.-H. J.-H., Lee, W., Kim, K., Kim, T., Shin, J., Song, J.-H. J.-H., Noh, Y.-H. Y.-H., Bang, H., & Lim, I. (2009). *Expression of Ca^{2+}-Activated K^+ Channels in Human Dermal Fibroblasts and Their Roles in Apoptosis.* Skin Pharmacol. Physiol., 23(2): 91–104.

Zhou, Y.-C., Liu, J.-Y., Li, J., Zhang, J., Xu, Y.-Q., Zhang, H.-W., Qiu, L.-B., Ding, G.-R., Su, X.-M., Mei-Shi, & Guo, G.-Z. (2011). *Ionizing radiation promotes migration and invasion of cancer cells through transforming growth factor-beta-mediated epithelial-mesenchymal transition.* Int. J. Radiat. Oncol. Biol. Phys., 81(5): 1530–7.

Zou, J., Ye, Y., Welshhans, K., Lurtz, M., Ellis, A. L., Louis, C., Rehder, V., & Yang, J. J. (2005). *Expression and optical properties of green fluorescent protein expressed in different cellular environments.* J. Biotechnol., 119(4): 368–78.

9. Apendix

9.1. Abbreviations

*OH - Hydroxyl radical
1-EBIO - 1-ethyl-2-benzimidazolinone; hIK channel opener
A549 - Adenocarcinomic human alveolar basal epithelial cell line
ATP - Adenosintriphosphat
BK$_{Ca}$ - Big conductance calcium-activated potassium-channel
BrdU - Bromodeoxyuridine; thymidine analogue
$[Ca^{2+}]_{cyt}$ - Cytosolic calcium concentration
CaM - Calmodulin
cAMP - Cyclic adenosine monophosphate
CLSM - Confocal laser scanning microscope
CLT - Clotrimazole; 1-[(2-Chlorphenyl)diphenylmethyl]-1H-imidazol; hIK channel blocker
CRAC - Calcium release-activated calcium channel
DCFDA - 2'-7'-dichlorodihydrofluorescein diacetate; a chemical ROS dye
DMEM - Dulbecco´s modified minimal essential medium
DMSO - Dimethyl sulfoxide
DNA - Deoxyribonucleic acid
e^{-}_{aq} - Hydrated electron
Eag1 - Voltage-gated potassium-channel; KCNH1; Kv10.1
EDTA - Ethylenediaminetetraacetic acid
EMT - Epithelial-mesenchymal transition
FCS - Fetal calve serum
FRET - Förster resonance energy transfer; fluorescence resonance energy transfer
G_1-phase - Gap1-phase; cell cycle
G_2-phase - Gap2-phase; cell cycle
GBM - Glioblastoma multiforme
Grx1-roGFP2 - ratiometric protein-based fluorescence sensor for the glutathione redox-potential
GSH / GSSG - Glutathione reduced / oxidized
GSI - Helmholtzzentrum für Schwerionenforschung GmbH (Darmstadt; Germany)
H_2O_2 - Hydrogen peroxide
HEK293 - Human embryonic kidney cell line
hERG - Voltage-gated potassium-channel; KCNH2; Kv11.1
hIK - Human intermediate-conductance Ca^{2+}-activated K^{+}-channel; KCNN4, K$_{Ca}$3.1
Hoechst33258 - 2′-(4-hydroxyphenyl)-5-(4-methyl-1-piperazinyl)-2,5′-bi-1*H*-benzimidazole trihydrochloride hydrate; DNA dye

HyPer - ratiometric, protein-based H_2O_2 fluorescence sensor
I_{inst} - Instantaneous current (definition Fig. 8)
IK_{Ca} - Intermediate-conductance calcium-activated potassium-channel
IM - Ionomycin
IR - Ionizing radiation
I_{td} - Time dependent current (definition Fig. 8)
Kv1.3 - Voltage-gated potassium-channel; KCNC1
Kv3.4 - Voltage-gated potassium-channel; KCNC4
Kv4.1 - Voltage-gated potassium-channel; KCND1
LET - Linear-energy transfer (LET; keV/µm)
M-phase - Mitosis phase; cell cycle
m.i. - Micro-irradiation
NAC - N-acetylcysteine
NADPH - Nicotinamide adenine dinucleotide phosphate
NEAA - Non-essential amino acids
O_2^{*-} - Superoxide radical
Orai - Calcium release-activated calcium modulator
PBS - Phosphate buffered saline
pH - Potential of hydrogen
RBE - Relative biological effectiveness
ROI - Region of interest
ROS - Reactive oxygen species
S-phase - Synthesis-phase; cell cycle
SD - Standard deviation
SK_{Ca} - Small conductance calcium-activated potassium-channel
SOCE - Store-operated calcium entry
STIM1 - Ca^{2+} sensor protein stromal interaction molecule
SypHer - HyPer-C199S H_2O_2 insensitive mutant
Tram-34 - 1-[(2-Chlorophenyl)diphenylmethyl]-1H-pyrazole; hIK channel blocker
TRP - transient receptor potential channels
UNILAC - Universal Linear Accelerator
UV - Ultraviolet (< 400 nm)
wt - Wildtype
X-ray - Roentgen radiation
YC3.60 - ratiometric FRET-based Ca^{2+} sensor; chameleon

9.2. List of figures

Fig. 1 Ion-channels are molecular switches. 6
Fig. 2 Schematic model of the complex interplay between Ca^{2+} and K^+-channels in mediating cytosolic calcium concentrations. 7
Fig. 3 Structure of the hIK channel. 8
Fig. 4 Dose distribution of X-rays and carbon-ions. 10
Fig. 5 Timeline of the early effects of ionizing radiation. 12
Fig. 6 Simulation of the distribution of ROS after an ion traversal. 12
Fig. 7 Pulse protocols used in this thesis to elicit currents in HEK293 and A549 cells. 18
Fig. 8 Representative current response of an A549 cell with a negative reversal potential. 21
Fig. 9 Representative current response of an A549 cell with a more depolarized membrane voltage. 22
Fig. 10 The instantaneous conductance is blocked with Clotrimazole. 22
Fig. 11 Calcium facilitates the activation of the instantaneous conductance in A549 cells. 23
Fig. 12 ROS mainly activate the instantaneous current component. 24
Fig. 13 ROS mediated ion-channel activation in A549 cells. 25
Fig. 14 I_{inst} is activated with low physiological H_2O_2 concentrations and the activation is dependent on the membrane voltage. 26
Fig. 15 The inhibitor Clotrimazole blocks the H_2O_2 activated conductance in A549 cells. 26
Fig. 16 Representative current response of a HEK293 cell and a HEK293 cell overexpressing hIK channels. 27
Fig. 17 Elevation of $[Ca^{2+}]_{cyt}$ activates heterologous expressed hIK channels. 28
Fig. 18 Clotrimazole blocks heterologous expressed hIK channels. 29
Fig. 19 ROS mediated activation of overexpressed hIK channels. 30
Fig. 20 Activation of overexpressed hIK channels by irradiation with 1 Gy X-rays. 31
Fig. 21 Radiation and ROS induced membrane hyperpolarization is dependent on the hIK channel activity. 32
Fig. 22 The calcium signal remains stable over a long time period. 33
Fig. 23 External applied ROS stimulate calcium signals in HEK293 cells. 34
Fig. 24 H_2O_2 stimulated increase of $[Ca^{2+}]_{cyt}$ in A549 cells. 34
Fig. 25 Fluorescence properties of the H_2O_2 sensor HyPer. 36
Fig. 26 Stability of the ratiometric HyPer signal over long time recording. 37
Fig. 27 *In vivo* calibration of the ratiometric fluorescence sensor HyPer. 38
Fig. 28 UV-laser micro-irradiation in HEK293 cells elicites the generation of H_2O_2. 39
Fig. 29 UV-laser micro-irradiation generates a rapid burst of H_2O_2 in the irradiated compartment. 40
Fig. 30 The ROS, which are elicited by laser micro-irradiation, are scavenged with the radical scavenger N-acetylcysteine. 40
Fig. 31 Laser micro-irradiation has no effect on the pH of the cytosol. 41
Fig. 32 Fluorescence properties of the redox sensor Grx1-roGFP2. 42

Fig. 33 The ratiometric Grx1-roGFP2 signal is stable in long time recordings. 42
Fig. 34 Repetitive micro-irradiation of the cytoplasm results in an increased glutathione-redox potential in the nucleus. 43
Fig. 35 Selected examples of redox-buffering after laser micro-irradiation. 44
Fig. 36 Cytoplasm and nucleus have different redox-buffering capacities. 45
Fig. 37 Reaction of HEK293 cells expressing HyPer to 1 Gy of X-ray irradiation. 48
Fig. 38 Generation of H_2O_2 in A549 cells after exposure to 1 Gy and 5 Gy of X-ray irradiation. 48
Fig. 39 Generation of H_2O_2 in A549 cells after exposure to 10 Gy of X-rays. 49
Fig. 40 Rapid buffering of X-ray radiation generated ROS. 50
Fig. 41 X-ray radiation induced ROS generation and buffering. 51
Fig. 42 Simulation of the generation and buffering of H_2O_2. 52
Fig. 43 Generation of ROS after heavy-ion irradiation with Pb. 52
Fig. 44 Generation of ROS after irradiation with carbon-ions. 53
Fig. 45 ROS and Ca^{2+} mediated signal cascade activating the hIK channel after ionizing radiation. 54
Fig. 46 Time-course of ROS and Ca^{2+} signaling leading to an increased K^+ conductance of hIK channels. 62

9.3. Own Work - List of contributions

Experiments, data analysis and writing were exclusively done by myself, with exception of:

- Internal perfusion with high Ca^{2+} concentrations of A549 cells and HEK293 cells overexpressing hIK channels were partial done by Anastasia Timofiiv (Bachelor Student; Vancouver, Canada): Fig. 11 A-C and Fig. 17 A - C.

- Live microscopy after X-ray irradiation and heavy-ion irradiation were performed at GSI (Helmholtzzentrum für Schwerionenforschung, Darmstadt, Germany) with the help and supervision of Dr. Burkhard Jakob.

- The Matlab Simulation (Fig. 42) was done with the help of Dr. Indra Schröder (TU-Darmstadt, Germany).

- Electrophysiological measurements of A549 cells after X-ray irradiation (Fig. 46) were done by Dr. Bastian Roth (TU-Darmstadt, Germany) and published in Roth (2013).

9.4. Declaration - Ehrenwörtliche Erklärung

"Ich erkläre hiermit ehrenwörtlich, dass ich die vorliegende Arbeit entsprechend den Regeln guter wissenschaftlicher Praxis selbstständig und ohne unzulässige Hilfe Dritter angefertigt habe.

Sämtliche aus fremden Quellen direkt oder indirekt übernommenen Gedanken sowie sämtliche von Anderen direkt oder indirekt übernommenen Daten, Techniken und Materialien sind als solche kenntlich gemacht. Die Arbeit wurde bisher bei keiner anderen Hochschule zu Prüfungszwecken eingereicht."

Darmstadt, den ___________________

____

Christine S. Gibhardt

9.5. Acknowledgements

An dieser Stelle möchte ich mich bei Herrn Prof. Dr. Gerhard Thiel bedanken, für die Möglichkeit meine Doktorarbeit in seiner Arbeitsgruppe durchzuführen. Die vielen Freiräume hinsichtlich Thematik und Methodik, sowie das entgegengebrachte Vertrauen die Arbeitsgruppe bei internationalen Konferenzen zu vertreten haben die Zeit dieser Doktorarbeit sehr bereichert.

Herrn Prof. Dr. Marco Durante von der Abteilung Biophysik der GSI bedanke ich mich für die Übernahme des zweiten Gutachtens und die erfolgreiche Kooperation mit seiner Abteilung.
Außerdem danke ich Herrn Prof. Dr. Harald Kolmar und Herrn Prof. Dr. Bodo Laube für die Übernahme des Prüfungsbeisitzes.

Mein großer Dank gilt Herrn Dr. Burkhard Jakob für die viele Zeit, die er für die Experimente an dem von ihm und Kollegen gebauten Mikroskopie-Setups für die real-time Röntgenbestrahlung investiert hat. Die an diesem Setup aufgenommenen Daten, waren essentiell für die Aussage dieser Arbeit. Außerdem danke ich ihm für die Betreuung bei den Schwerionen-Experimenten und seine Bereitschaft selbst zu nachtschlafender Zeit diese Experimente mit mir zusammen durchzuführen.

Bei der ganzen Membran-Biophysik Gruppe, die mir mit ihren wechselnden Mitgliedern in den vergangenen Jahren eine tolle Zeit bereitet hat, möchte ich mich ganz herzlich bedanken. Die Arbeitsatmosphäre war immer sehr angenehm und die gemeinsam verbrachte Zeit sowohl in der Uni, als auch Abends nach Arbeitsschluss wird mir immer in guter Erinnerung bleiben.

Aus der Arbeitsgruppe Thiel müssen einige Mitglieder noch persönlich namentlich genannt werden:

- Barbara Reinhards möchte ich für jegliche Hilfe bei bürokratischen Dingen, aber auch für die netten Gespräche zwischendurch danken.
- Danke an die TAs (Silva Haase, Mirja Manthey und Sylvia Lenz) im Hintergrund, ohne die vieles sicherlich nicht so glatt laufen würde und wir im Laboralltag manchmal aufgeschmissen wären.
- Indra danke ich für die netten Diskussionen und die Hilfe bei allen physikalischen und mathematischen Fragen die in den letzten Jahren aufkamen.
- Basti danke für die gute Zusammenarbeit an "unserem" Thema und die unvergesslichen Konferenztage bei denen wir versucht haben die Ionenkanäle in die Welt der Strahlenbiologen und die Strahlenbiologie in die Welt der Elektrophysiologen zu bringen.
- Meiner liebsten Büro-Kollegin Brigitte sage ich Danke für die tolle, lustige und liebevolle Atmosphäre. Mir werden die Eichhörnchen, die ab und zu "rüber gehuscht" kamen, obwohl wir Rücken an Rücken saßen, fehlen.
- Anne danke für die vielen gemeinsamen Samstags-Frühstücke in der Uni. Vor allem in den letzten Monaten haben die und die Motivase den Arbeitsalltag aufgelockert.

Ich bedanke mich bei der TU-Darmstadt und der DFG für die Bereitstellung des Stipendiums und des Arbeitsplatzes. Außerdem bedanke ich mich bei allen GRK1657 Mitgliedern für die angenehme Atmosphäre auf unseren Fahrten, den konstruktiven Austausch bei Seminaren und Kursen und die vielen Gespräche die mich nicht nur wissenschaftlich, sondern auch persönlich sehr bereichert haben.

Danke an meine Freunde, die ich jetzt nicht alle namentlich nennen werde (die richtigen werden sich angesprochen fühlen), für die viele Unterstützung während meines Studiums und der Promotion. Ihr seid ein wichtiger Teil meines Lebens und ohne euch wäre es manchmal nur halb so schön gewesen.

Zu guter Letzt möchte ich mich noch bei meiner Familie für die jahrelange Unterstützung bedanken, ohne die mir das Studium und die Promotion gar nicht erst möglich gewesen wären. Vor allem gilt mein Dank meinem großen, kleinen Bruder Johannes dafür, dass er immer für mich da ist!

9.6. Curriculum vitae

Personal information

Name: Gibhardt

Surname: Christine Silvia

Date of birth: 22.05.1986 in Kassel, Germany

Education and working experience

2011 – 2014	PhD thesis DFG-funded Graduiertenkolleg 1657 at the TU Darmstadt ("Molecular and cellular responses to ionizing radiation") Advisor: Prof. Dr. G. Thiel
2010 – 2011	Research assistant; Prof. Dr. G. Thiel at the TU Darmstadt tasks: cell culture, molecular biology methods, electrophysiology
20.09.2010	Diploma 1,0 (with distinction)
2005 – 2010	Study of biology at the Technische Universität Darmstadt Subjects: biochemistry, genetics, plant physiology cell- and radiation biology Diploma thesis: "Konstruktion, Funktionsanalyse und Etablierung einer Amber Suppressor tRNA zur Oberflächenpräsentation einer NNK randomisierten VHH-Fragmentbibliothek auf *Saccharomyces cerevisiae* Zellen." Advisor: Prof. Dr. H. Kolmar
2002 – 2005	Abitur in Kassel
1992 – 2002	Elementary school; secondary school

Publications, presentations and conferences

2014	B. Roth, C. S. Gibhardt, P. Becker, M. Gebhardt, J. Knoop, C. Fournier, A. Moroni, G. Thiel "Low dose photon irradiation alters cell differentiation via activation of hIK channels" (2014), Pflügers Archiv – European Journal of Physiology
2014	Poster presentation and short oral presentation at the "Experimentelle Strahlentherapie und Klinische Strahlenbiologie"; Tübingen; ISSN 1432-864X "Radiation induced activation of potassium-channels: the role of ROS and calcium"
2013	Oral presentation at GREWIS Workshop „Chronisch-entzündliche Erkrankungen und Strategien zur Behandlung“; Darmstadt
2013	Poster presentation at the EMBO|EMBL Symposium: Seeing is Believing – Imaging the Processes of Life; Heidelberg "Fluorescent reporter proteins monitor the role of ROS and calcium in radiation generated potassium-channel activation."
2013	Poster presentation at the 16th Annual Meeting of the GBS; Darmstadt "Radiation induced activation of potassium-channels: the role of ROS and calcium"
2013	Oral presentation at the „Dresden-Sydney - Workshop on Lipid Bilayers“; Dresden "Electrophysiological monitoring of membrane parameters in cells under stress."
2012	Poster presentation at the 15th Annual Meeting of the GBS; Munich "ROS mediated signal cascade leads to potassium-channel activation and membrane hyperpolarization"
2012	Poster presentation at the „International Meeting on Ion Transport and Cancer“ (ITC); Würzburg "ROS mediated signal cascade leads to potassium-channel activation and membrane hyperpolarization"
2012	GREWIS Workshop „Dosimetrie“; Darmstadt
2011	ISIMEP Workshop „Ionizing radiation epidemiology“; Mainz
2011	Poster presentation at the 14th Annual Meeting of the GBS; Cologne "Effects of ionizing radiation on ion-channel activity"